CHARACTERIZATION OF DIACYLGLYCEROL KINASES ETA AND IOTA IN ITCH, PAIN, AND PSYCHOPATHOLOGICAL BEHAVIOR IN MICE

Victoria Brings Bartsch

A dissertation or thesis submitted to the faculty at the University of North Carolina at Chapel Hill in partial fulfillment of the requirements for the degree of Doctor of Philosophy in the Department of Cell Biology and Physiology in the School of Medicine.

Chapel Hill
2018

Approved by:

Mark Zylka

Carol Otey

Andrea Nackley

Robert Nicholas

Robert Tarran

ABSTRACT

Victoria Brings Bartsch: Characterization of Diacylglycerol Kinases Eta and Iota in Itch, Pain, And Psychopathological Behavior in Mice
(Under the direction of Mark J. Zylka)

Diacylglycerol kinases (DGK) control diverse signaling functions. Expression of the iota and eta isoforms of DGK (*Dgki* and *Dgkh*, respectively) are enriched in mouse neuronal tissues. By overexpressing *Dgki* and *Dgkh* in HEK293 cells, we found that *Dgki* and *Dgkh* enhanced G-protein-coupled receptor signaling and phosphorylated diacylglycerol and monoacylglycerol. We acquired a *Dgki*-knockout mouse and generated a *Dgkh*-knockout mouse and a double *Dgki*/*Dgkh* knockout (dKO) mouse. Using the *Dgki*$^{-/-}$, *Dgkh*$^{-/-}$, and dKO mice, we elucidated the role of *Dgki* and *Dgkh* in regulating behaviors associated with the neuronal tissues in which they are expressed.

Dgki and *Dgkh* are highly expressed in small-diameter dorsal root ganglia (DRG) neurons, which detect pruritogenic (itch-causing) and algogenic (pain-causing) stimuli. We found that *in vivo* sensitivity to histamine—but not other pruritogens—was enhanced in male and female *Dgki*$^{-/-}$ mice, but was attenuated in *Dgkh*$^{-/-}$ males. Interestingly, dKO mice phenocopied the histamine sensitivity of the *Dgki*$^{-/-}$ mice. In contrast, baseline pain sensitivity and pain sensitization post-injury were equivalent between wild type (WT) and *Dgki*$^{-/-}$, *Dgkh*$^{-/-}$, or dKO mice. Even though diacylglycerol and monoacylglycerol kinase activity was reduced in DRGs from *Dgkh*$^{-/-}$ and dKO mice, *in vitro* signaling induced by pruritogens and algogens in DRG neurons was unaffected by *Dgki* or *Dgkh* deletion.

Genome-wide association studies linked *DGKH* and *DGKI* to mood disorders, and both genes are expressed throughout the brain. dKO mice—but not *Dgki*$^{-/-}$ or *Dgkh*$^{-/-}$ mice—showed

behavioral signs of anxiety and mania. *Dgki*$^{-/-}$ and dKO males showed hyperactivity and hyperexploratory behavior, as well. In addition to the psychopathological phenotypes, dKO females demonstrated deficits in maternal care. Fewer than 30% of newborn pups raised by dKO females survived to weaning; however, 85% of pups born from dKO dams survived when fostered by WT dams. Pups raised by dKO dams had smaller milk spots and reduced weight, indicative of impaired nursing. Together, our research suggests that *Dgki* and *Dgkh* regulate behavioral responses to histamine, without affecting responses to other pruritogens or algogens, and that combined deletion of *Dgkh* and *Dgki* disrupts mood-disorder-related phenotypes and impairs maternal behavior in the early postpartum period.

Dedicated to my brilliant and supportive parents, Liza and Bob Brings

ACKNOWLEDGEMENTS

The work presented in this dissertation was the combination of work by many people other than myself. Dr. Joe Rittiner laid the groundwork for the *Dgkh* study. Dr. JrGang Cheng developed the RFP-*Dgki* construct. Bonnie Taylor-Blake performed the immunohistochemical staining of mouse DRGs, and Dr. Megumi Aita performed the *in situ* hybridization. Dr. Eric McCoy performed the CFA injections for the dKO mice and also tested their responses in the electronic von Frey assay. Jesse Niehaus performed the SNI surgeries on the *Dgki*$^{-/-}$ mice and tested their filamentous von Frey responses.

In addition to performing these experiments, members of the Zylka lab have made an even-greater contribution to this work by supporting me throughout my graduate career. Not only did I find mentors, teachers, and sometimes therapists in many of my labmates, but I also found what are sure to be lifelong friends. I'll avoid listing all the lab members who made an impact on me because the list is too long, and the one person I end up forgetting to put on the list will probably be the one person who ends up reading these acknowledgements. And, of course, I'd like to give an immense thank you to my advisor, Dr. Mark Zylka, for his guidance and mentorship. It has been an absolute pleasure working for someone so brilliant and so patient.

Outside of the Zylka lab, this work was made possible by many cores and collaborators. Sperm from the *Dgki*$^{-/-}$ mice was generously provided by Dr. Matthew Topham at the University of Utah, and the Mutant Mouse Resource and Research Centers at the University of North Carolina at Chapel Hill performed the *in vitro* fertilization to recover the *Dgki*$^{-/-}$ mouse line. The Animal Models Core at UNC generated the *Dgkh*$^{-/-}$ founder mice. The psychopathological

behavioral assays were performed with the equipment in the Carolina Institute for Developmental Disabilities Behavioral Phenotyping Core. Additionally, my committee of Drs. Carol Otey, Andi Nackley, Rob Tarran, and Rob Nicholas provided great advice that significantly improved my progress and the quality of my research. I would also like to express my sincere gratitude for the hundreds of mice that contributed to this study.

Finally, I would like to thank my wonderful family. Houdini and Kaiser, I honestly don't think I would have finished graduate school without you. Otto, there are not enough words for me to express how grateful I am for all your encouragement, understanding, excitement, shared frustration, interest, patience, and love throughout this journey. Mom, Daddy, Katie, not only did you give me all the support I could have dreamed of, but you've also helped me by being incredible role models. Thank you for both telling me I could do anything I wanted and helping me to make that happen.

TABLE OF CONTENTS

LIST OF TABLES

LIST OF FIGURES

LIST OF ABBREVIATIONS

2-AG	2-Arachidonoylglycerol
^{32}P	Phosphorus-32
AA	Arachidonic acid
ADHD	Attention deficit hyperactivity disorder
ATP	Adenosine triphosphate
AUC	Area under the curve
BPD	Bipolar disorder
BSA	Bovine serum albumin
C1	Cysteine-rich
Cas9	CRISPR associated protein 9
CB1	Cannabinoid receptor 1
CFA	Complete Freund's adjuvant
CPM	Counts per minute (measure of radioactivity)
CRISPR	Clustered regularly interspaced short palindromic repeats
DAG	Diacylglycerol
DAGL	Diacylglycerol lipase
DAT	Dopamine transporter
DGK	Diacylglycerol kinase
Dgka	Diacylglycerol kinase alpha
Dgkb	Diacylglycerol kinase beta
Dgkd	Diacylglycerol kinase delta
Dgke	Diacylglycerol kinase epsilon
Dgkg	Diacylglycerol kinase gamma
Dgkh	Diacylglycerol kinase eta

Dgki	Diacylglycerol kinase iota
Dgkk	Diacylglycerol kinase kappa
Dgkq	Diacylglycerol kinase theta
Dgkz	Diacylglycerol kinase zeta
dKO	Double knockout of *Dgkh* and *Dgki*
DRG	Dorsal root ganglion
EGF	Epidermal growth factor
EGFR	Epidermal growth factor receptor
EPM	Elevated plus maze
ERK	Extracellular signal-regulated kinase
FST	Forced swim test
$G\alpha_q$-GPCR	$G\alpha_q$-protein-coupled receptor
GPCR	G-protein-coupled receptor
GWAS	Genome-wide association studies
H1R	Histamine receptor 1
HEK293	Human embryonic kidney 293 cells
IP_3	Inositol trisphosphate
LPA	Lysophosphatidic acid
MAG	Monoacylglycerol
MAPK	Mitogen-activated protein kinase
MEK	Mitogen-activated protein kinase kinase
mGluR-LTD	Metabotropic glutamate receptor-dependent long-term depression
mPFC, PFC	(Medial) Prefrontal cortex
Mrgprd	Mas-related GPR D
mTOR	Mammalian target of rapamycin

NGF	Nerve growth factor
P0, P1, P*n*	0, 1, *n* days post-birth
PA	Phosphatidic acid
PCR	Polymerase chain reaction
PH	Pleckstrin homology
PIP_2	Phosphatidylinositol 4,5-bisphosphate
PIP5K	Phosphatidylinositol 4-Phosphate-5 kinase
PKC	Protein kinase C
PLC	Phospholipase C
RasGRP	Ras guanyl-releasing protein
RFP	Red fluorescent protein
RNAseq	RNA (ribonucleic acid) sequencing
RTK	Receptor tyrosine kinase
SAM	Sterile alpha motif
SNI	Spared nerve injury
TRP	Transient receptor potential
TRPV1	Transient receptor potential vanilloid 1
UNC-CH	University of North Carolina at Chapel Hill
UTP	Uridine triphosphate
WT	Wild type (mice)

CHAPTER 1: INTRODUCTION TO DIACYLGLYCEROL KINASES (DGKs)

DGK is an important regulator of lipid signaling

Diacylglycerol kinase (DGK) plays an important role in mammalian physiology by altering the activity of the substrate diacylglycerol (DAG) and other effectors that control cellular functions [1-3]. Stimulation of G-protein-coupled receptors (GPCRs) and receptor tyrosine kinases (RTKs) leads to activation of phospholipase C (PLC), which cleaves PIP_2 to produce DAG. DGK phosphorylates DAG, converting it into phosphatidic acid (PA). Both DAG and PA affect the activity of a number of downstream targets [4]. For example, DAG's effectors include C1-domain-containing proteins (e.g. PKC [5] and chimaerins [6]) and TRPV1 [7], and PA's effectors include PIP5K [8] and mTOR [9]. By regulating the balance between two important lipid signaling mediators, DGK is poised to impart a large effect on multiple signaling cascades, with major implications for mammalian biology. Kinases represent the largest class of druggable targets in the human genome [10, 11]. Therefore, defining how phosphorylation of DAG regulates lipid levels, modulates cell signaling, and alters physiology may reveal an attractive candidate for pharmacological treatments.

DGK represents a diverse family of enzymes

There are ten different DGK genes in the murine and human genomes [1]. All have C1 domains and catalytic domains, although for some the catalytic region is split in two. Each DGK also has unique motifs, such as calcium-binding EF-hands or phosphoinositide-binding pleckstrin homology (PH) domains. Many of the DGK genes have alternative splice variants, creating additional diversity in this group of enzymes [4]. Variations in structure govern the

subcellular localization of DGK, the effect the DGK has on signaling, and how the function of the DGK can be regulated [2, 4]. DGK isoforms also have variations in their tissue distribution [3]. They are found in most tissues in the body, where they contribute to normal functions. Many tissues also have upregulated *DGK* expression in pathological conditions, such as cancer.

The unique domain structures and diverse tissue distribution enable DGKs to regulate several aspects of mammalian physiology. *Dgka* (alpha) and *Dgkz* (zeta) regulate immune function through their expression in T lymphocytes, promoting T cell anergy [12-16]. *Dgke* (epsilon) and *Dgkz* in cardiomyocytes are both protective against cardiac hypertrophy and dysfunction [17, 18]. A majority of research on DGK isoforms has focused on their role in different forms of cancer. *DGKA*, *DGKD* (delta), or *DGKH* (eta) depletion reduced growth in lung cancer cells [19-21], and reducing *DGKZ* expression attenuated invasiveness of colon, prostate, and breast cancer cells [22]. *DGKA* or *Dgki* (iota) depletion inhibited skin tumor growth [19, 23]. Additionally, epigenetic silencing of *DGKG* (gamma) is increased in colorectal cancer cells [24].

DGK regulates neuronal functions

All ten mammalian *Dgk* genes are expressed in the brain, each with a distinct regional expression pattern [25, 26]. Many have been implicated in the regulation of neuron physiology and mouse behavior [25-28]. *Dgkb* (beta) deletion and *Dgkz* knockdown were found to reduce spine formation and maintenance, respectively, and *Dgkk* (kappa) knockdown reduced spine maturation and stability [29-31]. *Dgkb*, *Dgkz*, *Dgki*, and *Dgkk* have all been shown to regulate synaptic plasticity [31-34]. Alterations in *Dgkb*, *Dgkz*, *Dgke*, or *Dgkk* coincided with differences in lipid levels in various neuronal tissues [31, 34-36]. On the behavioral level, seizure susceptibility was enhanced by *Dgkd* knockdown and *Dgkb* knockout [37, 38] and reduced by *Dgke* loss [35]. *Dgkb*$^{-/-}$ and *Dgkh*$^{-/-}$ male mice showed neurological phenotypes including hyperactivity and reduced depression [29, 39], while *Dgkk*-deficient mice showed Fragile X

syndrome-like social deficits and stereotypic behaviors [31]. Therefore, changing the balance of lipids in this network by targeting various *Dgk* genes appears to influence neurophysiology.

Dgki **(iota) and** ***Dgkh*** **(eta)**

The work presented in this dissertation focuses on the iota and eta isoforms of DGK (*Dgki* and *Dgkh*), which are primarily expressed in neuronal tissues (data presented in Chapter 2). These isoforms piqued our interest due to their high expression in dorsal root ganglia (DRG), a sensory organ relevant to our lab's work on itch and pain physiology. *Dgki* and *Dgkh* are also expressed in the brain, and *DGKH* and *DGKI* have been linked to mental and cognitive disorders, including schizophrenia, bipolar disorder, depression, and attention deficit hyperactivity disorder [40-44]. However, little was known about how they contribute to disease or even how they regulate neuronal function. Through this research we have developed a better understanding of the molecular functions of *Dgki* and *Dgkh* and have demonstrated the role of *Dgki* and *Dgkh* in behaviors associated with the neuronal tissues in which they are expressed.

CHAPTER 2: CHARACTERIZATION OF DGKI AND DGKH MOLECULAR FUNCTION AND KNOCKOUT MOUSE DEVELOPMENT

INTRODUCTION

DGKs have diverse signaling functions

As a result of their diversity in structure, DGK isoforms affect signaling in many different ways. DGKs largely affect signaling by metabolizing DAG, decreasing its signaling. DAG produced downstream of $G\alpha_q$-protein-coupled receptor ($G\alpha_q$-GPCR) or RTK activation activates protein kinase C (PKC) [5]. By decreasing DAG signaling, DGK can attenuate PKC activity, which in turn can alter the PKC-dependent functions downstream of both $G\alpha_q$-GPCRs and RTKs. For example, overexpressing *Dgke*, *Dgkz*, or *Dgkh* decreased $G\alpha_q$-GPCR-stimulated PKC activity [17, 18, 45]. Similarly, PKC activity and phosphorylation and inactivation of EGFR were decreased by *DGKQ* (theta) expression and increased by *Dgkd* loss [46, 47].

In addition to affecting downstream activation of PKC by DAG, DGKs can directly interact with non-lipid signaling molecules, including Ras GTPases and their regulators. *DGKH* facilitated C-Raf/B-Raf heterodimerization to enhance EGF-stimulated ERK signaling in HeLa cells [48]. *DGKG* interacted with β2-chimaerin, enhancing its activation and its suppression of Rac1 induced by EGF in fibroblasts [49], whereas *DGKZ* interacted with active Rac1 itself in a neuroblastoma cell line [50]. *Dgka* and *Dgkz* inhibited RasGRP1, leading to decreased Ras signaling in T cells [12-16], whereas *Dgki* inhibited RasGRP3, leading to increased Ras signaling (via Rap1 inhibition) in fibroblasts [23].

All of these modifications in signaling lead to changes in cellular function. Therefore, we aimed to characterize the molecular functions of *Dgki* and *Dgkh* in order to understand how they might affect the cellular functions of the tissues in which they are expressed. Previously, we

found that *Dgkh* enhances $G\alpha_q$-GPCR signaling in a PKC-dependent fashion [45]. Through the work presented in this chapter, we determined how *Dgki* affects GPCR signaling, investigated the substrate-specific kinase functions of *Dgki* and *Dgkh*, and developed tools to study these two kinases *in vivo*.

RESULTS

Dgki and *Dgkh* enhance $G\alpha_q$-GPCR-stimulated calcium activity

The cleavage of PIP_2 after receptor-mediated PLC activation produces IP_3 and DAG. IP_3 induces the release of calcium from intracellular stores. The degree to which receptor activation affects signaling within a cell can be measured by monitoring calcium activity following receptor stimulation. By overexpressing *Dgkh* in HEK293 cells and stimulating GPCR activity, we previously found that *Dgkh* prolongs GPCR signaling by decreasing the activation of PKC by DAG. This, in turn, diminishes the rate at which PKC phosphorylates and desensitizes the receptor [45]. We also demonstrated that *Dgki* enhances GPCR-stimulated calcium activity to the same degree as *Dgkh* in this HEK293 cell paradigm (Figure 2.1).

Dgki and *Dgkh* phosphorylate multiple acylglycerol substrates

Because *Dgki* and *Dgkh* are expressed in many of the same tissues despite their redundant functions as diacylglycerol kinases, we explored the possibility that they might differ in their substrate preferences (i.e. one *Dgk* could prefer DAG species with saturated fatty acid chains, while the other prefers unsaturated). There is precedence for this, as *DGKE* shows stearoyl arachidonoyl substrate specificity [51]. Activation of effectors of DAG, such as PKC, depends on the acyl chain composition of DAG [52, 53]. Therefore, the substrate specificity of a *Dgk* isoform could have major implications for which signaling pathways *Dgki* and *Dgkh* may regulate.

To characterize the degree to which these DGKs phosphorylate various substrates, we utilize a radioactivity-based kinase activity assay [45]. In this assay, protein lysates from HEK293 cells transfected with one of five constructs (RFP-*Dgki* or RFP-*Dgkh*; the kinase-dead version of either enzyme, RFP-*Dgki* G431D or RFP-*Dgkh* G389D; or an RFP control) were combined in a reaction with ATP labeled with ^{32}P in the gamma phosphate, and the amount of ^{32}P-labeled product was measured (Figure 2.2A). The phosphorylation of each substrate by lysates expressing RFP-*Dgki* or RFP-*Dgki* G431D (Figure 2.2B) or RFP-*Dgkh* or RFP-*Dgkh* G389D (Figure 2.2C) was normalized to the phosphorylation of that substrate by RFP. Statistical significance was then tested between RFP-*Dgki* and RFP-*Dgki* G431D and between RFP-*Dgkh* and RFP-*Dgkh* G389D.

We used four different biologically-relevant DAG substrates that varied in acyl chain length and degree of saturation, including 16:0-18:1 (1-palmitoyl-2-oleoyl-glycerol), 18:1-18:1 (1,2-dioleoyl-glycerol), 18:0-20:4 (1-stearoyl-2-arachidonoyl-glycerol), and 18:0-22:6 (1-stearoyl-2-docosahexaenoyl-glycerol) [54]. Both *Dgki* and *Dgkh* showed significantly more phosphorylation of one or more DAG species than their kinase-dead counterparts (Figure 2.2B-C; 1,2-DAG). We found that *Dgki* showed greater kinase activity than *Dgkh* on all DAGs tested. All five constructs were tested simultaneously, so the responses of *Dgki* and *Dgkh* can be compared, even though they are shown on different graphs.

While exploring substrate differences between *Dgki* and *Dgkh*, our attention turned to monoacylglycerol (MAG) as potential substrates. Monoacylglycerol kinases were purified from swine and bovine brains [55, 56], but there has been no further characterization of these kinases in nearly 30 years. Both MAGs and DAGs have fatty acid acyl chains, which DGKs bind to, and are phosphorylated at the 3rd position in glycerol to yield lysophosphatidic acid (LPA) and PA, respectively (Figure 2.2A). We hypothesized that *Dgki* and *Dgkh* could serve as kinases for MAGs. Using MAG substrates with different acyl chain position on glycerol (2nd or 1st

position in glycerol) or composition (oleoyl [18:1] or arachidonoyl [20:4]), we found that *Dgki* and *Dgkh* could both use MAG as a kinase substrate (Figure 2.2B-C).

Deletion of *Dgki* and/or *Dgkh* in mice disrupts DGKI and/or DGKH expression in neuronal tissues

Genetically-engineered mice lacking expression of *Dgki* and/or *Dgkh* are valuable tools we used to determine how these lipid kinases modulate various signaling pathways and how that may translate to differences in pruriception, nociception, and psychopathological behaviors.

A *Dgki*-knockout mouse was developed by another team of researchers [23]. They found that *Dgki* normally enhances Ras activation, and in the absence of *Dgki*, Ras signaling is reduced. Activation of the Ras-Raf-MEK-ERK pathway is a mediator of receptor tyrosine kinase signaling in nociceptive neurons, leading to their sensitization [57]. Other scientists demonstrated that metabotropic glutamate receptor-dependent long-term depression (mGluR-LTD) was dampened in hippocampal slices from neonatal (two weeks post-birth) *Dgki*$^{-/-}$ mice [32]. This impaired mGluR-LTD was dependent on increased PKC activation. This effect on signaling mediated by a $G\alpha_q$-GPCR holds promise for the hope of inhibiting *Dgki* to attenuate GPCR activity. Despite this *in vitro* phenotype, the only behavioral difference observed was a slight latency to habituate to a novel environment. They found no change in learning, anxiety, or motor behaviors. The lack of an overt phenotype makes this mouse an attractive model for studying pain sensitivity, as some of the behaviors that could possibly confound the results if aberrant are shown to be normal in these mice.

We acquired sperm from the *Dgki*$^{-/-}$ mice and generated mice using *in vitro* fertilization in collaboration with the Mutant Mouse Regional Resource Core at the University of North Carolina at Chapel Hill (UNC-CH). The mice were on a mixed background of C57BL/6 and 129; to correct for any background-strain-dependent effects, we backcrossed these mice to C57BL/6 for 5

generations. We confirmed absence of DGKI protein in the DRG, spinal cord, and brain of male and female mice (Figure 2.3).

We generated a *Dgkh*-knockout mice using CRISPR-Cas9 technology [58] in collaboration with the Animal Models Core at UNC-CH. A guide RNA was designed to insert a three-frame stop cassette into exon 9 (Figure 2.4A-B). We targeted exon 9 to prevent any portion of the first catalytic domain from being produced, while attempting to avoid having potential translational start sites between the inserted stop cassette and the catalytic domain to cause disruption of all known transcripts of *Dgkh*. In the founder mice produced from microinjections of the guide RNA, the mutant *Dgkh* alleles were cloned and sequenced to demonstrate successful integration of the stop cassette in exon 9 (Figure 2.4C). The genotypes of the *Dgkh* mutant mice were confirmed using PCR amplification of the *Dgkh* allele and digestion with KpnI (Figure 2.4D). We confirmed the absence of DGKH protein in DRG, spinal cord, and cortex tissue in male and female $Dgkh^{-/-}$ mice (Figure 2.4).

To address the potential for compensations in *Dgki* and *Dgkh* expression, we examined protein levels of DGKH in WT and $Dgki^{-/-}$ mice and protein levels of DGKI in WT and $Dgkh^{-/-}$ mice. We found no differences in protein levels between mouse lines in DRG, spinal cord, or cortex tissue (Figure 2.5). Therefore, neither DGKI nor DGKH expression increases in the absence of the other.

To account for the potential of redundancy in *Dgki* and *Dgkh* functions *in vivo*, we crossed the $Dgki^{-/-}$ and $Dgkh^{-/-}$ mice to generate a double knockout (dKO) mouse. We also confirmed absence of DGKI and DGKH in various neuronal tissues of these mice (Figure 2.6).

DISCUSSION

The *in vitro* analyses using HEK293 cells overexpressing *Dgki* and *Dgkh* provided valuable insight into the molecular functions of these enzymes. We found that both *Dgki* and *Dgkh* enhance $G\alpha_q$-GPCR-stimulated calcium signaling. Additionally, we showed that *Dgki* and

Dgkh phosphorylate both DAG and MAG lipids. Finally, we developed *Dgki*$^{-/-}$, *Dgkh*$^{-/-}$, and dKO mice that enabled us to study these kinases on the cellular and behavioral levels, as presented in subsequent chapters.

Kinase function vs. signaling function

We have demonstrated that *Dgki* and *Dgkh* are effective kinases for multiple acylglycerol substrates, and both kinases are able to enhance $G\alpha_q$-GPCR signaling. Our lab previously showed that *Dgkh*'s kinase function was required for the increased calcium activity post-$G\alpha_q$-GPCR stimulation [45]. Interestingly, the kinase assay experiments presented here showed that *Dgki* was a stronger kinase than *Dgkh* for all substrates tested, however the effect on $G\alpha_q$-GPCR calcium signaling was similar between *Dgki*- and *Dgkh*-overexpressing cells. Thus, the kinase function may not represent all of the roles *Dgki* or *Dgkh* play in modulating GPCR signaling. Indeed, others found that a kinase-dead mutant of *DGKH* enhanced EGF-induced ERK signaling by acting as a substrate for B-Raf and C-Raf [48]. This dual functioning of *Dgkh* as both a diacylglycerol kinase and a substrate is not uncommon for this kinase family. For example, *Dgkg* prevents lamellipodia formation in a kinase-dependent fashion [49, 59] but enhances filopodia-like process formation in kinase-independent fashion [59]. Therefore, the kinase function or substrate function of *Dgki* and *Dgkh* may both be important factors in regulating cellular functions.

Kinase function is dependent on cellular environment

Others have recently shown that *DGK* isoforms overexpressed in COS-7 cells can phosphorylate MAG [60]. However, they found that kinase activity on MAG substrates by *DGKH* was only about 8% of the kinase activity on DAG substrates, and *DGKI* had no MAG kinase activity at all. While the use of mouse vs. human *Dgk* constructs likely contributed to differences in our results, it may also be the case that *Dgk* kinase function is highly dependent on the

cellular environment. Indeed, some *Dgk* isoforms have shown very different functions in different tissues, and even affect the same signaling pathway in opposite directions in different tissues. For example, even though they inhibit Ras activity in T cells [12, 13, 15], *Dgka* and *Dgkz* enhance Ras-Raf-MEK-ERK signaling in liver cancer [19] or heart cells [17], respectively. This suggests that in order to analyze the most important functions of *Dgki* and *Dgkh*, they need to be analyzed *in situ*, in the tissues in which they are expressed. The knockout mice provided a tool to study these kinases in the tissues in which they are endogenously expressed, both looking at the *in vitro* function of these tissues and analyzing the behaviors associated with the neuronal tissues in which they are expressed.

METHODS

Molecular biology

The mouse *Dgkh* and *Dgkh* G389D constructs in the pcDNA3.1(+) vector with N-terminal red fluorescent protein (RFP) tags described in [45] were used in this study. The mouse *Dgki* was generated by JrGang Cheng in the pcDNA3.1(+) vector with an N-terminal RFP tag, based on Gene ID 320127. The RFP-*Dgki* G431D mutant was generated with polymerase chain reaction (PCR)-directed mutagenesis.

HEK293 cell culture

HEK293 cell culturing, plating, and transfection were performed similar to [45]. HEK293 cells were cultured in Dulbecco's modified Eagle's medium (DMEM, 11995-065, Gibco, Grand Island, New York) supplemented with 10% fetal bovine serum (10437-010, Gibco) and 100 U/mL penicillin/streptomycin (15140, Gibco). For calcium imaging assays, glass-bottom MatTek dishes (product info, MatTek Corporation, Ashland, Massachusetts) were plated with 300,000 cells each. For kinase activity assays, 6-well plates (Corning, Corning, New York) were plated with 450,000 cells each. The glass bottoms of the MatTek dishes and the bottoms of the 6-well

plates were precoated with 1 mg/mL poly-D-lysine (P7886, Sigma, St. Louis, Missouri). The following day, each dish or well of HEK293 cells was transfected with 500 ng of RFP, RFP-*Dgki*, RFP-*Dgki* G431D, RFP-*Dgkh*, or RFP-*Dgkh* G389D and 500 ng of pcDNA3.1(+) using Lipofectamine (18324012, Invitrogen, Carlsbad, California) with Plus Reagent (11514015, Invitrogen) in DMEM supplemented with antibiotics for 4 hours. Transfection medium was then replaced with DMEM supplemented with serum and antibiotics. Cells were kept a 37°C incubator with 5% CO_2 and used for assays within 24 hours.

HEK293 calcium imaging

Similar to previous work [45], on the day of imaging cells were washed 2 times with assay buffer: Hanks' balanced salt solution (14025-126, Gibco; 140 mg/L $CaCl_2$, 100 mg/L $MgCl_2$-$6H_2O$, 100 mg/L $MgSO_4$-$7H_2O$, 400 mg/L KCl, 60 mg/L KH_2PO_4, 350 mg/L $NaHCO_3$, 8 g/L NaCl, 48 mg/L Na_2HPO_4, 1 g/L D-glucose) supplemented with 2.4 g/L HEPES, 2 g/L D-glucose, and 0.1% w/v fatty acid–free BSA (A6003, Sigma), at pH 7.3. Cell were then incubated with 2 μM Fura-2, AM (F1221, Invitrogen) in 0.02% Pluronic F-127 (P-3000MP, Invitrogen) in assay buffer for 1 h at room temperature (approximately 23°C). Cells were washed 3 times with assay buffer, then maintained at room temperature for 30 min before imaging.

Assays were performed on an Eclipse Ti microscope (Nikon, Tokyo, Japan) with a CFI Plan Fluor 20x objective (Nikon) and a DG-4 light source (Sutter, Novato, California). To image Fura-2, cells were alternately excited for 500 ms at 340 nm and for 250 ms at 380 nm, and emission was measured at 510 nm. Cells were recorded using a Clara DR-328G-C01-SIL CCD camera (Andor, Belfast, United Kingdon) and NIS Elements imaging software (Nikon).

Assay buffer was changed directly before imaging. An image was taken in the RFP channel to identify which cells were expressing the RFP-tagged construct. Baseline Fura-2 ratios were collected for 40 s, then assay buffer was removed an agonist was added manually

as quickly as possible. Imaging continued for 3 min. The agonist used was 10 μM carbamoylcholine chloride (carbachol; C4382, Sigma) in assay buffer.

For analysis, we calculated the Fura-2 ratio (ratio of the emission following excitation at 340 nm/380 nm) for all cells that had RFP expression. We excluded cells that had high baseline Fura-2 ratios (>0.6) or failed to respond to agonist (did not reach ratio of at least 0.8 during carbachol exposure). To normalize to baseline, the 30 s of Fura-2 ratios measured immediately preceding agonist exposure were averaged for a given cell, and that average was subtracted from each data point for that cell throughout the whole assay period. Area-under-the-curve (AUC) values were calculated on a cell-by-cell basis, using the baseline-normalized values, for the 3-min period of agonist exposure. RFP-transfected HEK293 cells were tested each day, along with HEK293 cells transfected with RFP-*Dgki* and/or RFP-*Dgkh*, alternating dishes in a random order. The data presented here included the responses of 104 RFP-transfected cells, 85 RFP-*Dgki*-transfected cells, and 67 RFP-*Dgkh*-transfected cells.

HEK293 kinase activity assay

Kinase activity was measured similar to previous work [45]. HEK293 cells plated into 6-well plates and transfected with one of five constructs (RFP-*Dgki*; RFP-*Dgkh*; the kinase-dead version of either enzyme, RFP-*Dgki* G431D or RFP-*Dgkh* G389D; or an RFP control) were washed with ice-cold PBS. We then added 200 μL of kinase assay lysis buffer (50 mM Tris pH 7.4, 150 mM NaCl, 1 mM EDTA pH 8.0, 1% v/v Triton-X100, 1 mM phenylmethanesulfonyl fluoride, 1 mM sodium deoxycholate, 1× cOmplete Mini EDTA-free Protease Inhibitor Cocktail [4693159001, Roche, Basel, Switzerland], 1x phosphatase inhibitor cocktail 2 [P5726, Sigma]) to each well. After 10 min on ice, cells were scraped into lysis buffer and transferred to a microcentrifuge tube. Following sonication on ice for 10 s, lysates were centrifuged at 10,000 × g at 4°C for 10 min to separate the debris. Lysates were kept on ice (never frozen) until use in the kinase activity assay the same day.

The diacylglycerol substrates used were 1-palmitoyl-2-oleoyl-glycerol (16:0-18:1; 800815C, Avanti Polar Lipids, Alabaster, Alabama), 1,2-dioleoyl-glycerol (18:1-18:1; 800811C, Avanti), 1-stearoyl-2-arachidonoyl-glycerol (18:0-20:4; 800818C, Avanti), and 1-stearoyl-2-docosahexaenoyl-glycerol (18:0-22:6; 800819C, Avanti). The monoacylglycerol substrates used were 1-oleoyl-glycerol (18:1; M7765, Sigma), 2-oleoyl-glycerol (18:1; M2787, Sigma), and 2-arachidonoyl-glycerol (20:4; 870450O, Avanti). Lipids in chloroform were transferred to a glass tube, and the chloroform was evaporated under a gentle stream of nitrogen gas. Lipids were resuspended in sodium deoxycholate and mixed with kinase assay buffer. The final concentrations of the components of the kinase assay buffer were: 50 mM Tris-HCl pH 7.4, 100 mM NaCl, 20 mM NaF, 10 mM $MgCl_2$, 1 mM DTT, 1 mM EDTA, and 1 mM sodium deoxycholate. Each 50-µL reaction had 10 µL of cell lysate, 25 nmol of lipid, and 1 mM ATP (50 uCi [γ-^{32}P]-ATP; NEG035C005MC, Perkin Elmer, Waltham, Massachusetts). The reaction was initiated by addition of lysate. After 10 min at 30°C, the reaction was stopped by adding 25 µL of 12 N HCl then 750 µL butanol-saturated water.

Lipid extraction was performed by mixing 500 µL butanol into the sample and spinning at 1,000 × g at room temperature for 5 min. 425 µL of the upper organic phase was washed with 500 µL butanol-saturated water. Following another spin, 300 µL of the organic phase was again washed with 500 µL of butanol saturated-water. Following a final spin, 250 µL of the organic phase was mixed with 2 ml of ScintiSafe Econo 2 scintillation fluid (SX21-5, Thermo Fisher Scientific, Waltham, Massachusetts) in a scintillation vial (03-341-72A, Thermo Fisher) and counted on a Wallac Rackbeta 1209 liquid scintillation counter (LKB Instruments, Mount Waverley, Victoria, Australia) with counts per minute (CPM) as the readout.

After performing the kinase assay, the lysates were run on a western stained for RFP and β-actin. Blotting for RFP confirmed expression of the transfected construct. Blotting for β-actin allowed us to determine the relative protein concentration in each sample. All samples tested on a given day were run on the same western; the intensity of the ACTB band for each

sample was quantified using ImageJ image analysis software (NIH, Bethesda, MD), and the intensity relative to RFP's ACTB band was calculated. The CPM of each sample was normalized to the relative ACTB intensity of that sample, as a way of normalizing to protein level of the sample. For data analysis, the phosphorylation of each substrate by lysates expressing RFP-*Dgk* constructs was normalized to the phosphorylation of that substrate by RFP. Statistical significance was then tested between RFP-*Dgki* and RFP-*Dgki* G431D and between RFP-*Dgkh* and RFP-*Dgkh* G389D. All five constructs were tested in each experiment (although different lipid species were tested each day), so the responses of *Dgki* and *Dgkh* can be compared, even though they are shown on different graphs.

Mice

All procedures used in this study were approved by the Institutional Animal Care and Use Committee at the University of North Carolina at Chapel Hill. Mice were maintained on a 12 h:12 h light:dark cycle and given food (Teklad 2020X, Envigo, Huntingdon, United Kingdom) and water *ad libitum.* Mice were group housed with 3 to 5 mice per cage. Cages had Bed-o'Cobs bedding (Andersons Lab Bedding, Maumee, Ohio). Modifications in housing and bedding and specific methods related to mating and behavior are presented in the subsequent chapters. Because of the deficits in maternal care by dKO dams (discussed in Chapter 4), all dKO mice used in behavioral studies were raised by WT foster moms.

***Dgki*-knockout mice**

We acquired a *Dgki*$^{-/-}$ mouse line described previously [23], which was on a mixed 129 and C57BL/6 background. All data presented here from both the *Dgki*$^{-/-}$ and dKO lines were from mice that were backcrossed with C57BL/6J mice for at least five generations.

Dgkh-knockout mice

We generated a *Dgkh*-knockout mouse using CRISPR/Cas9 technology [58]. To arrest translation at the start of the first catalytic domain of DGKH, we designed a guide RNA (GTGTTCGTCAACTCTAAGAGTGG) and a homology-directed repair donor template (TTTCGTTCTGTGTCAGCCCCCTCTTGGTGTTCGTCAACTCTAA**ATAAAGGTACCTAGGATA AATA**GAGTGGAGATAATCAGGGAGTGAAGTTCCTTCGTCGCTTTAAA) to insert a three-frame stop cassette (bold) and *KpnI* site (bold underlined) in exon 9 of *Dgkh*. Pronuclear injections of the guide RNA and donor template produced founder mice from which we cloned and sequenced *Dgkh* alleles to demonstrate successful integration of the stop cassette. *Dgkh*$^{-/-}$ mice present no gross anatomical or overt motor phenotypes.

Genotyping

We performed PCR with genomic DNA isolated from tail clips to confirm genotypes of our mice. A region of *Dgkh* containing exon 9 was amplified using primers 5'-GCAGATACTGAACCGTTTAGCCAG-3' and 5'-CGCATGAGAGCAACAAAGATGTC-3', on a PCR cycle that consisted of 35 rounds of 15 s of denaturing at 95°C, 15 s of annealing at 55°C, and 60 s of extending at 72°C. The products of this reaction were PCR purified and digested with *KpnI* (R0142, New England BioLabs, Ipswich, Massachusetts). *Dgki* was analyzed as described previously [23]. A forward primer of 5'- AGGATGGTCCAGGAATGGCTTC -3' was combined with reverse primers 5'-AGGTGAGTGAGGCCAACTAGGC-3' (to amplify WT *Dgki*) and 5'-GAGGGAAGCGTCTACCTACTGG -3' (to amplify mutant *Dgki*). The PCR cycle consisted of 35 rounds of 30 s of denaturing at 95°C, 90 s of annealing at 65°C, and 90 s of extending at 72°C. *KpnI*-digested *Dgkh* PCR products and *Dgki* PCR products were run on 2% agarose gels containing SybrSafe (S33102, Invitrogen).

Neuronal tissue protein isolation

Frontal cortex, spinal cord, and DRG tissue was dissected (in that order) from 4-week-old WT and *Dgki*$^{-/-}$ male and female mice, 2- to 3-month-old WT and *Dgkh*$^{-/-}$ male and female mice, and 5-month-old WT and dKO female mice. Tissues were rinsed in ice-cold PBS (9 g/L NaCl, 795 mg/L Na_2HPO_4-$7H_2O$, 144 mg/L KH_2PO_4, pH7.4) then placed in ice-cold lysis buffer (50 mM Tris pH 7.4, 150 mM NaCl, 1 mM EDTA pH 8.0, 1% v/v Triton-X100, 1 mM phenylmethanesulfonyl fluoride, 1 mM sodium deoxycholate, 1× cOmplete Mini EDTA-free Protease Inhibitor Cocktail [4693159001, Roche]) for 10 min. Following sonication on ice for 10 s, lysates were centrifuged at 10,000 × g at 4°C for 15 min to separate the debris.

Western blotting

Protein (30 µg) from each lysate was combined with sample buffer (125 mM Tris-HCl pH 6.8, 40% v/v glycerol, 2% v/v SDS, 0.02% w/v bromophenol blue 10%, v/v β-mercaptoethanol [161-0710, Bio-Rad, Hercules, California]) and separated on a 4-20% SDS/PAGE gel (456-1094, Bio-Rad) in a running buffer of 25 mM Tris, 192 mM glycine, 1% v/v SDS, pH 8.3. Protein was then transferred to a 0.2 µm nitrocellulose membrane (1620095, Bio-Rad) in a transfer buffer of 25 mM Tris, 192 mM glycine, 20% v/v methanol, pH 8.3. Following 1 h of blocking in a solution of 5% w/v milk (170-6404, Bio-Rad) in tris-buffered saline with Tween 20 (TBST; 100 mM Tris pH 7.5, 165 mM NaCl, 0.1% v/v Tween 20) at room temperature, membranes were incubated overnight at 4°C with primary antibodies (details below) in a solution of 5% w/v bovine serum albumin (BSA; A3912, Sigma) in TBST. Blots were probed with secondary antibodies of 1:10,000 IRDye 680RD-conjugated goat anti-mouse (925-68070, LI-COR Biosciences, Lincoln, Nebraska) and 1:10,000 IRDye 800RD-conjugated donkey anti-rabbit (926-32213, LI-COR) in 5% w/v milk in TBST for 2 h at room temperature. Blots were washed with TBST between each step. Blots were imaged on a LI-COR Odyssey system.

The primary antibodies used for the HEK293 kinase activity assay were for β-actin (1:3,000 mouse anti-ACTB, ab6276, Abcam, Cambridge, United Kingdom) and RFP (1:3,000 rabbit anti-RFP, R10367, Invitrogen). The primary antibodies used to validate the *Dgki*$^{-/-}$ and *Dgkh*$^{-/-}$ mice were for β-actin (1:3,000 mouse anti-ACTB, ab6276, Abcam) and either DGKH (1:1,000 rabbit anti-DGKH, HPA040355, Sigma) or DGKI (1:1,000 rabbit anti-DGKI, LS-C118721, Lifespan Biosciences, Seattle, Washington) in a solution of 5% w/v bovine serum albumin (A3912, Sigma) in TBST.

Statistics

Data were analyzed with Prism version 7.04 (GraphPad Software Inc., La Jolla, California). Two-tailed t-tests with Welch's correction were used to test for significance for all comparisons in this chapter: AUC of carbachol-induced calcium responses of HEK293 cells overexpressing RFP-*Dgki* or RFP-*Dgkh* versus cells overexpressing RFP; normalized CPM values of HEK293 cells overexpressing RFP-*Dgki* or RFP-*Dgkh* versus cells overexpressing their kinase dead counterparts; levels of DGKH protein in WT versus *Dgki*$^{-/-}$ DRG tissue western blots and levels of DGKI protein in WT versus *Dgkh*$^{-/-}$ tissue western blots.

FIGURES

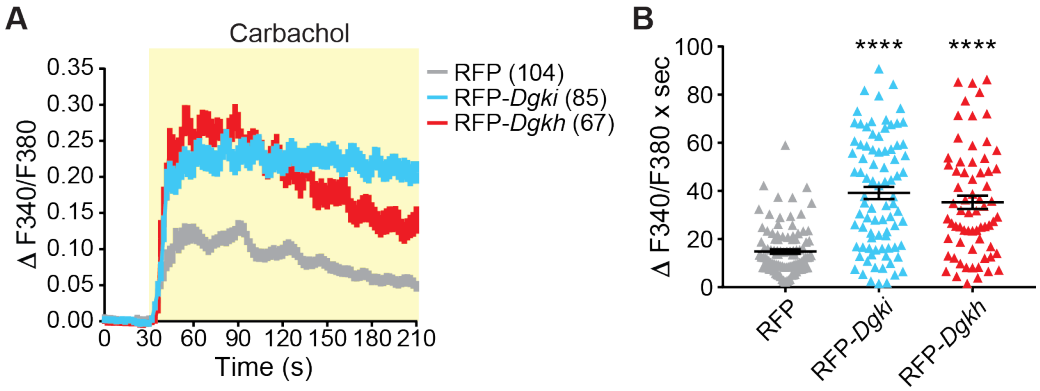

Figure 2.1. Overexpression of *Dgki* and *Dgkh* enhances $G\alpha_q$-GPCR-induced calcium activity. A) Calcium mobilization induced by 10 μm carbachol, a $G\alpha_q$-GPCR agonist, is prolonged by overexpression of RFP-*Dgki* or RFP-*Dgkh* in HEK293 cells. B) Area under the curve (AUC) of responses in (A). Data represent mean ± SEM. ****p<0.0001 vs. RFP.

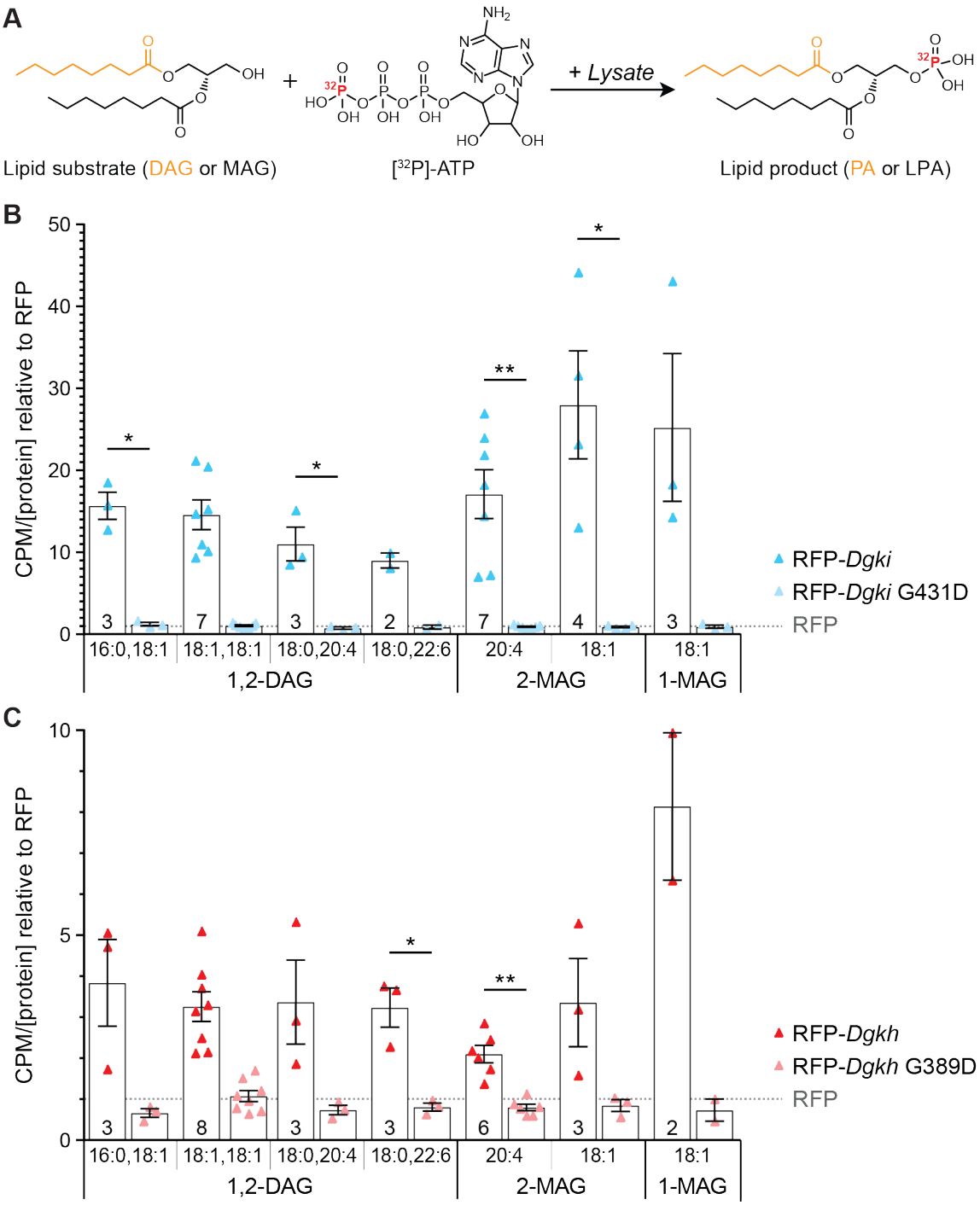

Figure 2.2. *Dgki* and *Dgkh* phosphorylate multiple DAG and MAG substrates. A) A kinase reaction combining an acylglycerol substrate (either DAG, with 2 acyl chains, or MAG, with 1 acyl chain), ^{32}P-labeled ATP, and a cell lysate yielded a lipid (PA from DAG, LPA from MAG) phosphorylated with ^{32}P. B,C) Counts per minute, CPM, of ^{32}P-PA or ^{32}P-LPA produced when the indicated lipid substrates were combined with lysates from HEK293 cells overexpressing RFP-*Dgki* or RFP-*Dgki* G431D (B) or RFP-*Dgkh* or RFP-*Dgkh* G389D (C), relative to the CPM of reactions with lysates from HEK293 cells overexpressing RFP (gray line in B and C). All CPM values were normalized to the protein level of the sample before the relative difference from the

RFP was calculated. Data represent mean ± SEM. Number of samples indicated on graphs; the N for the kinase dead construct for each substrate was the same as the N for the catalytically active construct for that substrate. *$p<0.05$, **$p<0.01$ vs. kinase-dead mutant.

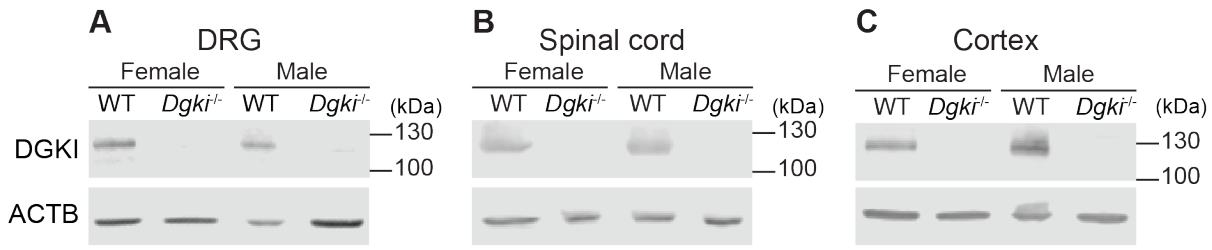

Figure 2.3. Deletion of *Dgki* in mice causes loss of DGKI in neuronal tissues. Immunoblotting with lysates from female and male WT and *Dgki*$^{-/-}$ mouse DRG (A), spinal cord (B), and cortex (C) shows that genetic deletion of *Dgki* eliminates the DGKI protein. ACTB=β-actin.

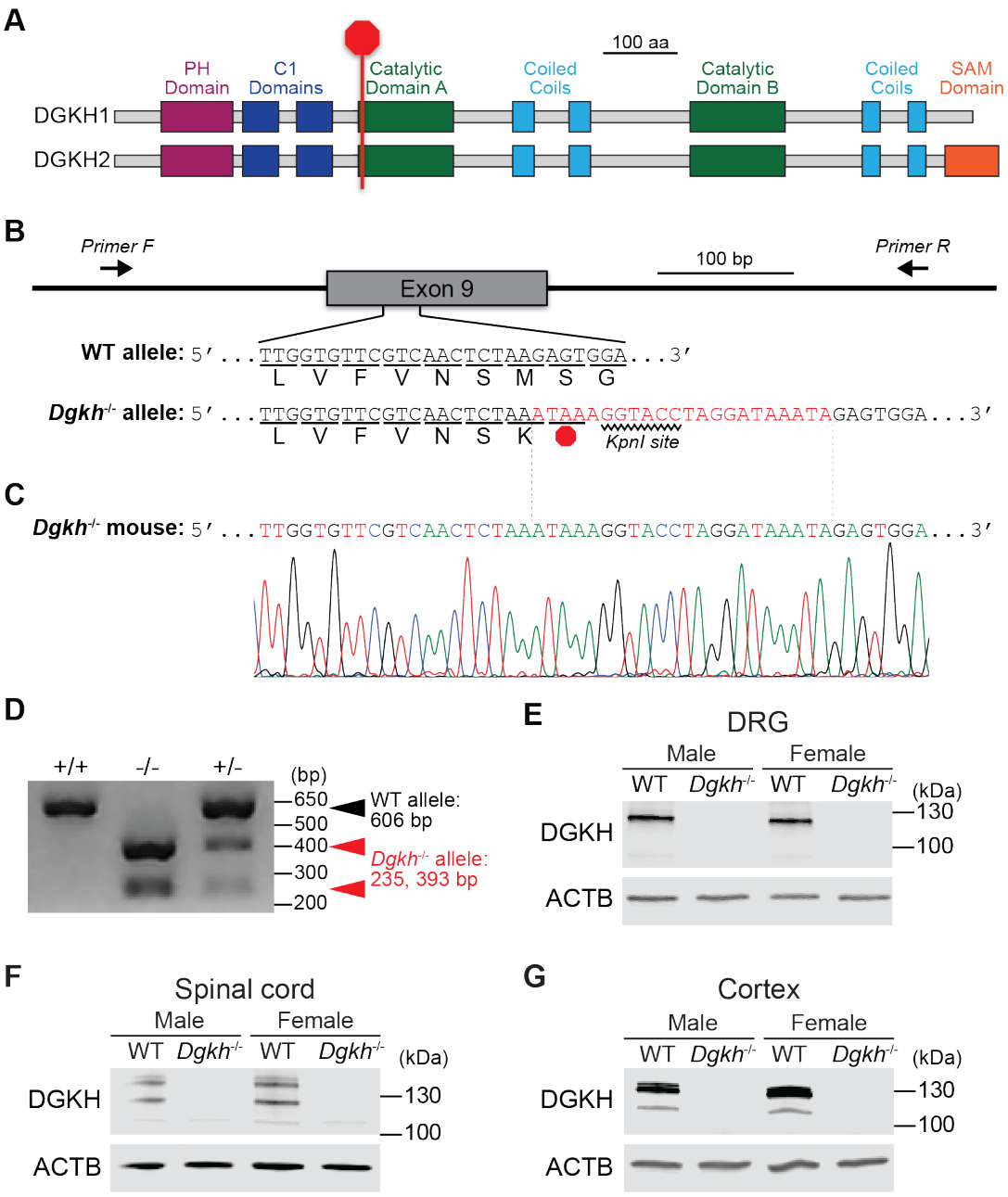

Figure 2.4. Generation of *Dgkh*-knockout mice using CRISPR-Cas9. A) Integration of a STOP cassette arrests translation at the start of the first catalytic domain of DGKH. PH = pleckstrin homology. C1 = cysteine-rich (diacylglycerol-binding). SAM = sterile alpha motif. B) The 22-base-pair cassette (red), containing a STOP codon and *KpnI* restriction site, was inserted into Exon 9 of the *Dgkh* gene, as confirmed by sequencing in (C). D) PCR amplification of tail DNA and digestion with *KpnI*. Without *KpnI* digestion, the amplified fragment from the *Dgkh*$^{-/-}$ allele is 628 bp. E-G) Western blot using 30 µg of protein isolated from DRG (E), spinal cord (F), and cerebral cortices (G) of WT and *Dgkh*$^{-/-}$ male and female mice.

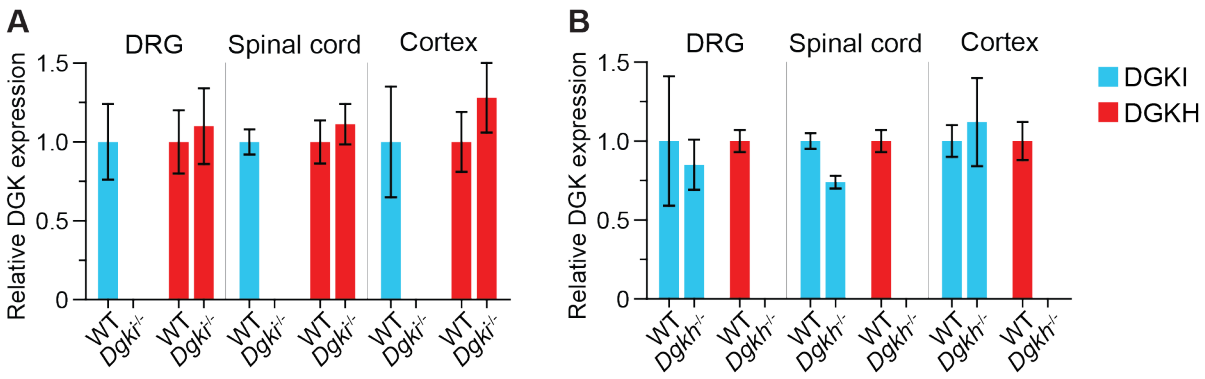

Figure 2.5. Expression of neither DGKI nor DGKH is upregulated in the others' absence. Quantification of western blots of protein from DRG, spinal cord, and cortical tissue demonstrates that DGKH protein levels are equal in WT and *Dgki*$^{-/-}$ tissues (A) and DGKI protein levels are equal in WT and *Dgkh*$^{-/-}$ tissues (B). Data represent mean ± SEM.

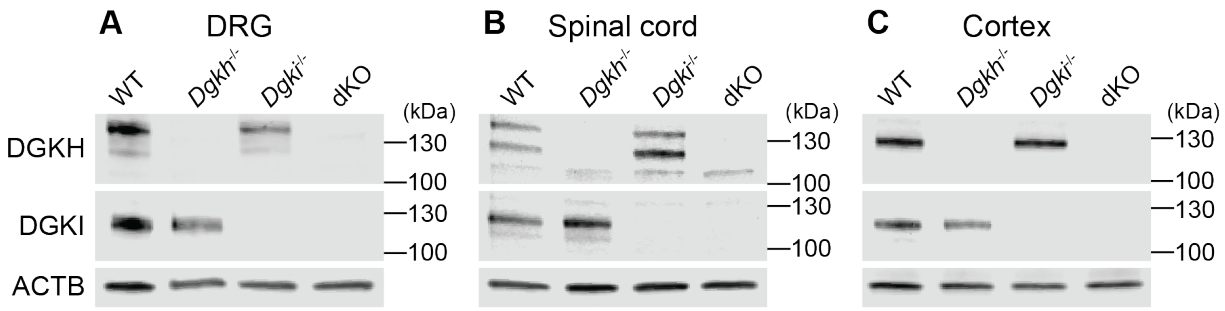

Figure 2.6. Deletion of *Dgki* and *Dgkh* in dKO mice causes loss of both DGKI and DGKH in neuronal tissues. Immunoblotting with lysates from female WT, *Dgki*$^{-/-}$, *Dgkh*$^{-/-}$, and dKO mouse DRG (A), spinal cord (B), and cortex (C) shows that genetic deletion of *Dgki* and/or *Dgkh* eliminates the DGKI and/or DGKH protein, respectively.

CHAPTER 3: DGKI AND DGKH REGULATE HISTAMINE-INDUCED ITCH WITHOUT ALTERING DRG FUNCTION IN MICE

INTRODUCTION

Primary afferent DRG neurons mediate itch and pain sensation and sensitization

The societal burden of chronic pain, which affects nearly one third of American adults, is substantial [61]. The economic impact is estimated to be at $600 billion annually, when accounting for health care costs and lost productivity due to patients' inability to work. Estimates of the consequences of chronic pain on society are likely to be inaccurately low, as pain is a symptom of other chronic diseases, such as ulcerative colitis [62], and frequently predisposes patients to other conditions, such as depression [63]. Medications available to treat chronic pain come with harmful side effects [64] or lack the ability to reduce pain with high efficacy [65]. Similarly, chronic itch (pruritus) is notoriously difficult to manage, often causing patients to develop skin lesions from excessive scratching [66]. Antihistamines comprise the majority of available itch medications; while effective against allergen-induced itch, they do not treat other pathological itch conditions [67, 68]. Expanding knowledge of nociceptive (pain-sensing) and pruriceptive (itch-sensing) signaling may reveal better targets for future pharmacological therapies.

The primary sensory neurons whose cell bodies cluster in the dorsal root ganglia (DRG) innervate peripheral tissues and send projections to the dorsal horn of the spinal cord, where signals are transmitted to the brain. Pruritogenic (itch-causing) compounds released by immune cells activate itch fibers of the DRG that innervate the skin. While this activation enables recognition of allergens, many patients suffer from aberrant, unprovoked activity of itch fibers, leading to extreme scratching behavior [67]. Similarly, algogenic (pain-causing) compounds

released following nerve or tissue injury can both activate and sensitize peripheral pain fibers of the DRG [69]. This sensitization leads to increased responsiveness to painful stimuli (hyperalgesia) and sensitivity to previously innocuous stimuli (allodynia). Unfortunately, in some cases these neurons remain sensitized even after the injury has healed, or demonstrate this sensitivity without any injury, leaving the patients in a state of chronic pain [70].

DRG neurons are the primary responders to pruritogenic and algogenic stimuli, and their dysfunction contributes to chronic pain and itch. Subsets of itch- and pain-specific DRG neurons and their accompanying molecular markers have been identified [67, 71, 72]. However, despite being distinct sensations, nociceptive and pruriceptive neuron populations widely overlap, and pain and itch activate many of the same receptors [73-75]. Characterizing mechanisms of pain and itch processing in DRG neurons could lead to advancements in understanding and treating both conditions.

DAG and MAG are important signaling lipids in DRG neurons

Algogenic and pruritogenic stimuli induce the release of signaling mediators from immune cells, injured tissue, and primary afferent fibers that contribute towards activating and sensitizing DRG neurons. Algogens commonly activate $G\alpha_q$-GPCRs or transient receptor potential (TRP) channels [69, 76, 77], and many pruritogens activate $G\alpha_q$-GPCRs that signal through TRP channels [68, 78]. Some receptors are involved in both nociception and pruriception, such as TRPV1 (transient receptor potential vanilloid 1), which signals both thermal pain and histamine-dependent itch [75]. Molecules that regulate signaling from these receptors would be compelling new targets for pain and itch medications.

$G\alpha_q$-GPCR activation in DRG neurons produces diacylglycerol (DAG) [77]. Removal of the acyl chain in the *sn*-1 position of DAG produces *sn*-2-monoacylglycerol (MAG) [79]. When the *sn*-2 acyl chain is arachidonoyl, the MAG produced is 2-arachidonoylglycerol (2-AG). DAG and 2-AG are important lipid signaling molecules that can regulate DRG activity (Figure 3.1).

DAG activates PKC [5], which phosphorylates GPCRs and TRP channels linked to itch and pain [45, 80]. Phosphorylation by PKC desensitizes $G\alpha_q$-GPCRs [81], terminating their signaling, but sensitizes TRPV1 [80], lowering its threshold for activation. By regulating the activation of PKC by altering DAG levels, DGK has the potential to modulate activity of many receptor families. Further, both DAG and 2-AG can directly manipulate the activity of receptors themselves. 2-AG is an endogenous agonist for inhibitory cannabinoid receptors (e.g. CB1) [82]. DAG and 2-AG are partial agonists for TRPV1 [7, 83].

Dgki and *Dgkh* may alter itch and/or pain signaling

Decreasing activity of lipases that act on DAG and MAG alters neuronal lipid levels and attenuates pain signaling [84-86]. Therefore, changing the levels of lipids in this network can control somatosensory responses. As shown in the previous chapter (Figure 2.2B-C), DAG and MAG levels can also be altered through phosphorylation by *Dgki* or *Dgkh*, converting them into PA and LPA, respectively, and terminating their signaling. In addition to phosphorylating DAG and MAG, *Dgki* and *Dgkh* interact with mediators of the Ras-Raf-MEK-ERK pathway, modulating the effects of RTK activation [20, 23, 48]. Altering this signaling pathway also affects pain signaling [57]. Therefore, *Dgki* and *Dgkh* have the potential to impact somatosensory signaling by controlling the phosphorylation of DAG and MAG and/or by regulating the function of other signaling mediators in the DRG. Here, we have characterized the roles of *Dgki* and *Dgkh* in DRG function and sensory behavior.

RESULTS

Dgki and *Dgkh* are highly expressed in itch- and pain-sensing DRG neurons

Of the ten mammalian *Dgk* genes [1], *Dgkh*/*DGKH* is one of the most highly expressed in both mouse and human DRG [87]. Additionally, among the tissues that express *Dgkh* and *Dgki* in mice, the neuronal tissue in which they are most highly expressed is the DRG (Table

3.1) [88]. This suggests that these two *Dgk* genes play important roles in regulating the function of peripheral sensory neurons. Whereas others have examined the role of *Dgki* and *Dgkh* in the brain [32, 39], no one has yet looked at the function of either kinase in the DRG.

Single-cell RNA-sequencing of mouse DRG has shown that *Dgki* and *Dgkh* are enriched in the subclasses of DRG neurons that express genes important for pruriception and nociception, whereas *Dgki* and *Dgkh* expression is low in other subclasses, including those expressing genes involved in sensing light touch [89]. DRG neuron subclasses can generally be distinguished based on size; itch- and pain-sensing neuronal cell bodies typically have small diameters [69]. Immunostaining of mouse DRG revealed that DGKI is expressed in small diameter neurons (Figure 3.2A-B). Additionally, DGKI localizes to the cytoplasm, suggesting a role in signaling following receptor activation. *In situ* hybridization demonstrates this same distribution of RNA for each *Dgk* isoform based on cell size (*Dgkh* in Figure 3.2C, *Dgki* in [90]). Others who examined localization of *Dgkb*, *Dgkg*, *Dgke*, *Dgkz*, and *Dgki* in rat DRG likewise found *Dgki* to be the only one with expression specific to the cytoplasm of small-diameter neurons [90]. Taken together, the gene and protein expression data support the hypothesis that *Dgki* and *Dgkh* may mediate signaling involved in pruriception and nociception.

Sensory behavior is disrupted by deletion of *Dgki* and/or *Dgkh* in mice

Using the *Dgki*$^{-/-}$, *Dgkh*$^{-/-}$, and dKO mice presented in the previous chapter, we aimed to determine how *Dgk* lost manifests in altered somatosensory processing *in vivo*. Behavioral assays were used to determine sensitivity to pruritogenic and algogenic stimuli in these mice, relative to wild type (WT) mice. Investigating differences in behavior related to somatosensation helped us understand the potential for *Dgk* modulation as a method for treating itch and pain.

Deletion of *Dgki* and/or *Dgkh* primarily affects scratching responses to histamine

Male and female mice of WT, *Dgki*$^{-/-}$, *Dgkh*$^{-/-}$, and dKO genotypes were assayed for their scratching responses to injections of the pruritogens histamine, chloroquine, or β-alanine. Histamine is released by mast cells after allergen exposure and is a target of many antipruritic drugs [67, 74]. Chloroquine is an anti-malaria drug that causes severe pruritis in black Africans that contributes to low patient compliance [78]. β-alanine is a supplement commonly taken by body builders to regulate muscular pH levels that causes a minor itch side effect [91].

Histamine caused significantly greater scratching responses in both male and female *Dgki*$^{-/-}$ mice relative to their WT counterparts, especially in the first 5 minutes after injection (Figure 3.3A-B). Chloroquine induced slightly more scratching in *Dgki*$^{-/-}$ females than WT females, but did not differentially affect males based on genotype (Figure 3.3C-D). β-alanine elicited scratching behavior equally in *Dgki*$^{-/-}$ and WT animals (Figure 3.3E-F).

Contrary to the effect of *Dgki* loss, *Dgkh* loss caused increased histamine-induced scratching, although the effect was specific to male mice in the first 15 minutes after injection (Figure 3.4A-B). Similar to the effect of *Dgki* loss, *Dgkh* loss caused slightly more scratching in response to chloroquine in female, but not male, mice (Figure 3.4C-D). Additionally, the scratching behavior elicited by β-alanine was unaffected by *Dgkh* expression in male or female mice (Figure 3.4E-F).

Histamine caused significantly greater scratching responses in both male and female dKO mice relative to their WT counterparts, with differences peaking in the first 5 minutes post-injection (Figure 3.5A-B). Neither chloroquine (Figure 3.5C-D) nor β-alanine (Figure 3.5E-F) elicited differential scratching behavior between WT and dKO mice of either sex.

Overall, the greatest differences in *in vivo* pruritogen responses were seen in the *Dgki*$^{-/-}$ and dKO animals' enhanced scratching behavior immediately following histamine injection. Interestingly, the greatest impact of *Dgkh* loss was seen in the males' decreased scratching in

the first 15 minutes following histamine injection. The phenotype of the mice lacking both *Dgki* and *Dgkh* more closely resembled the phenotype of the *Dgki*$^{-/-}$ mice.

Acute pain sensitivity is slightly altered in *Dgkh*$^{-/-}$ and dKO mice

To determine if acute pain was altered in these mice, we tested responses to thermal and mechanical stimuli applied to the tail (Figure 3.6A-D, Figure 3.7A-D, Figure 3.8A-D) and the hindpaw (Figure 3.6E-G, Figure 3.7E-G, Figure 3.8E-G) of WT, *Dgki*$^{-/-}$, *Dgkh*$^{-/-}$, and dKO male and female mice. To examine thermal sensitivity in the tail, we measured the latency for a mouse to flick its tail after immersing it in a 75% ethanol solution cooled to -10°C [92] or a water bath heated to 46.5°C or 49°C [93]. To examine thermal sensitivity in the hindpaw, we measured the latency for a mouse to withdraw its hindpaw following applications of heat via placement on a 55°C hot plate [94] or cold via dry ice application in the cold plantar assay [95]. To examine sensitivity to painful mechanical stimulation in the tail, we measured the latency for a mouse to attempt to remove a small clothespin attached to the distal tip of tail [96]. To examine sensitivity to innocuous mechanical stimulation in the hindpaw, we assessed the frequency of response to a light touch with a “fluffed out” cotton swab brushed across the hindpaw [97]. The latter assay was used to determine if *Dgki* and/or *Dgkh* loss affected large-diameter, low-threshold mechanosensory neurons of the DRG, whereas the other assays were meant to probe the function of the small-diameter, nociceptive DRG neurons.

Sensitivity to noxious (Figure 3.6A, Figure 3.7A, Figure 3.8A) or innocuous (Figure 3.6E, Figure 3.7E, Figure 3.8E) mechanical stimuli was unaffected by deletion of *Dgki* and/or *Dgkh* in either sex. Loss of *Dgki* had no effect on responses to painful cold (Figure 3.6B,F) or painful hot (Figure 3.6C-D,G) stimuli. However, thermal pain sensitivity was altered in sex- and modality-dependent ways in *Dgkh*$^{-/-}$ and dKO mice. Interestingly, *Dgkh*$^{-/-}$ females had *decreased* sensitivity to immersion of the tail in 49°C, but not 46.5°C, water, as shown by in increased withdrawal latency (Figure 3.7C-D), yet they had *increased* sensitivity to exposure of the

hindpaws to a 55°C hot plate (Figure 3.7G). Loss of *Dgkh* had no effect on responses to painful cold stimuli (Figure 3.7B,F). The dKO mice also demonstrated some small but statistically significant differences in acute pain sensitivity in the hindpaw: dKO *females* had decreased sensitivity to cold stimuli and dKO *males* had increased sensitivity to heat (Figure 3.8F-G). Simultaneous deletion of *Dgki* and *Dgkh* had no effect on tail responses to thermal stimuli (Figure 3.8B-D). While the effect sizes in these pain assays were small, the differences were statistically significant.

Sensitization and recovery following inflammatory injury is unchanged in the absence of *Dgki* and/or *Dgkh*

Although baseline pain sensitivity was not strongly disrupted in the *Dgki*$^{-/-}$, *Dgkh*$^{-/-}$, and dKO animals, we hypothesized that *Dgki* and/or *Dgkh* loss may alter sensitization to nerve or tissue injury. We analyzed responses to the complete Freund's adjuvant (CFA) model of inflammatory injury [98]. We used the electronic von Frey assay [99], in which we measured the force taken to cause a mouse to withdraw its hindpaw, to demonstrate changes in mechanical sensitivity. We used the Hargreaves assay [100], in which we measured the latency to withdraw the hindpaw from a focused beam of light, to demonstrate changes in thermal sensitivity. In addition to measuring the baseline responses to these stimuli, the change in responses following injury were measured.

In these experiments, the *Dgki*$^{-/-}$ and *Dgkh*$^{-/-}$ males and their simultaneously-tested WT male counterparts failed to sensitize to von Frey stimulation post-CFA; therefore, in the absence of proper controls, only the Hargreaves responses are shown for *Dgki*$^{-/-}$ and *Dgkh*$^{-/-}$ males (Figure 3.9A, Figure 3.10A). The WT and dKO males did show sensitization to von Frey post-CFA, so those data are shown in Figure 3.11C in addition to their Hargreaves responses in Figure 3.11A. Both Hargreaves and von Frey response are shown for *Dgki*$^{-/-}$, *Dgkh*$^{-/-}$, and dKO females (Figure 3.9B-C, Figure 3.10B-C, Figure 3.11B,D).

Overall, expression of *Dgki* and/or *Dgkh* did not influence how hypersensitive the ipsilateral paws became to heat in the Hargreaves assay following CFA injection (Figure 3.9A, Figure 3.10A, Figure 3.11A-B). Likewise, there was little difference in the recovery to baseline heat sensitivity levels; however, while the dKO males did recover in the 7-day period, they did not recover to the same levels as WT males (Figure 3.11A). Additionally, there were no differences between genotypes in the level of sensitization to mechanical stimulation that developed after CFA injection, nor were there differences in the recovery from this sensitization in either the *Dgki*$^{-/-}$, *Dgkh*$^{-/-}$, or dKO females (Figure 3.9C, Figure 3.10C, Figure 3.11D) or the dKO males (Figure 3.11C). For mice of both sexes, the responses of the contralateral paw to thermal or mechanical stimuli did not vary significantly over time and did not differ based on genotype.

Sensitization following neuropathic injury is unaffected by *Dgki* deletion

We analyzed responses to the spared nerve injury (SNI) model of neuropathic injury [101, 102], using the filamentous von Frey assay [103] to demonstrate changes in sensitivity to a range of mechanical stimuli in male (Figure 3.12A-D) and females (Figure 3.12E-H) WT and *Dgki*$^{-/-}$ mice. Here, we show responses of the ipsilateral and contralateral paws to a range of von Frey filaments of different forces at baseline (Figure 3.12A,E) and Days 1 (Figure 3.12B,F), 7 (Figure 3.12C,G), and 14 (Figure 3.12D,H) post-surgery. Apart from a small increase in the response rate of the ipsilateral paw to a force of 0.692 g in *Dgki*$^{-/-}$ males on Day 14, the overall degree of sensitization did not differ between WT and *Dgki*$^{-/-}$ mice in either sex. There were no differences between ipsilateral and contralateral paws at baseline, and no changes in responses from the contralateral paw over time.

Signaling in mouse DRG neurons is unaltered in absence of *Dgki* and/or *Dgkh*

Nociceptors are flooded with a diverse milieu of signaling mediators in response to injury or exposure to pruritogenic stimuli, activating multiple classes of receptors. In gain-of-function studies, we showed that *Dgki* or *Dgkh* overexpression enhances $G\alpha_q$-GPCR signaling (Figure 2.1). Work done by others demonstrated that reducing *Dgki* or *Dgkh* expression decreases Ras-MAPK signaling [20, 23, 48]. Therefore, *Dgki* and *Dgkh* are in a position to regulate responses after activation of multiple receptor types. We characterized how these pathways are affected in the absence of *Dgki* or *Dgkh* in order to contribute to a better understanding of how DRG neurons regulate responses to pruriceptive and nociceptive mediators.

Deletion of *Dgki* or *Dgkh* does not alter in vitro calcium responses to pruritogens or algogens in DRG neurons

Using cultured WT, *Dgki*$^{-/-}$, and *Dgkh*$^{-/-}$ DRG neurons loaded with a fluorescent ratiometric calcium dye, we measured changes in intracellular calcium concentrations induced by stimulation of receptors involved in itch and pain signaling. The agonists used to stimulate DRG neurons for these experiments were histamine, capsaicin, lysophophatidic acid (LPA), or uridine triphosphate (UTP). Histamine activates the H1 receptor on sensory neurons to induce itch responses [74]. Capsaicin is the chemical ligand for the ion channel TRPV1 (transient receptor potential vanilloid 1), an important receptor for itch and pain signaling [74, 104]. LPA acts on LPA receptors and induces nociception in peripheral neurons [105, 106]. UTP binds to P2Y receptors and activates and sensitizes small-diameter DRG neurons [107, 108]. We used histamine because of the *in vivo* scratching phenotypes we observed in response to histamine injection (Figure 3.3, Figure 3.4, Figure 3.5). We used capsaicin, LPA, and UTP for algogens because their receptors are expressed in a relatively high percentage of rodent DRG neurons [107, 109, 110].

Because *Dgki* and *Dgkh* are highly expressed in DRG neurons, we hypothesized that the altered responses to histamine *in vivo* were caused by altered signaling activity in DRG neurons. Despite enhancing scratching responses to histamine injection *in vivo* (Figure 3.3A-B), *Dgki* loss had no effect on calcium responses to histamine in cultured DRG neurons (Figure 3.13A-B). Despite decreasing scratching responses to histamine injection *in vivo* (Figure 3.4A-B), *Dgkh* loss had no effect on calcium responses to histamine in cultured DRG neurons (Figure 3.14A-B). Based on the lack of differential responses to painful stimuli *in vivo*, we were not surprised to see neither *Dgki*$^{-/-}$ nor *Dgkh*$^{-/-}$ neurons did not respond differently from WT after exposure to the algogenic compounds capsaicin, LPA, or UTP (Figure 3.13C-H, Figure 3.14C-H).

In addition to the magnitude of the response (represented by area under the curve of the agonist responses), the response rate—the proportion of healthy neurons responding to the agonist—was similar between WT and *Dgki*$^{-/-}$ and between WT and *Dgkh*$^{-/-}$ neurons for all four agonists tested (Figure 3.15).

Neither *Dgki* nor *Dgkh* deletion alters NGF-induced ERK signaling in mouse DRG

The ligands stimulating afferent nociceptors after injury also include peptides and neurotrophic factors, such as nerve growth factor (NGF), that activate receptor tyrosine kinases. NGF activates the TrkA receptor on DRG neurons, which is involved in pain signaling and sensitization [111]. Both *Dgki* and *Dgkh* have been shown to positively regulate Ras activity downstream of activation of epidermal growth factor receptors (EGFR, a receptor tyrosine kinase activated by EGF) in other cell types, though via different mechanisms from each other. *Dgkh* enhances associate of B-Raf and C-Raf [48], while *Dgki* inhibits RasGRP3 to attenuate Rap1 activation and enable Ras activation [23]. Deletion of either *Dgk* isoform has the potential to desensitize TrkA by increasing PKC activation by DAG, but both isoforms also have

alternative mechanisms of modulating RTK signaling that could be attenuated by DGK inhibition.

Because *Dgki* and *Dgkh* positively regulate Ras-MAPK signaling downstream of RTK activation, we measured activity of this pathway by measuring ERK phosphorylation following NGF exposure to determine if this signaling pathway is regulated by *Dgki* and *Dgkh* in mouse DRGs (Figure 3.16). NGF induced slightly less ERK phosphorylation after 5 minutes in DRGs from *Dgki*$^{-/-}$ mice relative to DRGs from WT mice (Figure 3.16B). However, because the *Dgki*$^{-/-}$ DRGs had lower baseline ERK phosphorylation, the increase in ERK phosphorylation after 5 minutes was comparable between the two genotypes (185% for WT, 187% for *Dgki*$^{-/-}$). NGF-induced ERK phosphorylation was not affected by *Dgkh* expression in DRGs (Figure 3.16D).

Dgki$^{-/-}$, *Dgkh*$^{-/-}$, and dKO DRG lysates phosphorylate DAG and/or MAG substrates less than WT DRG lysates

To characterize the degree to which *Dgk* loss alters the phosphorylation of various substrates in the DRG, we again used a radioactivity-based kinase assay, as in Figure 2.2A. Here, instead of using lysates from HEK293 cells overexpressing *Dgk* constructs, we used lysates from DRGs dissected from mice lacking *Dgki* and/or *Dgki*. Protein was isolated from WT, *Dgki*$^{-/-}$, *Dgkh*$^{-/-}$, and dKO mouse DRG tissue. Lysates were combined in a reaction with ^{32}P-labeled ATP and DAG or MAG substrates, and the amount of ^{32}P-phosphorylated PA or LPA produced was measured (Figure 3.17). We used the DAG substrates 16:0-18:1 (1-palmitoyl-2-oleoyl-glycerol) and 18:0-20:4 (1-stearoyl-2-arachidonoyl-glycerol), which are the two most prevalent DAG species in rodent peripheral nerves [54]. We also tested the MAG species 20:4 (2-AG) and 18:1 (2-oleoyl-glycerol).

Dgki loss had a little-to-no impact on the phosphorylation of DAG or MAG substrates by DRG lysates, resulting in a less than 20% reduction in kinase activity relative to WT DRG lysates. On the other hand, DRG lysates lacking *Dgkh* expression (both *Dgkh*$^{-/-}$ and dKO

genotypes) had significantly reduced phosphorylation of all four lipid substrates tested. Despite the small effect of deleting *Dgki* alone, the combined deletion of *Dgki* and *Dgkh* had a greater impact that deleting *Dgkh* alone.

DISCUSSION

Summary of sensory behavior and DRG activity phenotypes

We sought to determine how *Dgki* and/or *Dgkh* loss in mice manifests in altered somatosensory processing, combining itch and pain behavior assays and analyses of DRG function. A summary of the phenotypes seen in the *Dgki*$^{-/-}$, *Dgkh*$^{-/-}$, and dKO mice in the *in vivo* itch assays, the *in vivo* baseline pain sensitivity assays, and the *in vitro* DRG kinase assay are shown in Table 3.2. Not included in the table are the results of experiments in which none of the mouse models showed major differences from WT mice, including the *in vivo* inflammatory and neuropathic injury models, the *in vitro* DRG calcium signaling, and the *in vitro* ERK phosphorylation assays. The baseline pain sensitivity summary tables shows the responses to the stimuli presented in Figure 3.6, Figure 3.7, and Figure 3.8, as well as the baseline responses to the von Frey and Hargreaves stimuli used to demonstrate sensitization to CFA. The summary table is a heat map indicating how significantly each mouse differed from WT mice and in which direction (greater or smaller *in vivo* sensitivity or *in vitro* activity than WT). Note that the intensity of the color for the itch results represents the 5-min period with the peak difference from WT, which may not have been seen throughout the 30-min assay; see Figure 3.3, Figure 3.4, Figure 3.5 for more detailed data.

The most significant behavior phenotypes were seen in the itch assays (Table 3.2A). *Dgki* deletion significantly enhanced scratching responses to histamine. *Dgkh* deletion significantly attenuated scratching responses to histamine in males. Simultaneous deletion of *Dgki* and *Dgkh* in the dKO mouse phenocopied the *Dgki*-knockout. Small differences in chloroquine sensitivity were observed in single *Dgk*-knockout females, in the same direction as

histamine: increased in *Dgki*$^{-/-}$ mice and decreased in *Dgkh*$^{-/-}$ mice (although the histamine sensitivity in *Dgkh*$^{-/-}$ mice was male-specific). However, the fact that chloroquine sensitivity was not disturbed in the dKO mice suggests that, unlike with histamine sensitivity, neither *Dgki* or *Dgkh* loss affects chloroquine sensitivity strongly enough to persist in the absence of the other.

Of the 48 comparisons of baseline pain sensitivity (3 mouse models $\times$ 2 sexes $\times$ 8 pain tests), there were 4 comparisons in which there was a sex- and genotype-dependent different between one of our mouse models and WT mice (Table 3.2B). However, no pattern of effects was seen. *Dgkh*$^{-/-}$ females showed both increased and decreased sensitivity to heat (though at different stimulations sites: hindpaw and tail, respectively). Further, *Dgkh*$^{-/-}$ females did not differ from WT females in their sensitivity to other heat stimuli applied to those same sites (55°C hot plate and 46.5°C tail immersion, respectively). Additionally, the phenotypes seen in *Dgkh*$^{-/-}$ females were not seen in the dKO females, suggesting that the absence of *Dgkh* expression does not sufficiently cause these differences. The pain sensitivity phenotypes seen in the dKO mice were likewise without a pattern: females had decreased cold sensitivity, and males had increased heat sensitivity, both of which were not seen in all tests of that modality. Overall, the baseline pain assays showed that deletion of *Dgkh*, with or without concurrent *Dgki* deletion, had minor effects on acute pain sensitivity.

Even though overexpressed *Dgki* had greater kinase activity than *Dgkh* in the HEK293 cell paradigm (Figure 2.2B-C), we found that *Dgkh* loss had a much larger impact on acylglycerol phosphorylation than *Dgki* loss in mouse DRG (Figure 3.17). Even in the absence of both *Dgki* and *Dgkh*, the dKO DRG lysates still had over 50% of WT levels of kinase activity for all substrates tested (Table 3.2C). Therefore, other *Dgk* genes expressed in mouse DRG likely play a role in phosphorylating DAG and MAG in this tissue.

Dgki deletion enhances *in vivo* histamine sensitivity but does not alter *in vitro* DRG neuron functions

The effect of *Dgki* loss on noxious somatosensory behavior was mostly specific to histamine-induced itch, as there were no alterations in baseline pain or pain sensitization in *Dgki*$^{-/-}$ animals. Additionally, our data suggest that enhanced responses to histamine *in vivo* following *Dgki* deletion is not mediated by DRG neurons. Histamine signaling in DRG neurons requires coupling of histamine receptors to the ion channel TRPV1 [74]. Not only do *Dgki*$^{-/-}$ neurons respond normally to histamine, but they also have normal responses to the TRPV1 ligand capsaicin. Thus, *Dgki* loss does not appear to affect the function of either receptor involved in histamine response in DRG neurons, when using calcium influx as the readout.

Other measures of DRG function not directly related to histamine responses indicate that the function of this tissue is not greatly affected in other ways. We observed slight reductions in NGF-induced ERK phosphorylation (Figure 3.16B) and DAG kinase activity (Figure 3.17) in *Dgki*$^{-/-}$ DRG samples, but the effect sizes were very small. Additionally, these assays would suggest that *Dgki*$^{-/-}$ DRG function is reduced, which would oppose the hypothesis that the *in vivo* hypersensitivity to histamine seen in these animals was a result of increased DRG activity. Further, there was a lack of significant changes in response to chloroquine, β-alanine, and various algogenic stimuli *in vivo*, all of which involve the DRG in mediating their effects. Therefore, it stands to reason that the enhanced histamine sensitivity in *Dgki*$^{-/-}$ mice is mediated by cells other than DRG neurons.

The only tissue in which *Dgki* is expressed more highly than in the DRG is in mast cells (Table 3.1A) [88]. In response to allergen exposure mast cells release histamine, which activates receptors on nearby sensory neurons [74]. Recent research has shown that mast cells can respond to histamine themselves, as well. Mast cells can chemotax toward histamine, and histamine can induce calcium signaling and degranulation [112, 113]. Interestingly, other *Dgk* isoforms have been shown to affect mast cell function. *Dgkz* loss decreases FcεRI-induced

degranulation in bone marrow-derived mast cells but increases cytokine production [114]. Additionally, knockdown of *Dgkg* reduces degranulation in RBL-2H3 cells, a histamine-releasing, mast-cell-like line [115]. Because the mechanisms by which mast cells response to histamine are not yet known, it is difficult to hypothesize what mechanism could be altered by *Dgki* loss. That being said, it would still be worth investigating the role of *Dgki* in functions of these immune cells as a future direction of this study.

Dgkh deletion reduces *in vivo* histamine responses and *in vitro* DRG kinase activity but not *in vitro* DRG signaling

The phenotypes of the *Dgkh*$^{-/-}$ male mice most closely resemble our hypothesis how *Dgk* loss might affect sensory signaling. Because $G\alpha_q$-GPCR signaling is activated by *Dgkh* overexpression in HEK293 cells and by algogenic and pruritogenic stimuli in DRG neurons, we expected *Dgkh* loss to decrease activation of DRG neurons by noxious stimuli. Indeed, scratching induced by histamine was significantly reduced in *Dgkh*$^{-/-}$ males relative to WT males. Histamine activates a $G\alpha_q$-GPCR that that signals to PKC [116], a mechanism we expected *Dgkh* to regulate. However, there were also many sensory phenotypes that were not perturbed, including mechanical pain, which is partially driven by GPCR signaling [71].

Additionally, DAG and MAG phosphorylation by DRG lysates was significantly reduced by the loss of *Dgkh*, which also matched our hypothesis. However, none of the signaling functions analyzed in *Dgkh*-null DRGs differed from WT, including calcium activity in response to histamine receptor activation. This was unexpected, as the effect on $G\alpha_q$-GPCR signaling resulting from *Dgkh* overexpression in HEK293 cells was dependent on *Dgkh*'s kinase activity [45]. The kinase activity assay was performed using DRGs dissected from both male and female mice; *Dgkh* loss decreased DAG and MAG kinase activity equally in male and female DRG lysates (data not shown). Because *Dgkh*$^{-/-}$ males had decreased histamine sensitivity and

females did not, this suggests that histamine sensitivity was not linked to kinase activity in the DRG.

Thus, even though some phenotypes of the *Dgkh*$^{-/-}$ mice support our original hypotheses, the disruption of DRG kinase activity and, subsequently, $G\alpha_q$-GPCR signaling may not be the mechanism by which *Dgkh* deletion affects somatosensation in mice. Many of the same arguments against a DRG-dependent mechanism that I presented for *Dgki* also apply to *Dgkh*. *In vitro* DRG calcium and ERK signaling pathways are not affected in the knockout mice, and there are no major disruptions in baseline pain responses. However, the *presence* of a pain phenotype would do more to argue *for* a DRG-dependent mechanism than the *lack* of a pain phenotype would do to argue *against* a DRG mechanism for itch sensitivity. While itch-sensing DRG neurons respond to algogenic stimuli, far more DRG fibers are involved in pain than itch [75], so disrupting itch fibers would only affect a small population of pain fibers. Whereas the expression patterns of *Dgki* implicate mast cells in *Dgki*-dependent histamine sensitivity, the expression patterns of *Dgkh* do not suggest an alternative tissue that may drive *Dgkh*-dependent histamine itch. However, many neuronal subtypes have been shown to regulate histamine-induced itch, included inhibitory BHLHB5+ and excitatory TR4+ interneurons of the spinal cord [117, 118]. There are many potential avenues for further investigation to determine how *Dgkh* deletion alters histamine sensitivity.

dKO mice have enhanced *in vivo* histamine sensitivity and decreased *in vitro* DRG kinase activity

Interestingly, both *Dgk* isoforms affected *in vivo* responses to histamine more than other pruritogens, and did so in opposite directions of each other; histamine-induced scratching was enhanced by *Dgki* loss and reduced by *Dgkh* loss. Both female and male dKO mice phenocopied the *Dgki*-knockout's histamine hypersensitivity. However, DRG lysates from the

dKO mice phenocopied the decreased DAG and MAG phosphorylation seen in *Dgkh*-knockout DRG lysates.

Pairing the results from the *in vivo* histamine assay and the *in vitro* DRG kinase activity assay gives support to two hypotheses about the single *Dgk* knockout mice. First, it suggests *Dgki* loss could enhance histamine scratching in a non-DRG-dependent way. Even though dKO DRG lysates had lower kinase activity than *Dgki*$^{-/-}$ DRG lysates, the *in vivo* histamine phenotype was not stronger in dKO mice. This suggests that the reduction in kinase activity in the DRG is not directly correlated to the increased *in vivo* histamine response. Second, it suggests that reduced histamine scratching in the *Dgkh*$^{-/-}$ mice is not caused by reduced kinase activity in the DRG. Because DAG and MAG phosphorylation by DRG lysates was reduced far more by the loss of *Dgkh* than *Dgki*, and *Dgkh* deletion reduced histamine-induced scratching, one could be tempted to conclude that DAG/MAG kinase activity in the DRG may be required for histamine response (in male mice at least). However, like the *Dgkh*$^{-/-}$ males, dKO mice have decreased lipid phosphorylation, but they also have *increased* scratching in response to histamine. Therefore, decreased DRG kinase activity caused by *Dgkh* deletion is not sufficient to impair *in vivo* histamine sensitivity, and the presence of *Dgkh* is not necessary for *in vivo* histamine response.

Connections between pain and itch

As mentioned in the introduction to this chapter, many of the same receptors and the same cells are used to signal both itch and pain. Therefore, the results of the pain assays can help us identify and exclude potential mechanisms by which the itch phenotypes arise. For example, activation of the histamine receptor H1R causes opening of the heat-sensitive TRPV1 channel [75]. Heat responses were not altered in the *Dgki*$^{-/-}$ or *Dgkh*$^{-/-}$ mice, which suggests that their histamine-related phenotypes were *not* caused by disrupted TRPV1 function. Similarly, DRG neurons that express the β-alanine receptor, *Mrgprd* (Mas-related GPR D), mediate

mechanical pain [71]. dKO mice showed a slight hyperresponsiveness to β-alanine *in vivo*. However, because dKO mice did not also show increased mechanical sensitivity, we hypothesize that the β-alanine phenotype was *not* caused by increased excitability of the *Mrgprd*$^{+}$ neuronal population.

Our hypotheses on mechanism may also be informed by the ways that itch and pain interact on the physiological level. Scratching is perceived as a painful stimulus that overrides the itch signal [67]. However, patients with atopic dermatitis (a chronic pruritus disorder) become sensitized to itch such that even algogenic stimuli are interpreted as pruritogenic [73, 119]; not only does scratching fail to inhibit itch, but the scratching itself enhances the itch sensation. However, our behavioral tests appear to exclude this mechanism as an explanation of the *Dgk* mutant mouse scratching behaviors. If our *Dgki*$^{-/-}$ or dKO mice were unable to suppress histamine-induced itch via pain (scratching), we would expect to see one of two things in the pain assays. The first would be a reduction in pain sensitivity. Because pain suppresses itch, if there is reduced pain signaling, then that would allow for increased itch. Although there was reduced kinase activity in the DRG (a primarily pain-sensing organ), the *in vivo* responses to algogens were normal. The second would be a scratching response when exposed to an algogenic stimulus. If the pain fibers were sensitized to itch, as is the case in atopic dermatitis patients, painful stimuli would become pruritogenic. Unfortunately, we did not note scratching behaviors when performing these assays. Additionally, it is difficult to distinguish pain and itch responses behaviors with the sensory assays we used: mice would lick their hindpaw whether they were feeling either pain or itch. As a future direction, we could determine if algogenic stimuli induce scratching by utilizing an assay that can distinguish between a mouse's responses to pain and itch [120]. In this assay, algogens or pruritogens are injected in the cheek, which they scratch when they feel itch but wipe with the back of the paw when they feel pain.

In addition to looking at overlaps in itch and pain pathology, we can get an idea of the potential mechanism of altered histamine sensitivity by reflecting on the cells and circuits that are unique to itch or pain. For example, histamine-sensitive DRG neurons do not respond to mechanical stimuli [74]. Therefore, if the *Dgk* mutant mice had alterations in mechanical pain, this would argue against the hypothesis that histamine hypersensitivity was caused by a hyperexcitability of the histamine-sensitive neuronal population in *Dgki*$^{-/-}$ and dKO mice.

In general, the presence of a pain phenotype would be better at suggesting a mechanism for itch than the absence of a pain phenotype would be at excluding a mechanism. Nevertheless, seeing only minor pain phenotypes in our *Dgk* mice gives us confidence that the disruptions in sensory biology in these mice were specific to itch. This is an interesting contribution to the debate of whether itch and pain can truly be separated [68, 75, 121]. However, more work will need to be done to identify the mechanisms by which *Dgki* or *Dgkh* deletion alters histamine sensitivity.

METHODS

Analysis of microarray data

The *Dgki* and *Dgkh* expression profile data were generated previously by others and was accessed through BioGPS (dataset “GeneAtlas MOE430, gcrma” and probe sets 1439986_at, 1457213_a_at, and 1459906_at) [88, 122, 123]. For this study, expression level for each tissue was normalized to the median expression level for all tissues, and averages were calculated of duplicate samples. The expression levels were ranked highest to lowest, and the 10 tissues with the highest expression are shown here.

Mice

See: “Mice” under METHODS from Chapter 2. During the spared nerve injury (SNI) experiments, the bedding was 1/8-inch diameter (8B, Andersons Lab Bedding). During all other experiments, the bedding was 1/4-inch diameter (4B, Andersons Lab Bedding).

Immunohistochemistry

Histology was performed by Bonnie Taylor-Blake as previously published [124]. After euthanasia, lumbar DRGs were dissected from a 7-week-old wild type (WT) male mouse (for DGKI staining) or a 5-week-old WT male mouse (for DGKH staining) and placed into 4% paraformaldehyde (PFA) in 0.1 M phosphate buffer (13.8 g/L Na_2HPO_4-H_2O, 26.8 g/L Na_2HPO_4-$7H_2O$, pH 7.4) on ice. After 4 hours in 4% PFA at 4°C, DRGs were moved to 30% sucrose for cryoprotection overnight at room temperature. DRGs were then embedded in Tissue-Tek O.C.T. Compound (4583, Sakura Finetek, Torrance, California). Sections of 20 µm thickness were collected onto SuperFrost Plus glass slides (12-550-15, Thermo Fisher) and stored at -20°C until staining. After hydrating sections with PBS and washing with a solution of tris buffered saline with Triton X-100 (TBSTX; 0.05 M Tris, 2.7% w/v NaCl, 0.3% v/v Triton-X 100, pH 7.6), sections were blocked in a buffer of 10% normal donkey serum (S30, Millipore, Burlington, Massachusetts) in TBSTX (NDS/TBSTX) for 1 h at room temperature. Sections were then incubated in primary antibodies for NeuN (1:300 mouse anti-NeuN, MAB377, Millipore) and either DGKI (1:1,000 rabbit anti-DGKI, LS-C118721, Lifespan Biosciences) or DGKH (1:1,000 rabbit anti-DGKH, HPA040355, Sigma) in NDS/TBSTX overnight at room temperature. The next day, sections were blocked with NDS/TBSTX for 1 h before incubating in a secondary antibody solution of 1:200 Alexa Fluor 568-conjugated goat anti-mouse IgG1 (A21124, Invitrogen) and 1:200 Alexa Fluor 488-conjugated goat anti-rabbit (A11008, Invitrogen) in NDS/TBSTX for 2 h at room temperature. Sections were rinsed with TBSTX between each step. Coverslips were added directly to slides with FluoroGel mounting medium (17985-10, Electron Microscopy

Sciences, Hatfield, Pennsylvania). Imaging was performed on a Zeiss LSM 510 confocal laser scanning microscope.

In situ hybridization

Lumbar DRGs were dissected from a 4-month-old WT male, and *in situ* hybridization (ISH) was performed by Megumi Aita using a probe targeting a 873-bp fragment of mouse *Dgkh*.

Sensory Behavior

All behavior assays were performed on 2- to 4-month-old mice during the light phase of the light:dark cycle. For each assay, mice within each cohort were tested in a random order that varied between days. After testing each mouse for itch or baseline pain responses, they were kept separate from the mice that had not yet been tested in that assay, to avoid empathetic pain responses [125]. For all behavior assays, the experimenters were blinded to the genotype.

Sensory behaviors assays were performed in a mesh platform apparatus or a glass platform apparatus, except for the tail immersion and clothespin assays. The mesh platform apparatus consisted of a 28 × 46 cm sheet of stainless-steel mesh elevated 28 cm from the bench surface. Mice were placed on top of the mesh platform, and each mouse was enclosed in an individual 9 × 9 × 11 cm 5-sided transparent plastic box. For the glass platform apparatus, we used an 86 × 35 cm pane of 0.6 cm thick glass elevated 21 cm from the bench. Mice were placed in square acrylic enclosures of 13 cm height that were separated with dividers into 4 equally-sized 10 × 10 cm chambers. Lids of the acrylic chambers had 3-cm-diameter holes, covered with copper wire mesh to prevent escape.

Itch, cold plantar, and Hargreaves assays were tested in the glass platform apparatus. Cotton swab and filamentous von Frey assays were tested in the mesh platform apparatus.

Mice were acclimated to these apparatuses for 2 hours per day for at least 5 days prior to testing. On the day of testing itch responses, mice were acclimated to test chambers for 30 min prior to injection, and only one animal was tested at a time. On the day of testing cotton swab, cold plantar, Hargreaves, and von Frey, mice were acclimated to the test chamber for 1 h prior to testing, and all mice in the cohort were tested together.

Itch assay

We used an acute scratching assay to test itch responses to histamine, chloroquine, and β-alanine in WT, *Dgki*$^{-/-}$, *Dgkh*$^{-/-}$, and dKO male and female mice. Following a 30-min acclimation period, mice were injected with 50 µL of pruritogen that was dissolved in 0.9% w/v NaCl, made fresh on the day of testing, and kept on ice throughout the day. The 50 µL injection contained 500 µg β-alanine (A9920, Sigma), 500 µg histamine (H7250, Sigma), or 200 µg chloroquine (C6628, Sigma). After injecting a pruritogen subcutaneously at the nape of the neck using a 13-mm 30-gauge needle (305106, BD, Franklin Lakes, New Jersey) attached to a 50-µL glass syringe (Model 705, Hamilton, Reno, Nevada), we counted scratching bouts at the site of injection performed by each mouse in 5-minute intervals over 30 minutes. All three pruritogens were tested in each mouse. Each cohort was tested on β-alanine and given at least 48 hours to recover. Each cohort was then tested on histamine or chloroquine (alternating for each cohort) and given 72 hours to recover.

WT and *Dgki*$^{-/-}$ males and females were tested in two cohorts. The first cohort had 10 mice each of WT males, *Dgki*$^{-/-}$ males, WT females, and *Dgki*$^{-/-}$ females; the second cohort had 12 WT males, 11 *Dgki*$^{-/-}$ males, 10 WT females, and 8 *Dgki*$^{-/-}$ females. WT and *Dgkh*$^{-/-}$ males and females were tested in three cohorts. The first cohort had 5 WT males, 4 *Dgkh*$^{-/-}$ males, 4 WT females, and 5 *Dgkh*$^{-/-}$ females and were only tested for histamine; the second cohort had 10 WT males, 10 *Dgkh*$^{-/-}$ males, 11 WT females, and 9 *Dgkh*$^{-/-}$ females; the third cohort had 8 WT males and 7 *Dgkh*$^{-/-}$ males. WT and dKO males and females were tested in two cohorts. The

first cohort had 4 WT males, 4 dKO males, 7 WT females, and 7 dKO females; the second cohort had 8 WT males, 8 dKO males, 3 WT females, and 3 dKO females. The same effects were found in each cohort of a given genotype individually, so we combined the data from those cohorts.

Acute pain sensitivity assays

Mice were tested on each baseline pain assay at least twice, on separate days, and the responses for an individual animal were averaged. Mice were given at least one hour to recover after each test. In a single day, mice were tested on 2 to 5 baseline pain assays. The assays were run in a random order that varied between days.

Tail immersion – To measure thermal sensitivity [92, 93], a 75% ethanol solution was cooled to -10°C or a water bath was heated to 46.5°C or 49°C. Each mouse was gently wrapped in a towel and inverted, submerging approximately half of the tail, and the latency for the mouse to flick their tail was measured. Without a response, tails were removed from -10°C after 60 s, 46.5°C after 40 s, and 49°C after 20 s.

Clothespin – To measure mechanical sensitivity [96], we measured the latency for a mouse to attempt to remove a 2.5-cm long clothespin (3438, Bazic Products, Los Angeles, California) attached to the tail, approximately 1 cm from the distal tip. Assays were performed in an empty 17 × 28 × 12.5 cm plastic cage (Allentown Caging, Allentown, New Jersey) with no lid. The time for a mouse to bite or attempt to remove the clothespin was measured. The clothespin was removed as soon as the mouse responded, or after 20 s if there was no response.

Cotton swab – To determine if *Dgki* loss affects large-diameter, low-threshold mechanosensory neurons of the DRG [97], we assessed responses to a light touch via a “fluffed out” cotton swab brushed across the hindpaw. The cotton swab was brushed from heel to toe, and any movement of the paw was counted as a response. Each paw was tested 5 times (total of 10 tests per mouse). After testing each paw once for each animal, the mice were given 10

min to settle before testing again. We alternated starting testing on either the left or right hindpaw.

Cold plantar – To examine sensitivity to cold, we measured withdrawal latency to applications of dry ice to the hindpaw [95]. Dry ice was packed into a 3-mL syringe (209657, BD) modified to expose a 0.8-cm-diameter cross section and pressed against the glass directly under the hindpaw. Without a response, the stimulus was removed after 20 s. Each hindpaw was tested two to three times, with at least 30 min rest between tests on a single paw. We alternated starting testing on either the left or right hindpaw.

Hot plate – To examine sensitivity to heat, we measured latency to respond to placement of the mouse onto a 55°C hot plate [94], using a Hot Plate Analgesia Meter (Series 8 Model 29, IITC Life Science Inc., Woodland Hills, California). Mice were placed on the surface of the hot plate, within an acrylic cylinder with an inner diameter of 10 cm and a height of 15.4 cm. The latency to demonstrate a painful response (licking or rapidly flicking either hindpaw or jumping) was timed. The mouse was removed from the plate after responding, or after 30 s if there was no response.

Hargreaves – To examine sensitivity to heat, we measured withdrawal latency to applications of heat via a focused beam of light to the hindpaw [100], using an infrared radiometer (72-6703, Harvard Apparatus, Holliston, Massachusetts) light source set to an intensity of 30 mW/cm^2. Without a response, the stimulus was removed after 20 s. Each hindpaw was tested two to three times, with at least 30 min rest between tests on a single paw. We alternated starting testing on either the left or right hindpaw.

Filamentous von Frey – To examine mechanical pain, we used von Frey filaments. Pressure is applied to the plantar surface of the hindpaw using a long, thin filament until either the filament bends or the mouse withdraws its paw [103]. Eight filaments with bend thresholds of 0.407, 0.692, 1.2, 1.5, 2.04, 3.63, 5.5, and 8.5 g (Research Designs Inc.) were tested, in that order. Each filament was tested five times on each hindpaw (alternating left and right for each

test). The percentage of total hindpaw withdrawals (out of 10) was calculated to assess sensitivity to mechanical stimuli. Mice were allowed to rest for at least 2 minutes between tests of an individual filament and a minimum of 15 minutes between filaments to ensure withdrawals were due to mechanical nociception rather than overstimulation.

Electronic von Frey – To examine mechanical pain, we used an electronic von Frey anesthesiometer (Model 2390, IITC Life Science Inc.) consisting of a rigid filament is attached to a pressure transducer [99]. The filament is pressed against the plantar surface of the hindpaw until the filament bends or the mouse withdraws its paw. The maximum force applied to the paw is recorded by the anesthesiometer. Each hindpaw was tested two to three times, with at least 2 min rest between tests on a single paw.

Chronic pain models

Inflammatory injury – We modeled inflammatory sensitization by injecting 30 µL of complete Freund's adjuvant (CFA; 855828, MP Biomedicals, Santa Ana, California) into the plantar surface of the left hindpaw, using a 13-mm 27-gauge needle (305109, BD) attached to a 50-µL glass syringe (Model 705, Hamilton) [98, 102]. Responses of both the ipsilateral and contralateral hindpaws to heat in the Hargreaves test were measured at baseline (0 to 3 days prior to CFA injection) and on Days 1, 2, 3, 4, and 7 after CFA injection. Observation days were chosen to observe development of and recovery from CFA-induced inflammatory sensitization. WT and *Dgki*$^{-/-}$ males and females were tested in one cohort of 10 mice each of WT males, *Dgki*$^{-/-}$ males, WT females, and *Dgki*$^{-/-}$ females. In this cohort, the females were tested on Day 5 instead of Day 4. WT and *Dgkh*$^{-/-}$ males and females were tested in two cohorts. The first cohort had 8 WT males, 7 *Dgkh*$^{-/-}$ males, 11 WT females, and 8 *Dgkh*$^{-/-}$ females and were only tested for histamine; the second cohort had 6 each of WT females and *Dgkh*$^{-/-}$ females. WT and dKO males and females were tested in three cohorts. The first cohort had 6 WT males, 5 dKO males, 7 WT females, and 7 dKO females; the second cohort had 9 WT males, 9 dKO males, 3 WT

females, and 3 dKO females. The third cohort had 7 each of WT males and dKO males. The same effects were found in each cohort of a given genotype individually, so we combined the data from those cohorts.

Neuropathic injury – Neuropathic sensitization was induced using the spared nerve injury (SNI) model of neuropathic pain, in which two of the three major branches of the sciatic nerve are ligated and transected while the third is left intact [101]. Animals were anesthetized via isoflurane insufflation. Once unconscious (confirmed by toe pinch reflex), hair was removed from the left hindleg before being stabilized via surgical pins (tissue was not pierced). The incision site was cleaned with three alternating washes of chlorohexidine and iodine solution. A 2-cm incision was made through the skin at the mid-thigh level. The biceps and semitendinosus muscles were gently teased apart using forceps, exposing the sciatic nerve. The peroneal and sural nerves were tightly ligated with 6-0 silk suture while the tibial nerve was left intact. The ligated nerves were then transected distal to the ligature and 2 mm of each branch distal to the nerve stump were removed to confirm complete transection. The muscles were repositioned back over the nerve and the skin wound closed via surgical clips. The animals were then placed in a cage on a heating pad until they woke before being returned to their home cage. Total time unconscious was approximately 20 minutes. Animals were monitored daily to ensure the wound remained sealed and clean. Surgical clips were removed 6 days post-surgery. Responses of both the ipsilateral and contralateral hindpaws to mechanical stimulation in the filamentous von Frey assay were tested at baseline (1 to 3 days prior to SNI surgery), and Days 1, 7, and 14 after surgery. Due to the length of time of each surgery, the 40 total mice were tested in 4 cohorts. The first cohort had 7 WT and 6 *Dgki*$^{-/-}$ males, the second had 5 WT and 5 *Dgki*$^{-/-}$ males, the third had 5 WT and 3 *Dgki*$^{-/-}$ females, and the fourth had 5 WT and 4 *Dgki*$^{-/-}$ females.

Primary DRG neuron culture

Similar to previous work [124], DRGs were dissected from 4- to 8-week-old male and female WT, *Dgki*$^{-/-}$, or *Dgkh*$^{-/-}$ mice and placed into a 1.5-mL microcentrifuge tube containing 1 mL of calcium- and magnesium-free Hank's balanced salt solution (HBSS; 14175-145, Gibco; 400 mg/L KCl, 60 mg/L KH_2PO_4, 350 mg/L $NaHCO_3$, 8 g/L NaCl, 48 mg/L Na_2HPO_4, 1 g/L D-glucose) on ice. After a quick spin, HBSS was gently removed and replaced with 1 mL of a solution of 2 mg/mL collagenase (CLS1, Worthington Biochemical, Lakewood, New Jersey) and 5 mg/mL dispase (17105-041, Gibco) in HBSS. The tube was placed in a 37°C water bath for 30 min, inverting every 5 min. At 20 min, DRGs were triturated with a flame-polished glass Pasteur pipette, then returned to the water bath. At 30 min, the 1-mL DRG suspension was mixed with 1 mL of 37°C supplemented media containing Neurobasal A (10888, Gibco), 0.5% B-27 (17504, Gibco), 100 U/mL penicillin/streptomycin (15140, Gibco), 2 mM L-glutamine (25030, Gibco), 50 ng/mL glial derived neurotrophic factor (GF030, Millipore), and 25 ng/mL nerve growth factor (01-125, Millipore). The 2-mL DRG suspension was triturated with a fresh Pasteur pipette and placed on a pre-moistened 70 μm filter (22-363-548, Thermo Fisher). The filtrate was spun at 1000 × g for 5 min at room temperature. The supernatant was carefully removed, and the pellet was resuspended in 37°C supplemented media with a fresh Pasteur pipette. For the ERK assays, the supplemented media did not contain growth factors.

For calcium imaging assays, neurons were plated onto 12-mm diameter coverslips (354087, Corning) that were precoated with 1 mg/mL poly-D-lysine (P7886, Sigma) and 10 μg/mL laminin (L2020, Sigma), prewarmed to 37°C, and each placed in a well of a 24-well plate. Using a pipette with a plastic tip, 90 μL of the cell suspension was plated onto each coverslip, 7-12 coverslips/mouse. After 1-2 h, 410 μL of 37°C supplemented media was added to each well. For the ERK phosphorylation assays, neurons were plated into a 12-well plate precoated with poly-D-lysine and laminin and prewarmed to 37°C. Using a pipette with a plastic tip, 500 μL of

the cell suspension was plated into each well, 6 wells/mouse. DRGs from WT and knockout mice were plated on the same 12-well plate.

Cells were kept a 37°C incubator with 5% CO_2 and used for assays within 24 hours. For each preparation, DRGs from one WT and one *Dgki*$^{-/-}$ or *Dgkh*$^{-/-}$ mouse (age- and sex-matched) were dissected and cultured concurrently and were plated at equal densities.

DRG calcium imaging

Prior to imaging, neurons were washed and loaded with Fura-2, AM in the same manner as described in the methods of the previous chapter for HEK293 cell calcium imaging. The same imaging equipment was used, except for coverslips were placed in a chamber (Model RC-26GLP, Warner Instruments, Hamden, Connecticut) mounted on microscope stage adapter. The same excitation/emission parameters were used for imaging, except for there was no use of the RFP channel. Instead of manually changing the buffers, the coverslips were perfused with 30°C buffers (heated with SH-27B inline heater, Warner Instruments) at a flow rate of 4.2 mL/min (using a Minipuls 3 Peristaltic Pump, Gilson, Middleton, Wisconsin). After collecting 90 s of baseline Fura-2 ratios while perfusing with assay buffer, cells were perfused with agonist for 90 s, followed by assay buffer for 120 s, then 100 mM KCl for 30 s to test for neuron health. Agonists and 100 mM KCl solutions were made with assay buffer.

For analysis, we calculated the Fura-2 ratio (ratio of the emission following excitation at 340 nm/380 nm). We excluded cells that had high baseline Fura-2 ratios (>1.0) or failed to respond to KCl (did not reach ratio of at least 1.0 during KCl exposure). To normalize to baseline, the 60 s of Fura-2 ratios measured immediately preceding agonist exposure were averaged for a given cell, and that average was subtracted from each data point for that cell throughout the whole assay period. Only cells that responded to agonist (had a minimum increase in Fura-2 ratio of 0.1 over baseline average for 2 consecutive time points during period of agonist exposure) were included in our analyses. Area-under-the-curve (AUC) values were

calculated on a cell-by-cell basis, using the baseline-normalized values, for the 90-s period of agonist exposure.

DRG cultures from one WT and one *Dgki*$^{-/-}$ or *Dgkh*$^{-/-}$ mouse were tested each day, alternating coverslips in a random order. For histamine, we used 1 male and 2 female mice each for WT and *Dgki*$^{-/-}$ (6 mice total) and 2 males and 1 female each for WT and *Dgkh*$^{-/-}$. For capsaicin, we used 2 males each for WT and *Dgki*$^{-/-}$ and 1 male each for WT and *Dgkh*$^{-/-}$. For LPA, we used 2 males and 1 female each for WT and *Dgki*$^{-/-}$ and 2 males and 1 female each for WT and *Dgkh*$^{-/-}$. For UTP, we used 4 males each for WT and *Dgki*$^{-/-}$ and 1 male each for WT and *Dgkh*$^{-/-}$. Results from mice of both sexes were combined for each genotype (WT samples tested concurrently with *Dgki*$^{-/-}$ samples were combined, and WT samples tested with *Dgkh*$^{-/-}$ samples were combined). The number of healthy neurons and the numbers of neurons responding to agonist that we analyzed are indicated in Figure 3.15.

DRG ERK phosphorylation assay

ERK phosphorylation induced by nerve growth factor (NGF) in cultured DRG neurons was tested similarly to [126]. For testing *Dgki*$^{-/-}$ DRG neurons, cultures were prepared from 2 WT and 2 *Dgki*$^{-/-}$ 6-week-old males, dissected and cultured concurrently. For testing *Dgkh*$^{-/-}$ DRG neurons, cultures were prepared from 2 WT and 2 *Dgkh*$^{-/-}$ 4-week-old males, dissected and cultured concurrently. Before plating, neurons from the 2 mice of the same genotype were combined before plating into 12 wells. For the ERK assay, we used the same supplemented media as was used for DRG culturing (no growth factors). On the day of the assay, media was removed and replaced with 500 µL of 37°C supplemented media containing no NGF (baseline) or containing 100 ng/mL NGF (01-125, Millipore). Cells were incubated in NGF for 2, 5, or 10 min. Cells were incubated in the baseline control for 5 min. Cells were immediately washed with ice-cold HBSS (see “Primary DRG neuron culture” above). We removed the HBSS, added 100 µL of lysis buffer to each well, and froze plate at -80°C.

The next day, the plate was thawed and cells were scraped into lysis buffer (same as kinase assay lysis buffer above), and the contents of each well were collected into individual microcentrifuge tubes. Following sonication on ice for 10 s, lysates were centrifuged at 10,000 × g at 4°C for 15 min to separate the debris. Protein (20 µg) was run on duplicate westerns, following the same protocol from Chapter 2 above, using the following primary antibodies: 1:3,000 mouse anti-ACTB (ab6276, Abcam) and either 1:1,000 rabbit anti-ERK1/2 (4695S, Cell Signaling Technology, Danvers, Massachusetts) or 1:1,000 rabbit anti-phosphorylated-ERK1/2 (4370S, Cell Signaling Technology).

For each test day (*Dgki*$^{-/-}$ or *Dgkh*$^{-/-}$) there were triplicates of the 8 genotype × NGF conditions; we ran 3 pairs of westerns, each with 1 of the 3 triplicate samples of the 8 conditions. To quantify ERK phosphorylation, the intensity of both ERK1/2 bands for each sample were quantified together, as were both p-ERK1/2 bands for each sample. The ERK1/2 and p-ERK1/2 intensities were normalized to the actin band on the respective blot. The ratio of [(p-ERK1/2 / ACTB) / (ERK1/2 / ACTB)] was calculated to represent the amount of ERK phosphorylation in each sample.

DRG kinase activity assay

Assay was performed similarly to the HEK293 kinase activity assay protocol described in the methods of the previous chapter. Instead of HEK293 cells, we used protein isolated from DRGs that were dissected from 1- to 5-month-old WT, *Dgki*$^{-/-}$, *Dgkh*$^{-/-}$, and dKO male and female mice (age- and sex-matched on the day of testing). DRGs were dissected into HBSS (recipe under “Primary DRG neuron culture” above) on ice. Following DRG dissection, HBSS was removed, protein was isolated, and lysates were immediately used in the kinase assay.

Statistics

Data were analyzed with GraphPad Prism version 7.04. WT vs. mutant (*Dgki*$^{-/-}$, *Dgkh*$^{-/-}$, and dKO) responses (by sex) in all baseline pain assays were tested for significance using two-tailed t-tests with Welch's correction, as were WT vs. mutant AUC responses in calcium activity assays and WT vs. mutant ERK phosphorylation. For each sex, scratching responses to pruritogens, von Frey or Hargreaves responses in the CFA model, and von Frey responses in the SNI model were compared between WT and mutant using Sidak's multiple comparisons tests used for pairwise comparisons within each 5-min time bin (pruritogens), day (CFA), or filament (SNI) within two-way repeated measures analysis of variance (ANOVA) tests.

FIGURES

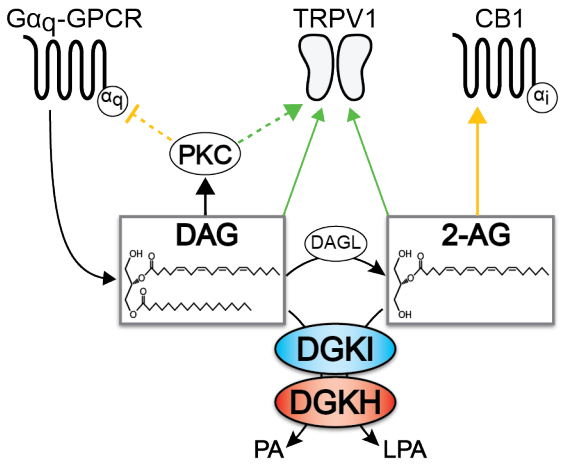

Figure 3.1. Diacylglycerol (DAG) and 2-arachidonoylglycerol (2-AG) regulate signaling in DRG neurons. DAG and 2-AG modulate activity of important secondary messengers and receptors. DGKI and DGKH terminate DAG and 2-AG signaling via phosphorylation. Green pathways promote itch/pain, orange pathways inhibit itch/pain.

A

Tissue	Relative *Dgki* expression
Mast cells	27.02
Dorsal root ganglia	12.59
Dorsal striatum	8.74
Olfactory bulb	3.75
Nucleus accumbens	3.52
Hippocampus	3.44
Spinal cord	3.10
Cerebral cortex	3.05
Natural killer cells	2.82
Amygdala	2.22

B

Tissue	Relative *Dgkh* expression
Dorsal root ganglia	95.62
Testis	31.46
Pituitary	9.53
Hippocampus	9.27
Large intestine	8.06
Nucleus accumbens	6.59
Dorsal striatum	6.38
Macrophage, bone marrow	6.19
Cebrebral cortex	6.17
Lung	4.66

Table 3.1. Expression of *Dgki* and *Dgkh* in mouse tissues. Microarray data reveal the murine tissues with the highest expression levels of *Dgki* (A) or *Dgkh* (B).

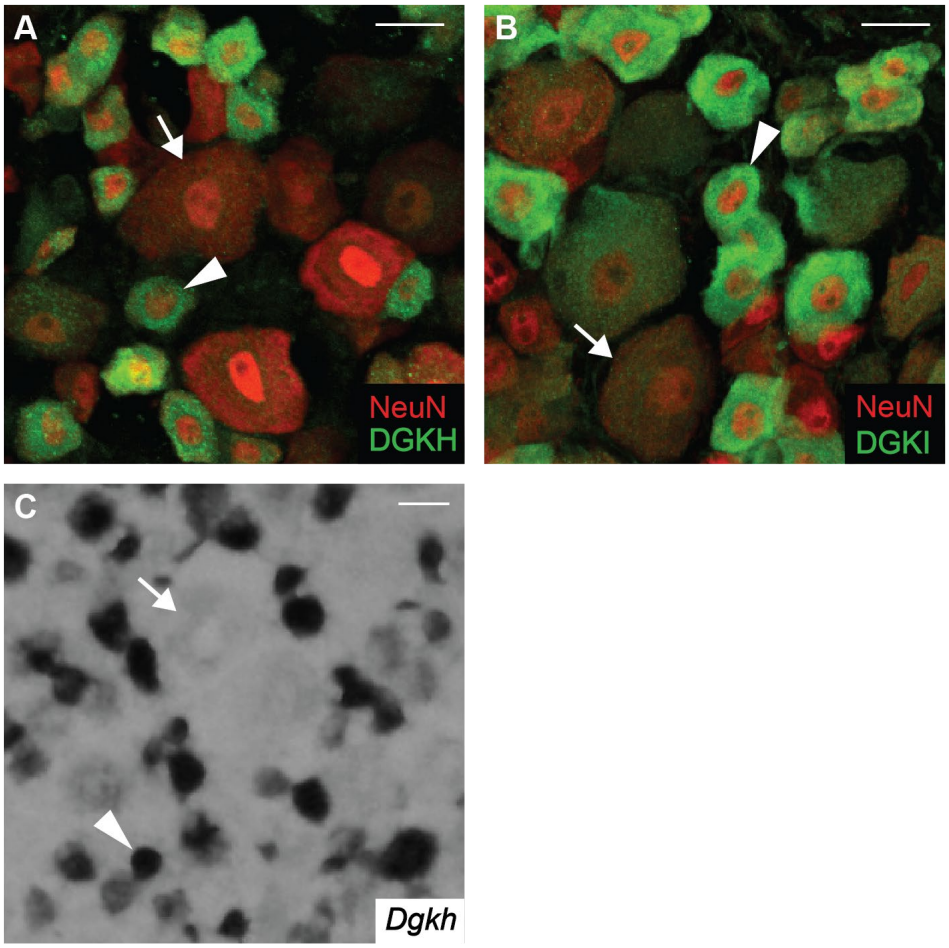

Figure 3.2. DGKH and DGKI are enriched in small-diameter DRG neurons. A-B) Protein immunohistochemical staining shows that DGKH (A) or DGKI (B) expression is cytoplasmic and is higher in small-diameter (arrowheads) than in large-diameter (arrows) mouse DRG neurons. C) In situ hybridization shows that Dgkh RNA has a similar expression pattern to DGKH protein. Scale bar = 20 μm.

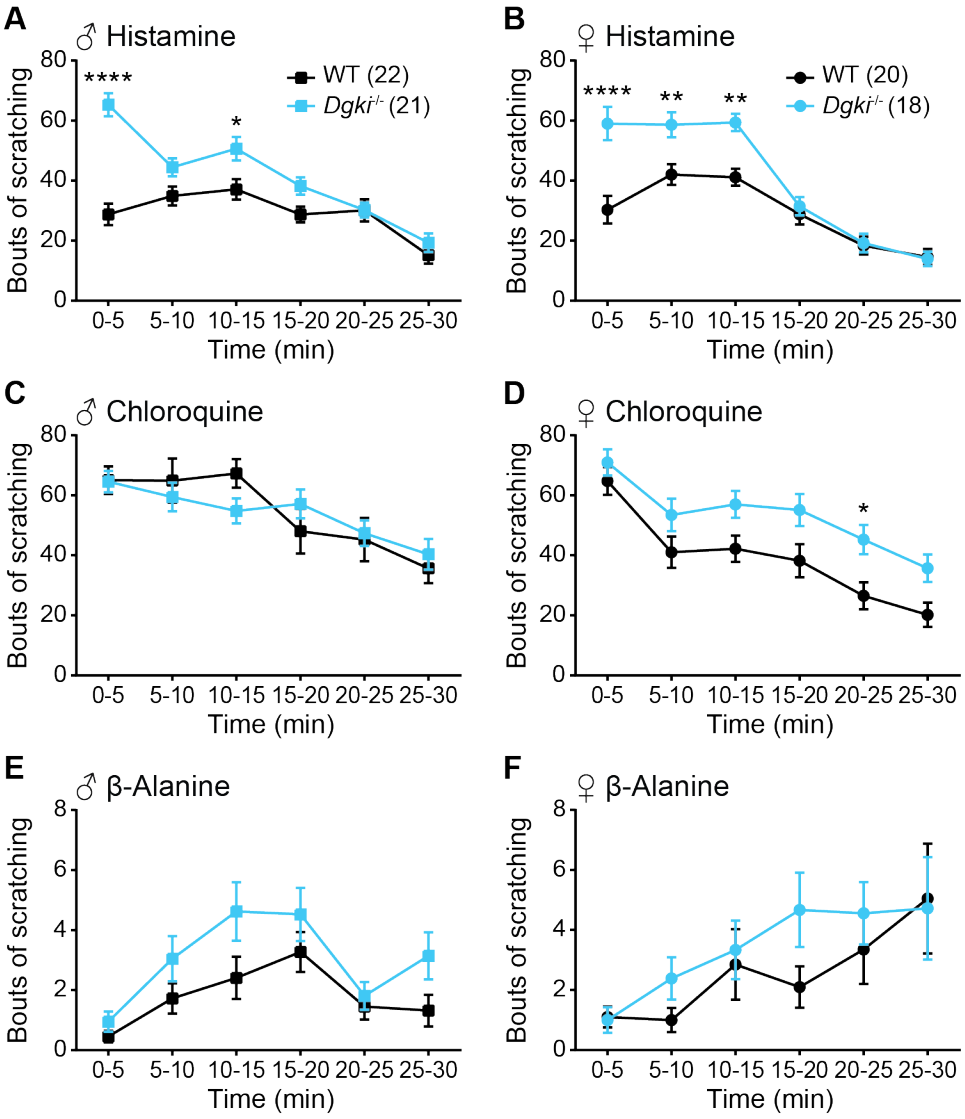

Figure 3.3. Loss of *Dgki* enhances histamine-induced scratching in male and female mice. An acute scratching assay was used to test itch responses in *Dgki*$^{-/-}$ mice following an injection of 500 ug histamine (A-B), 200 ug chloroquine (C-D), or 500 ug β-alanine (E-F) in WT and *Dgki*$^{-/-}$ male (A,C,E) and female (B,D,F) mice in 5-min intervals for 30 min. Data represent mean ± SEM. Number of mice for all assays indicated on graphs in (A) and (B). p< *0.05, **0.01, ****0.0001 vs. WT at individual time point.

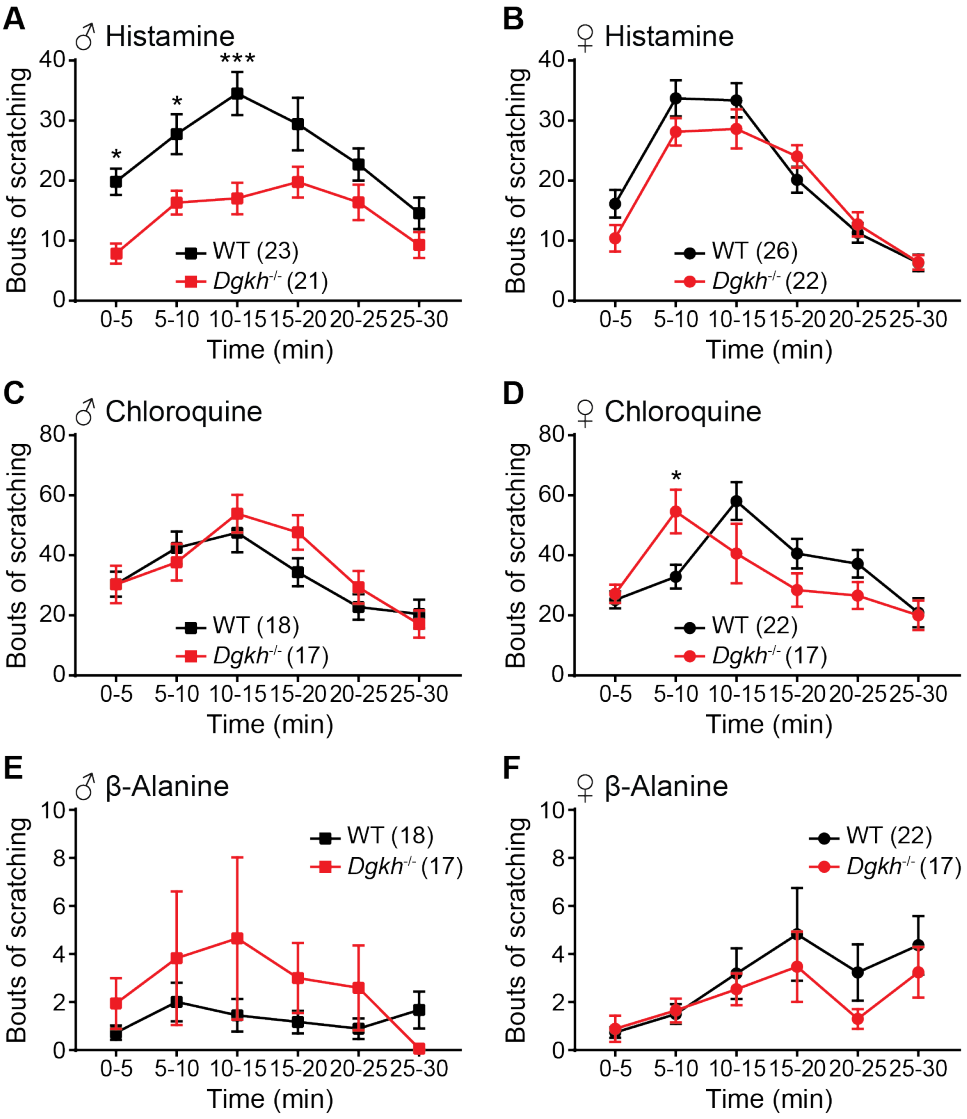

Figure 3.4. Loss of *Dgkh* reduces histamine-induced scratching in male mice. An acute scratching assay was used to test itch responses in *Dgkh*$^{-/-}$ mice following an injection of 500 ug histamine (A-B), 200 ug chloroquine (C-D), or 500 ug β-alanine (E-F) in WT and *Dgkh*$^{-/-}$ male (A,C,E) and female (B,D,F) mice in 5-min intervals for 30 min. Data represent mean ± SEM. Number of mice for all assays indicated on graphs in (A) and (B). p< *0.05, ***0.001 vs. WT at individual time point.

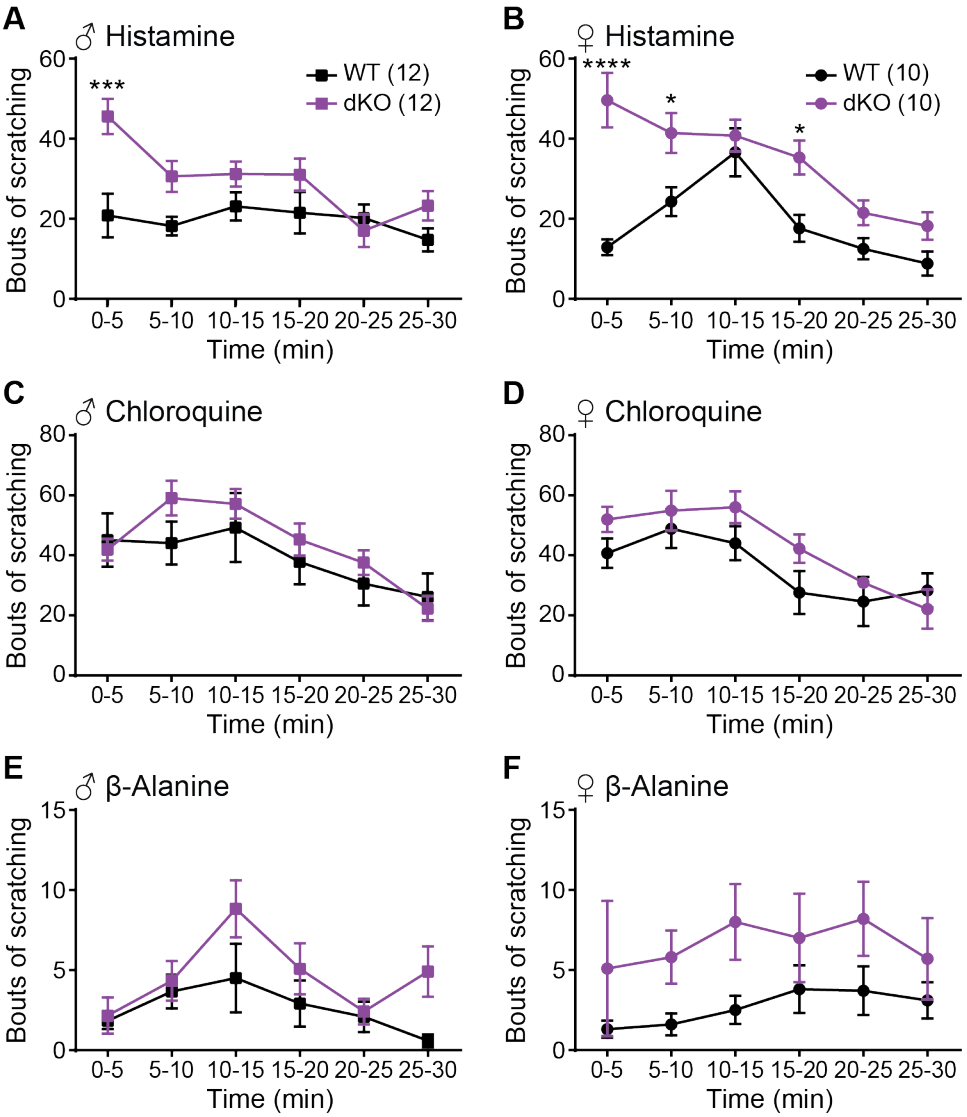

Figure 3.5. Loss of both *Dgki* and *Dgkh* enhances histamine-induced scratching in male and female mice. An acute scratching assay was used to test itch responses in dKO mice following an injection of 500 ug histamine (A-B), 200 ug chloroquine (C-D), or 500 ug β-alanine (E-F) in WT and dKO male (A,C,E) and female (B,D,F) mice in 5-min intervals for 30 min. Data represent mean ± SEM. Number of mice for all assays indicated on graphs in (A) and (B). p< *0.05, ***0.001, ****0.0001 vs. WT at individual time point.

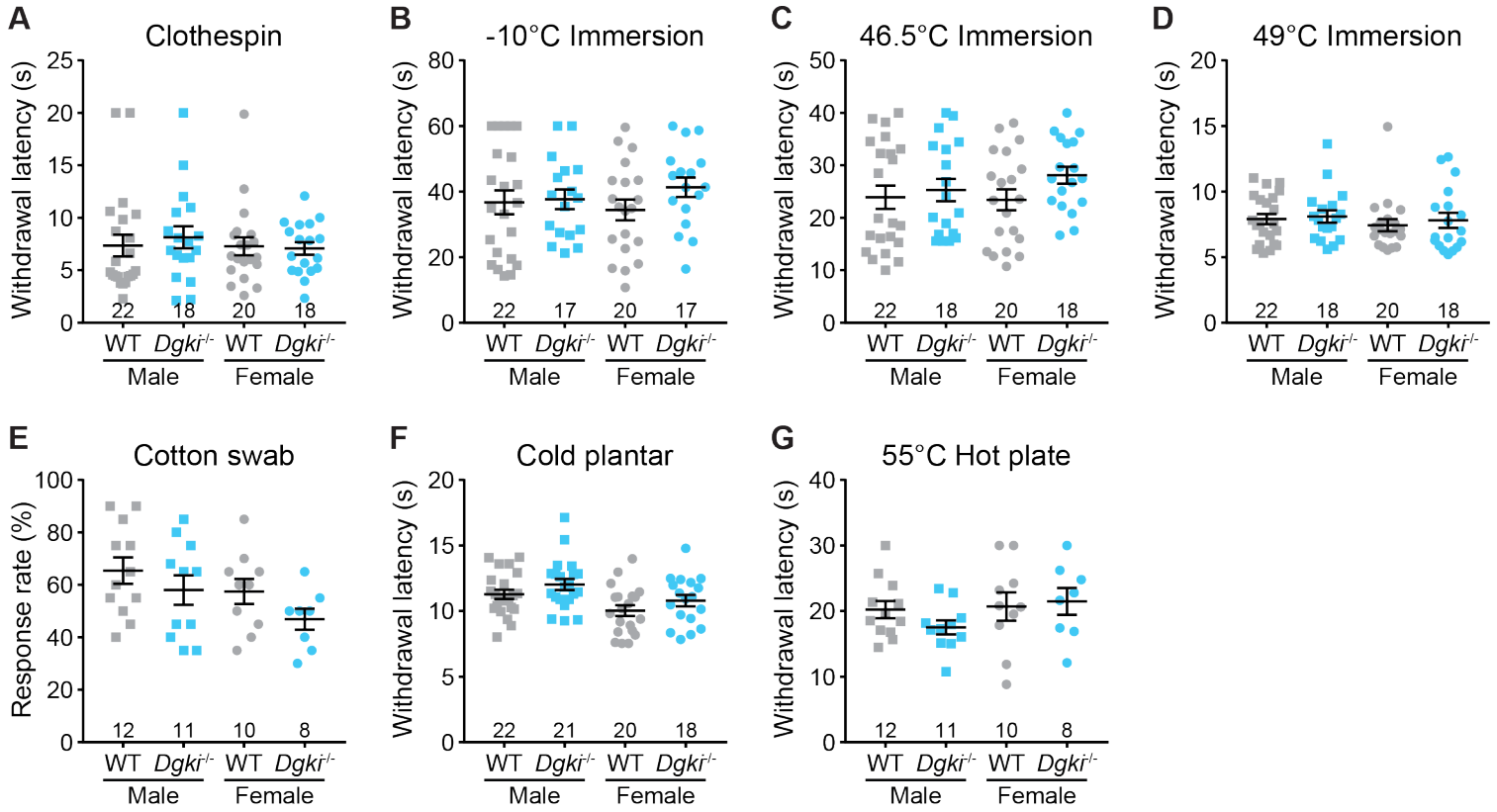

Figure 3.6. Loss of *Dgki* does not alter acute pain sensitivity in mice. A) The latency to respond to a small clothespin attached to the tail. B-D) The latency to respond to immersion of the tail in a bath set to a temperature of -10°C (B), 46.5°C (C), or 49°C (D). E) The rate of response to a light touch with a fluffed-out cotton swab. F-H) The latency to withdraw the hindpaw from an application of dry ice (F). Latency to lick hindpaw or jump after placement on a 55°C hot plate (G). Data represent mean ± SEM. Number of mice indicated on graphs.

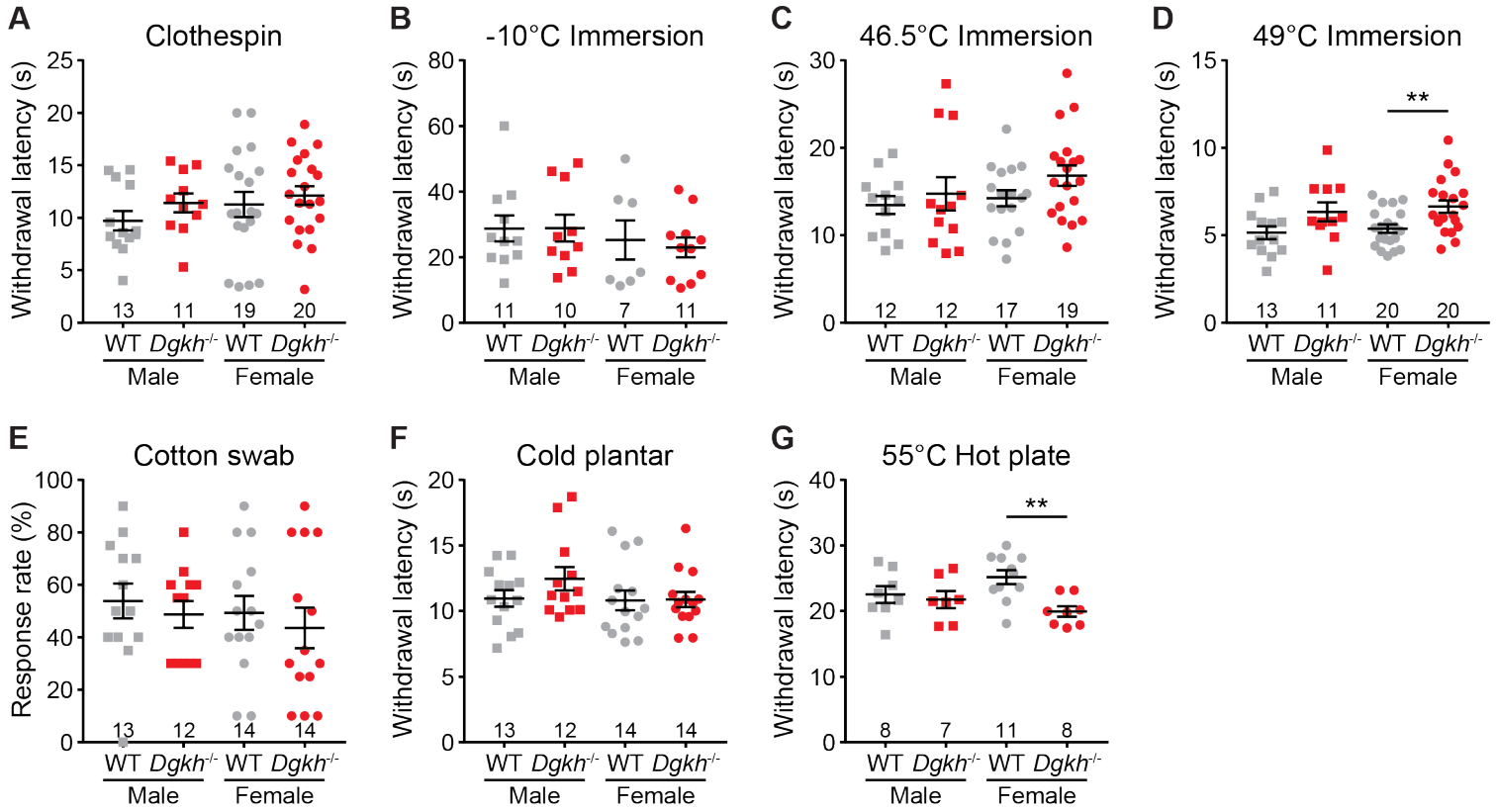

Figure 3.7. Loss of *Dgkh* alters some acute pain sensitivity metrics in mice. A) The latency to respond to a small clothespin attached to the tail. B-D) The latency to respond to immersion of the tail in a bath set to a temperature of -10°C (B), 46.5°C (C), or 49°C (D). E) The rate of response to a light touch with a fluffed-out cotton swab. F-H) The latency to withdraw the hindpaw from an application of dry ice (F). Latency to lick hindpaw or jump after placement on a 55°C hot plate (G). Data represent mean ± SEM. Number of mice indicated on graphs. **p<0.01 vs. WT.

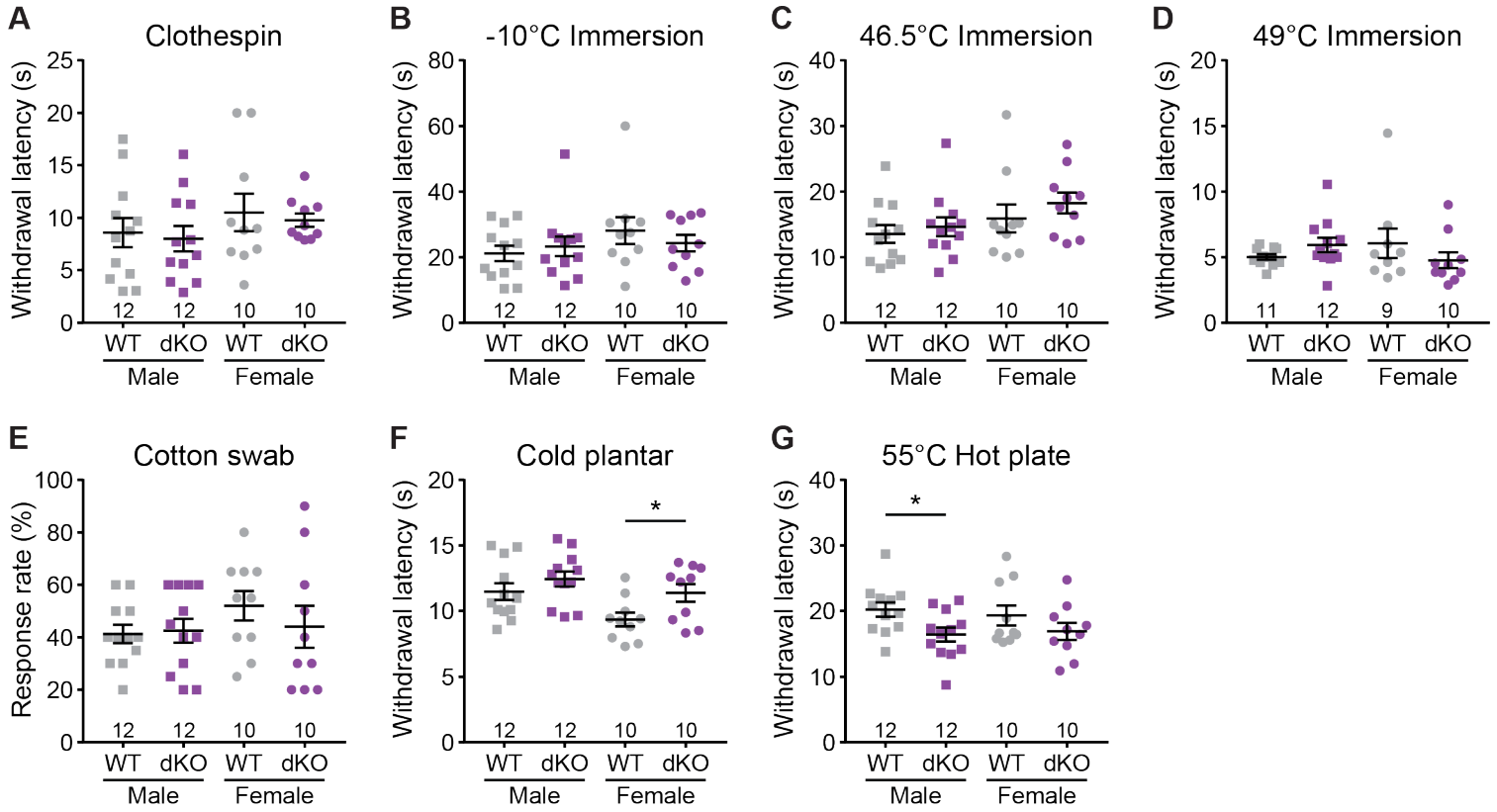

Figure 3.8. Loss of both *Dgki* and *Dgkh* alters some acute pain sensitivity metrics in mice. A) The latency to respond to a small clothespin attached to the tail. B-D) The latency to respond to immersion of the tail in a bath set to a temperature of -10°C (B), 46.5°C (C), or 49°C (D). E) The rate of response to a light touch with a fluffed-out cotton swab. F-H) The latency to withdraw the hindpaw from an application of dry ice (F). Latency to lick hindpaw or jump after placement on a 55°C hot plate (G). Data represent mean ± SEM. Number of mice indicated on graphs. *p<0.05 vs. WT.

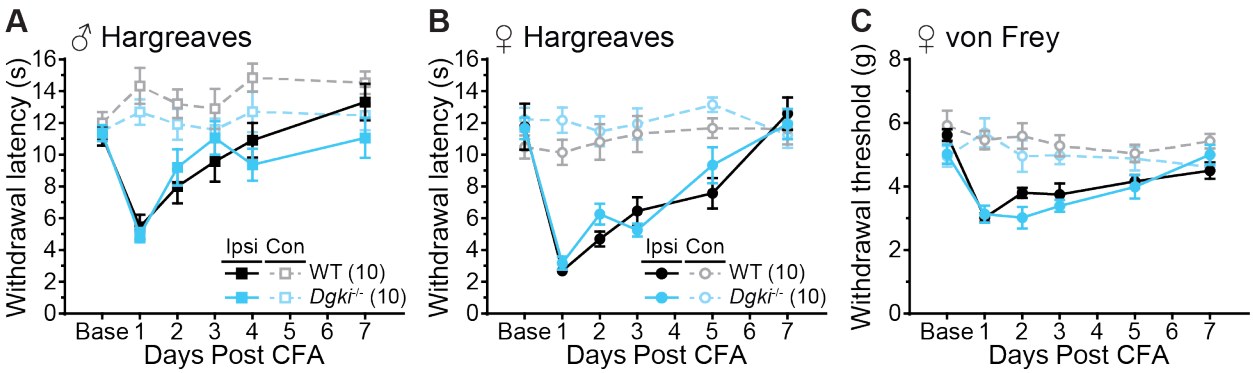

Figure 3.9. Loss of Dgki does not alter sensitization or recovery in the CFA model of chronic inflammatory pain. A-B) Withdrawal latencies to heat in the Hargreaves assay for 1 week following injection of CFA into the plantar surface of the hindpaw in male (A) and female (B) mice. C) Threshold of withdrawal from an electronic von Frey filament pressed to the plantar surface of the hindpaw in female mice. Data represent mean ± SEM. Number of mice indicated on graphs in (A) and (B).

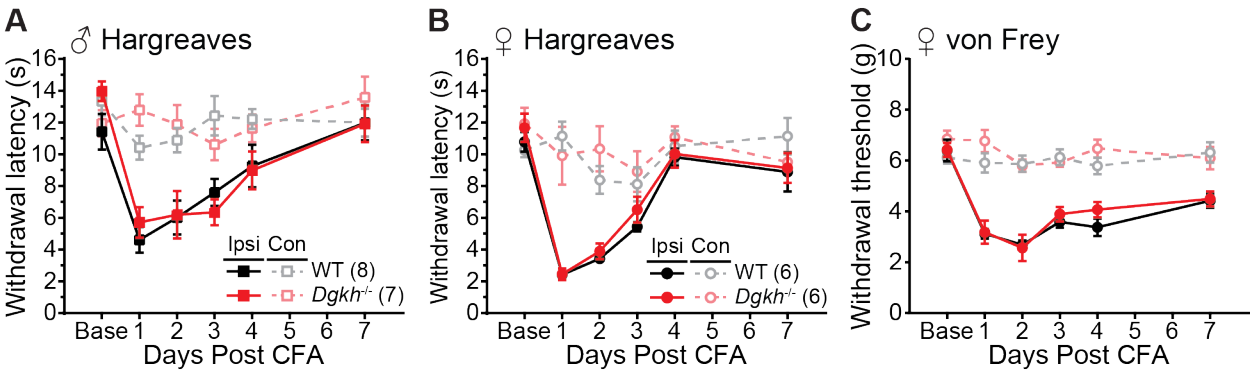

Figure 3.10. Loss of *Dgkh* does not alter sensitization or recovery in the CFA model of chronic inflammatory pain. A-B) Withdrawal latencies to heat in the Hargreaves assay for 1 week following injection of CFA into the plantar surface of the hindpaw in male (A) and female (B) mice. C) Threshold of withdrawal from an electronic von Frey filament pressed to the plantar surface of the hindpaw in female mice. Data represent mean ± SEM. Number of mice indicated on graphs in (A) and (B).

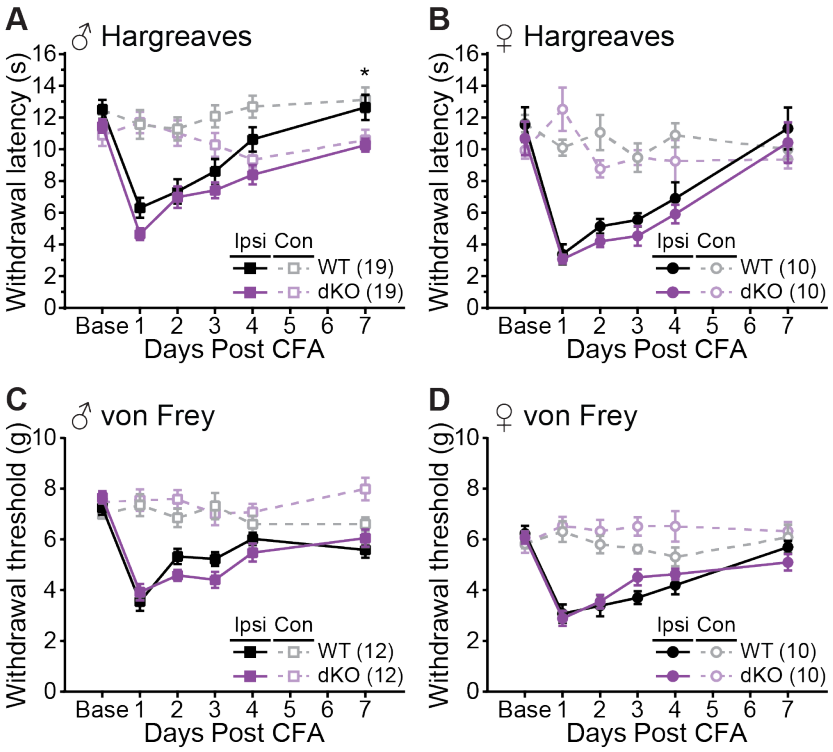

Figure 3.11. Loss of both *Dgki* and *Dgkh* in dKO mice does not alter sensitization or recovery in the CFA model of chronic inflammatory pain. A-B) Withdrawal latencies to heat in the Hargreaves assay for 1 week following injection of CFA into the plantar surface of the hindpaw in male (A) and female (B) mice. C) Threshold of withdrawal from an electronic von Frey filament pressed to the plantar surface of the hindpaw in female mice. Data represent mean ± SEM. Number of mice indicated on graphs. *p<0.05 vs. WT at individual time point in ipsilateral paw.

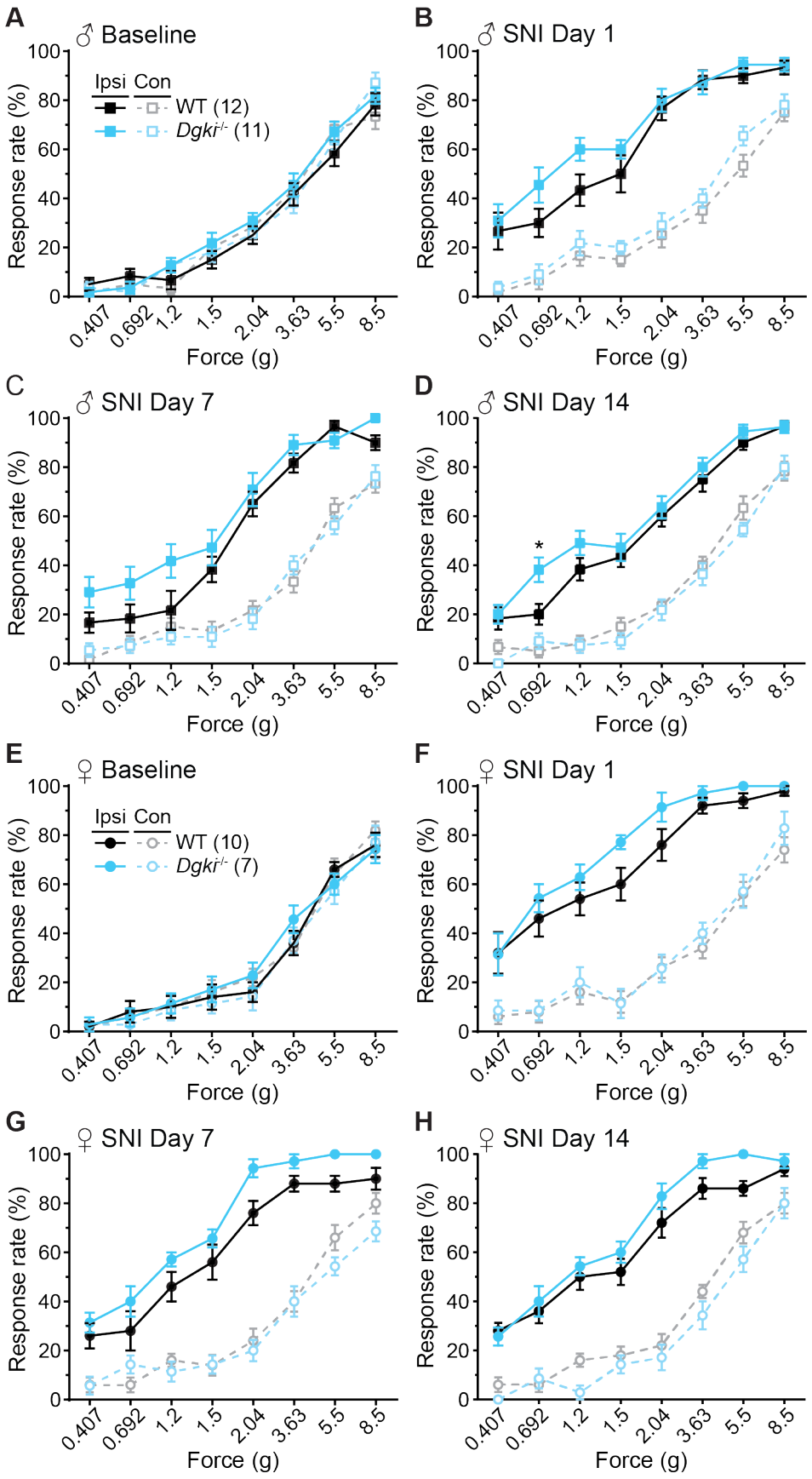
A
♂ Baseline
Ipsi Con
WT (12)
Dgki-/- (11)
B
♂ SNI Day 1
C
♂ SNI Day 7
D
♂ SNI Day 14
*
E
♀ Baseline
Ipsi Con
WT (10)
Dgki-/- (7)
F
♀ SNI Day 1
G
♀ SNI Day 7
H
♀ SNI Day 14
Response rate (%)
Force (g)
0.407
0.692
1.2
1.5
2.04
3.63
5.5
8.5

Figure 3.12. Loss of *Dgki* does not alter sensitization in the SNI model of chronic neuropathic pain. Response rates to von Frey filaments of the indicated forces pressed into the plantar surface of the hindpaw in male (A-D) and female (E-H) WT and *Dgki*$^{-/-}$ mice at baseline (A,E) and 1 (B,F), 7 (C,G), and 14 (D,H) days after SNI. Data represent mean ± SEM. Number of mice indicated on graphs in (A) and (E). *$p<0.05$ vs. WT at individual time point in ipsilateral paw.

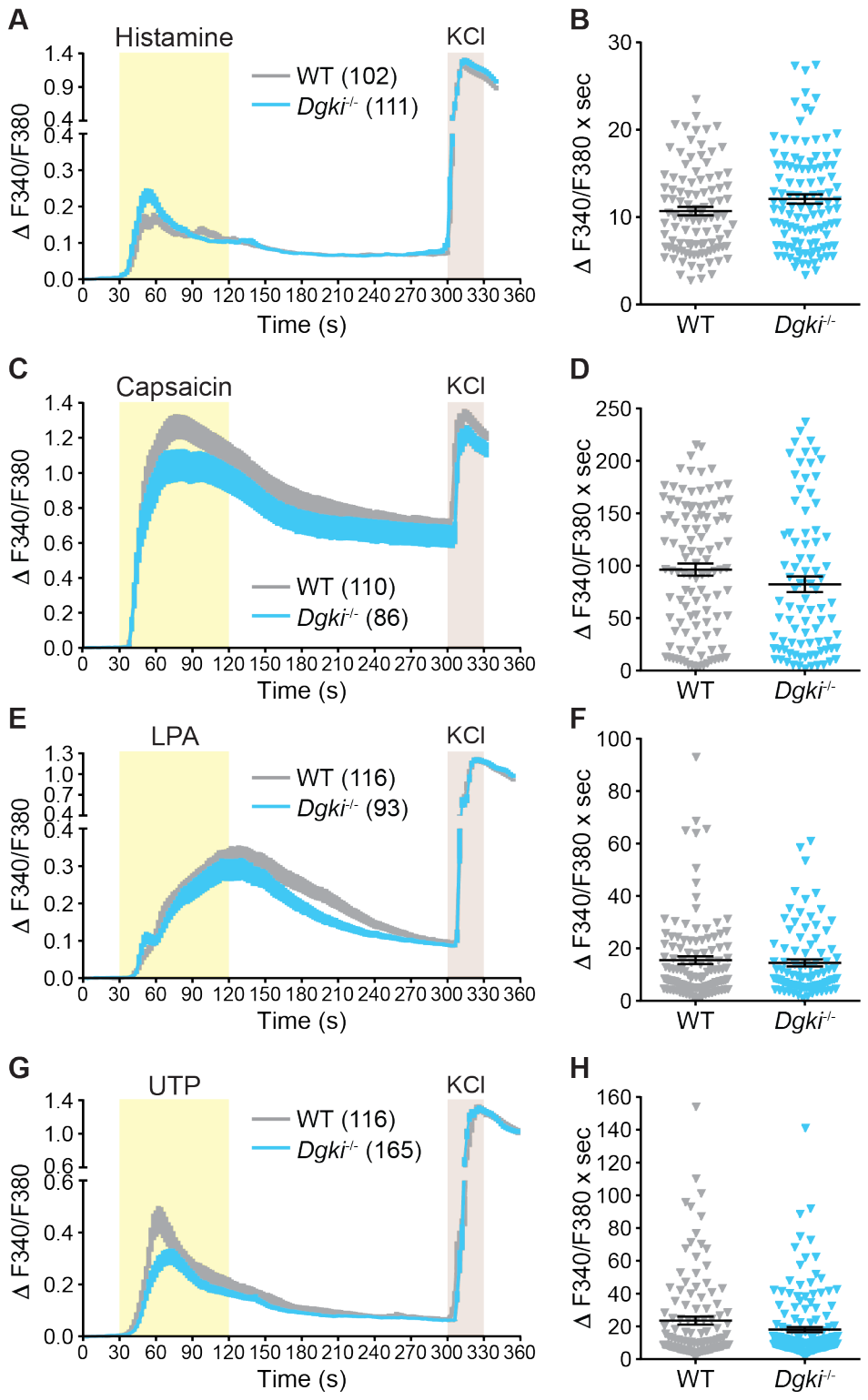

Figure 3.13. *In vitro* calcium responses to pruritogenic or algogenic agonists in cultured mouse DRG neurons are unchanged after *Dgki* loss. Calcium activity of DRG neurons dissected and cultured from WT and *Dgki*$^{-/-}$ mice in response to 100 μM histamine (A,B), 1 μM capsaicin (C,D), 10 μM LPA (E,F), or 100 μM UTP (G,H). Each experiment ended with exposure

to 100 mM KCl to ensure neuron health. Average calcium responses in WT and *Dgki*$^{-/-}$ DRG neurons over time are shown in (A), (C), (E), and (G). The AUC for the 90 s of agonist exposure was calculated for each neuron, plotted in (B), (D), (F), and (H). Data represent mean ± SEM. Number of neurons indicated on graphs in (A), (C), (E), and (G).

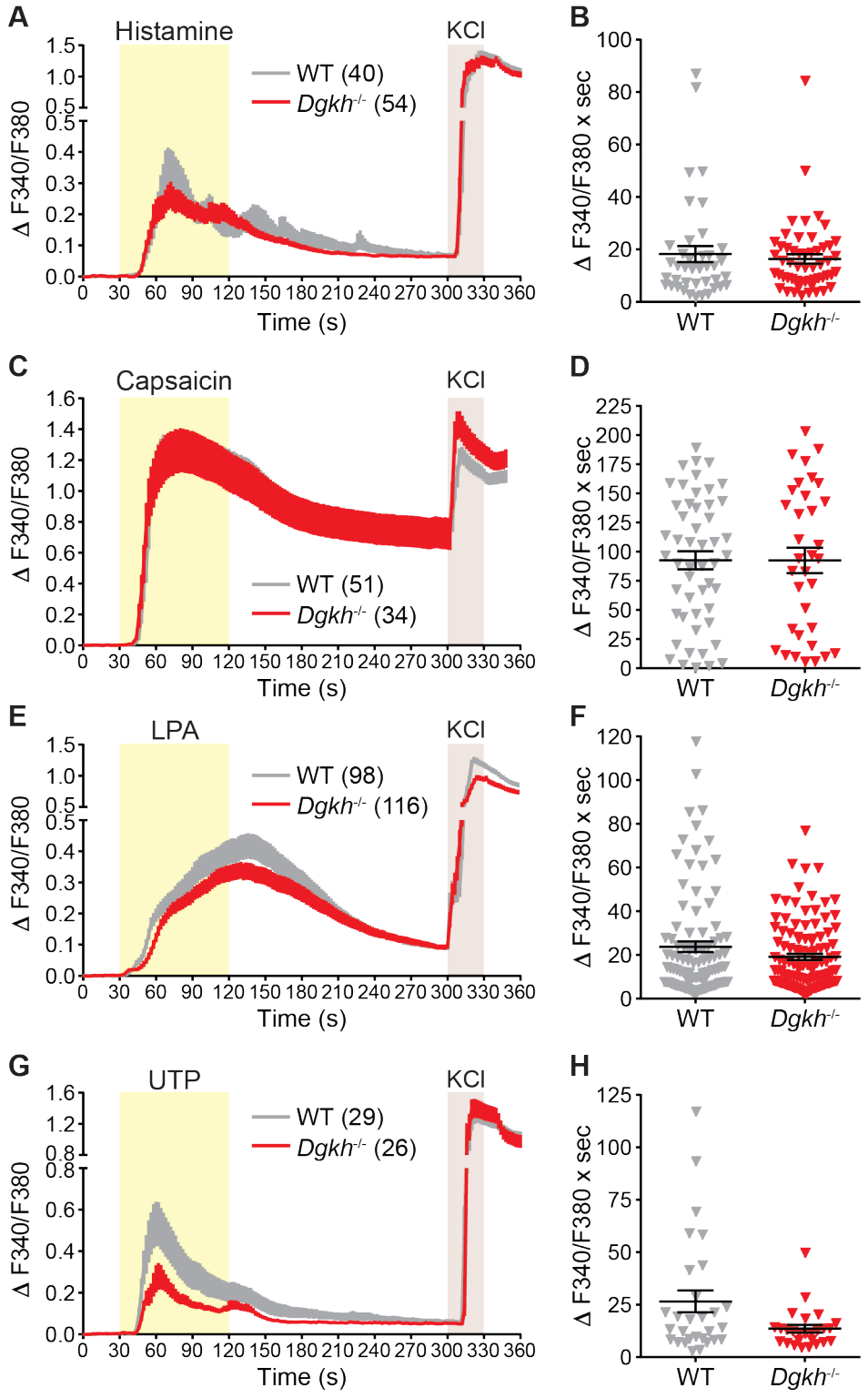

Figure 3.14. *In vitro* calcium responses to pruritogenic or algogenic agonists in cultured mouse DRG neurons are unchanged after *Dgkh* loss. Calcium activity of DRG neurons dissected and cultured from WT and *Dgkh*$^{-/-}$ mice in response to 100 μM histamine (A,B), 1 μM capsaicin (C,D), 10 μM LPA (E,F), or 100 μM UTP (G,H). Each experiment ended with exposure

to 100 mM KCl to ensure neuron health. Average calcium responses in WT and *Dgkh*$^{-/-}$ DRG neurons over time are shown in (A), (C), (E), and (G). The AUC for the 90 s of agonist exposure was calculated for each neuron, plotted in (B), (D), (F), and (H). Data represent mean ± SEM. Number of neurons indicated on graphs in (A), (C), (E), and (G).

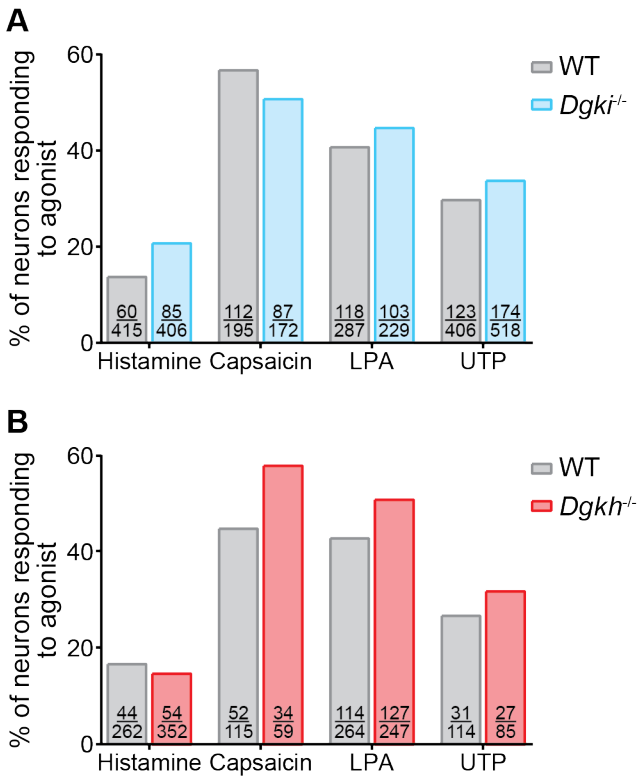

Figure 3.15. Response rate of mouse DRG neurons to pruritogens and algogens is not changed by deletion of *Dgki* or *Dgkh*. Of all healthy neurons (neurons responding to KCl), the proportion of neurons responding to the indicated agonists (same as Figure 3.13Figure 3.14) did not vary between WT and *Dgki*$^{-/-}$ (A) or between WT and *Dgkh*$^{-/-}$ (B) DRG cultures. On each bar, the top number indicates the number of neurons responding to the agonist and the bottom number indicates the total number of healthy neurons.

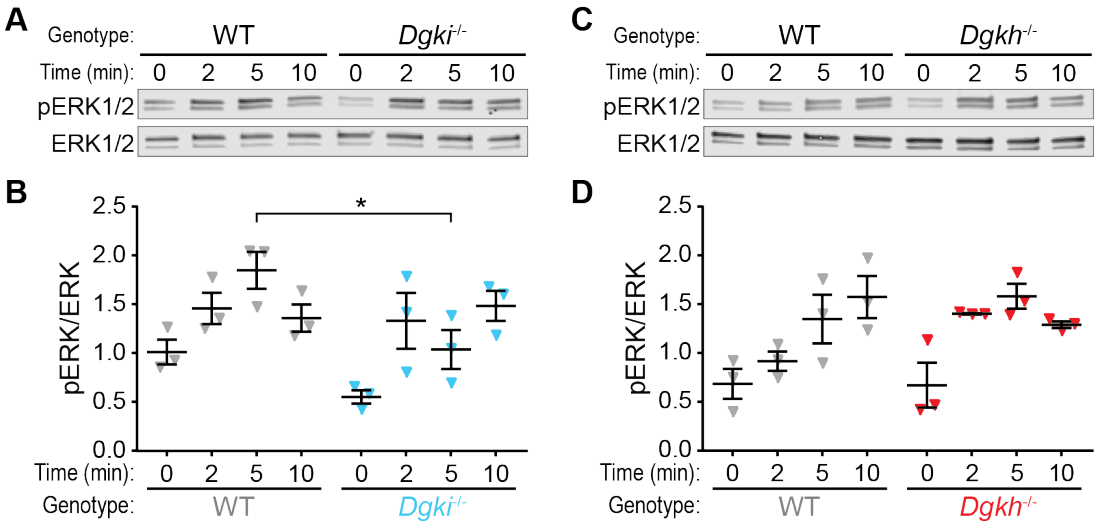

Figure 3.16. NGF-induced ERK phosphorylation in cultured DRG neurons is slightly diminished by loss of *Dgki*, but not *Dgkh*. DRG neurons cultured from WT or *Dgki*$^{-/-}$ (A-B) or WT or *Dgkh*$^{-/-}$ (C-D) mice were stimulated with NGF for 0, 2, 5, or 10 min and ERK phosphorylation was measured. A,C) Western blots show the presence of phosphorylated ERK (pERK1/2) and total ERK (ERK1/2) in protein isolated from NGF-stimulated DRG cultures. Ratio of pERK1/2 to total ERK1/2 was quantified for each time point, as shown in (B) and (D). Data represent mean ± SEM. N = 3 for each time point. *p<0.05 vs. WT at same time point.

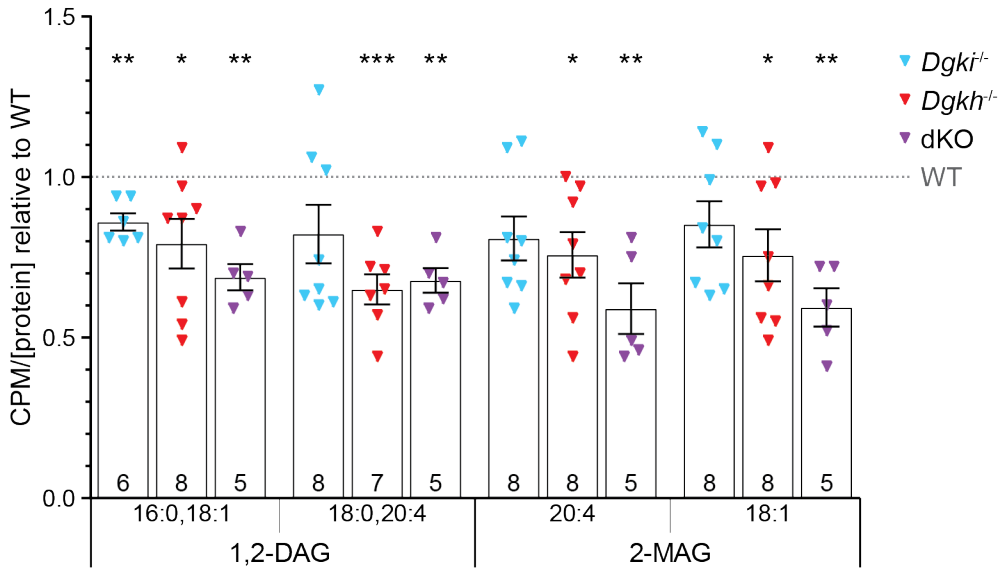

Figure 3.17. Phosphorylation of DAG and MAG substrates by DRG lysates is reduced in the absence of *Dgki* and/or *Dgkh*. CPM of ^{32}P-PA or ^{32}P-LPA produced when the indicated lipid substrates were combined in a reaction (see Figure 2.2A) with lysates from *Dgki*$^{-/-}$, *Dgkh*$^{-/-}$, or dKO DRGs, relative to the CPM of reactions with WT DRG lysates (gray line). All CPM values were normalized to the protein level of the sample before the relative difference from the RFP was calculated. Data represent mean ± SEM. Number of samples indicated on graph. *p<0.05, **p<0.01, ***p<0.001 vs. WT for indicated substrate.

A

	Modality	Stimulus site	Stimulus	*Dgki*$^{-/-}$ ♂	*Dgki*$^{-/-}$ ♀	*Dgkh*$^{-/-}$ ♂	*Dgkh*$^{-/-}$ ♀	dKO ♂	dKO ♀
in vivo	Itch	Back	Histamine						
		Back	Chloroquine						
		Back	β-Alanine						

B

	Modality	Stimulus site	Stimulus	*Dgki*$^{-/-}$ ♂	*Dgki*$^{-/-}$ ♀	*Dgkh*$^{-/-}$ ♂	*Dgkh*$^{-/-}$ ♀	dKO ♂	dKO ♀
in vivo	Pain – Cold	Tail	-10°C						
		Hindpaw	Cold plantar						
	Pain – Hot	Tail	46.5°C						
		Tail	49°C						
		Hindpaw	55°C						
		Hindpaw	Hargreaves						
	Pain – Mechanical	Tail	Clothespin						
		Hindpaw	von Frey						

C

	Modality	Stimulus site	Stimulus	*Dgki*$^{-/-}$	*Dgkh*$^{-/-}$	dKO
in vitro	Kinase activity – DAG	DRG	16:0,18:1			
		DRG	18:0,20:4			
	Kinase activity – MAG	DRG	20:4			
		DRG	18:1			

Legend

Direction of effect	Cell color	Statistical significance
Larger response than WT		p<0.0001
		p<0.001
		p<0.01
		p<0.05
Smaller response than WT		p<0.05
		p<0.01
		p<0.001
		p<0.0001

Table 3.2. Summary of sensory phenotypes in *Dgk* model mice relative to WT mice.
A) Subcutaneous injection of pruritogenic compounds in the back induced differential scratching responses in *Dgk* mouse models. The color intensity of each cell coordinates to the 5-min bin which had the greatest difference from WT over 30 min. B) Applications of noxious cold, noxious heat, or noxious mechanical stimuli on the tail or hindpaw of *Dgk* model mice induced slightly different responses relative to WT mice. C) DRG lysates from *Dgk* mouse models had decreased phosphorylation of DAG and/or MAG substrates *in vitro* relative to WT DRG lysates.

CHAPTER 4: DGKI AND DGKH REGULATE MATERNAL CARE AND PSYCHOPATHOLOGICAL BEHAVIORS IN MICE

INTRODUCTION

Psychiatric disorders

Psychiatric disorders can severely impair affect, energy, cognition, and quality of life. These include mood disorders, such as anxiety and bipolar disorder (BPD), as well as cognitive disorders, such as attention deficit hyperactivity disorder (ADHD). Each condition is defined by unique features, but many also have overlapping symptoms and pathologies. Patients with depression suffer from anhedonia and severe fatigue [127], and those with BPD endure additional manic episodes of impulsivity, irritability, and goal-directed and risk-taking behaviors [128-131]. ADHD also features impulsivity, along with hyperactivity and an inability to focus [132]. Anxiety imparts both fatigue and an enduring sense of nervousness and fear [133], and schizophrenia can cripple patients with hallucinations, delusions, and catatonia [134]. About 3-15% of the world's population will suffer from one of these conditions in their lifetime [131, 132, 135, 136]. Therefore, understanding the psychopathology behind these diseases could have major implications for treating millions of patients with mental health conditions.

Many psychiatric disorders are highly hereditary. Heritability rates for depression and anxiety are around 35% [127, 133] and for BPD, ADHD, and schizophrenia are as high as 70-85% [132, 134, 137]. Because genetics are strongly causative of these conditions, research on the genes that contribute to them will greatly improve our understanding of these diseases. Medications have been developed that can manage symptoms in many but not all patients [127, 133, 138-141]. Characterizing the underlying biology of psychiatric disorders by studying the genes implicated in their pathology will lead to additional treatments.

DGKI and *DGKH* in mood disorders

DGKI and *DGKH* are linked to multiple psychiatric disorders. Genome-wide association studies (GWAS) have linked mutations in *DGKI* to schizophrenia [42-44] and bipolar disorder [44]. GWAS have linked mutations in *DGKH* to bipolar disorder [40, 41, 142-144], schizophrenia [142], depression [41], and ADHD [41]. Additionally, high *DGKH* RNA expression was found in postmortem brain tissue of BPD patients relative to healthy controls [145], and patients with BPD risk mutations in *DGKH* had higher levels of circulating DGKH.

Recently, researchers examined the function of *Dgkh* in male mice [39]. Overall, they found that *Dgkh*-knockout males displayed mania-like behaviors that could be reversed with lithium, a common treatment for BPD [146]. Using *Dgki*-knockout mice [23], others found that *Dgki* loss caused no changes in learning, anxiety, or motor phenotypes other than a slightly diminished habituation to an open field [32]. Note that the sex of the mice in this latter study was not indicated.

As discussed in the introduction to Chapter 3, *Dgk* isoforms contribute strongly to neuronal function and neurological behaviors. A splice variant of *DGKB* was linked to BPD [147], and *Dgkb*-knockout mice show psychopathological phenotypes, including hyperactivity and decreased anxiety [29]. Therefore, genes identified in BPD patients are strong predictors of mood disorder symptoms in mammals, and genetically-engineered mice with *Dgk* deletions can be used to model neurological diseases. Here, we aimed to demonstrate the role of *Dgkh* and *Dgki* in mouse behaviors associated with aberrant psychopathology.

Maternal behavior

While maintaining our mouse colony, we noticed that the offspring of dKO female mice had poor survival rates due to deficits in dKO dams' nurturing abilities. In addition to being important for survival, maternal care influences the development of mood-disorder-related

symptoms—particularly anxiety, fear, and hyperactivity—in the adult offspring in rodents and humans [148-152]. Therefore, maternal behavior is incredibly important to mental health. Whereas the effect of poor maternal care on the young is well-appreciated, what causes female rodents to become poor care providers is understudied.

Important factors in the development of nurturing behaviors in rodents have neurological components. The neurohormone oxytocin controls the onset of many aspects of maternal care (e.g. milk ejection, sensory responses to offspring) [153], and the medial preoptic area of the hypothalamus has been shown to be critical for the initiation and maintenance of maternal behaviors [154]. Additionally, prenatal stress (a psychological stimulus) strongly predicts poor maternal care in rodents and humans [155, 156]. As part of the efforts to understand the role of *Dgkh* and *Dgki* in neurological behaviors, we investigated the nurturing behaviors and survival outcomes of dKO mothers and their litters.

RESULTS

dKO mice exhibit decreased immobility in the forced swim test (FST)

Given the genetic linkage of *DGKH* and *DGKI* to mood disorders in humans, we tested WT, *Dgkh*$^{-/-}$, *Dgki*$^{-/-}$, and dKO mice (both female and male) with neuropsychiatric disorder-related behavioral assays. To model depression or mania [157, 158], activity was monitored in the forced swim test (FST), in which a mouse is placed into a large cylinder of water and time spent immobile (as opposed to actively swimming) is measured. In this assay, both female and male dKO mice showed decreased immobility relative to WT mice (Figure 4.1), which is typically interpreted as mania [157]. Neither *Dgkh*$^{-/-}$ nor *Dgki*$^{-/-}$ females differed from WT females. However, the *Dgkh*$^{-/-}$ males showed increased immobility relative to WT male mice, suggesting a slight depression-like phenotype.

dKO mice prefer the closed arms in the elevated plus maze (EPM)

The elevated plus maze (EPM) was used to test for anxiety-like behavior [159]. In this test, we measured how much time mice spent in the protective closed arms versus the aversive open arms of an EPM (Figure 4.2). Deletion of *Dgkh* or *Dgki* alone had no effect on behavior in this assay in either sex. However, females and males lacking both *Dgkh* and *Dgki* spent significantly more time in the closed arms of the maze, considered a model of anxiety. Notably, the dKO males showed a preference for the protective closed arms of the maze, but not an avoidance of the aversive open arms.

Loss of *Dgkh* and/or *Dgki* affects behavior in an open field in males but not females

To test for exploratory behavior and activity levels [160], we monitored behavior of mice in an open field. We measured parameters of general activity (total horizontal distance covered and number of beam breaks from vertical movements) and of activity in the aversive center of the open field (distance covered and time spent in the center). When the behavior of the females was monitored in the open field test, none of the three genetic mouse models showed differences in activity relative to WT females (Figure 4.3A-F). However, when the males were monitored, we found that both *Dgki*$^{-/-}$ and dKO males were more active than their WT counterparts, in both horizontal and vertical activity metrics (Figure 4.4**Error! Reference source not found.**A-F). Additionally, in females the activity in the center of the open field did not significantly differ with genotype, in either distance or time (Figure 4.3G-E). However, in males the *Dgkh*$^{-/-}$, *Dgki*$^{-/-}$, and dKO mice showed enhanced activity in the center of the open field for at least one metric (Figure 4.4G-E).

Loss of *Dgkh* and/or *Dgki* in mice does not alter responses to startling acoustic stimuli

Deficits in prepulse inhibition (PPI) are used to model sensorimotor gating, a symptom of schizophrenia [161]. We found that responses to a startling acoustic tone of 120 dB (called the

acoustic startle response, or ASR) did not differ based on genotype in either sex (Figure 4.5A-B), nor did the inhibition of the startle response when paired with a softer prepulse tone of varying loudness (Figure 4.5C-D).

Poor survival rates of offspring raised by dKO mothers

While maintaining colonies of WT, *Dgkh*$^{-/-}$, *Dgki*$^{-/-}$, and dKO mice, we noticed a significantly diminished survival rate of litters raised by dKO females. Offspring of dKO mothers showed a significant decrease in survival within the first two days after birth (Figure 4.6A). Pups raised by WT mothers had a survival rate of 87.1%, whereas dKO-raised pups had a 29.5% survival rate. To evaluate the relative contribution of each *Dgk* gene to this phenotype, we examined survival rates of litters born from mothers of each genotype (Figure 4.6B). When raised by WT females, an average of 85.5% of the litter survived to weaning age, whereas dKO-raised litters had an average survival rate of 25.1%. At 72.1% average survival, litters raised by *Dgkh*$^{-/-}$ did not significantly differ from WT litters. At 54.0%, litters raised by *Dgki*$^{-/-}$ mothers fared slightly worse than those raised by WT dams, but the difference was most pronounced when both *Dgkh* and *Dgki* were deleted (dKO).

dKO dams show signs of deficient postnatal care

To determine if the poor survival rate was due to deficiencies in prenatal development or postnatal care, we fostered pups from dKO dams to recently postpartum WT dams. When fostered to a WT mother, an average of 83.9% of dKO-born pups survived (dKO Fostered; Figure 4.6B), which was a significant improvement over dKO-raised litters. These data suggest dKO-born pups can nurse and grow normally when under the care of a WT mother. Moreover, the normal litter size at birth (Figure 4.6C) ruled out the possibility that pup survival was impaired prenatally.

The severity of the survival phenotype was not dependent on the genotype of the pup, whether the dKO dam was a new or experienced mother, the age of the mother, or the size of the litter (Figure 4.6D-G).

dKO mothers show variable pup retrieval behavior

Since our data suggested poor pup survival was due to deficient maternal care, we next assayed an array of maternal behaviors. From observing their cages, we found that WT and dKO females both made protective nests, with tall sides and top coverings that fully enveloped both the dam and the litter (Figure 4.7A-B). In addition to making decent nests, mothers need to be able to retrieve pups that have strayed from the nest. In an assay of this maternal behavior, the latency to retrieve three stray pups was tested in WT and dKO moms on the day of (P0) or the day after (P1) birth of a new litter (Figure 4.7C). The average latency to return stray pups to the nest was higher in dKO dams at P0 (not significant) relative to WT (263.9 and 123.9 s, respectively) but was skewed by a subset of dKO mothers that failed to retrieve any pups during the entire 900-s assay period. Of the 14 P0 litters assayed with dKO mothers, 11 successfully retrieved all 3 pups (78.6%), compared to a success rate of 96.0% (24 out of 25) in trials with WT mothers (Figure 4.7D). All dams retrieved all three pups at P1 (Figure 4.7D), with comparable latencies between WT and dKO dams (Figure 4.7C).

Newborn offspring consume less milk when reared by dKO female mice

The protective nests built by WT and dKO females prevented the observation of nursing behavior directly, so we monitored the presence of milk spots in the pups to determine if the pups were consuming milk. Due to their transparent skin, milk in the stomach of newborn mice can be seen as a white spot on the abdomen. At P0, on average only 43.8% of pups from dKO-born litters had visible milks spots, compared to litters from WT dams with an average of 78.0% (Figure 4.7E). All dKO-raised pups had milk spots at P2, likely explaining why dKO pups that

survived to P2 then survived to weaning. Moreover, the presence of milk spots ruled out the possibility that dKO females were unable to produce milk.

Offspring of dKO mothers gain weight slowly in early postnatal period

The impact of insufficient nursing was seen in the average weight of mice raised by dKO mothers (Figure 4.7F). Pups raised by dKO dams weighed significantly less than those raised by WT dams at P0 (1.24 g and 1.38 g, respectively), P1 (1.29 g and 1.43 g), and P2 (1.43 g and 1.62 g). The differences between dKO and WT pup weights began to decrease at P3 (1.77 g and 1.99 g, respectively) and P4 (2.28 g and 2.51 g). From P5 to P21 (typical weaning age) there were no significant differences in offspring weight based on maternal genotype (partial data shown). The improvement in weight was preceded by the presence of milk spots at P2 (Figure 4.7E) and coincided with a decrease in lethality (Figure 4.6A).

DISCUSSION

Summary of behavioral assays

Here, we show that global loss of both *Dgkh* and *Dgki* in female mice causes anxiety and mania-like behaviors—phenotypes not seen from loss of *Dgkh* or *Dgki* alone. These behavioral phenotypes were paired with a significant deficit in early maternal care. The behaviors analyzed in all three genetic mouse models are summarized in Table 4.1A. For the dKO females, the lack of changes in general activity in the open field (Figure 4.3A-F) supports the conclusion that the increased activity in the FST (Figure 4.1A) was indicative of mania, not hyperactivity [162]. Additionally, the normal center behavior in the open field (Figure 4.3G-E) suggests that the phenotype of the dKO females in the EPM (Figure 4.2A) represented anxiety and not simply hypo-exploratory behavior [163].

We also observed differences from WT in how the male dKO mice behaved in the FST and EPM assays. However, unlike in the dKO females, we found additional aberrant behaviors

through the open field test. Interestingly, deletion of *Dgkh* or *Dgki* alone was sufficient to cause some of these phenotypes. The behaviors analyzed in the males are summarized in Table 4.1B. The preference for the protective closed arms of the EPM, as shown by the dKO males, is typically interpreted as anxiety (Figure 4.2B). Center behavior in the open field is analogous to EPM open-arm behavior; anxious mice will avoid the aversive center of the open field. Therefore, it was surprising to see that the dKO males actually had *increases* in time spent and distance traveled in the center of the open field (Figure 4.4G-E). Pairing the results of both the EPM and open field assays informs our interpretation of the dKO male behavior. Whereas dKO males showed a preference for the protective closed arms of the EPM, they actually did not avoid the open arms; they spent just as much time in the open arms as WT males. (Mice were able to stay in the middle of the plus maze, which was scored as neither closed or open arm time.)

In neither female nor male mice of any *Dgk*-mutant genotype were there changes in ASR or PPI responses. This suggests that startle reflexes and sensorimotor gating are not dependent on *Dgkh* and/or *Dgki* expression in mice, and exclude the interpretation that these mice have broad cognitive deficits [164].

Sex differences in psychopathological behavior

In the assays of psychopathological behavior in mice, there were two obvious differences between males and females. First, the dKO males, but not the females, showed increased activity and decreased center avoidance in the open field. Second, the *Dgkh*$^{-/-}$ and *Dgki*$^{-/-}$ females had no variations from WT females in their behavior, but the *Dgki*$^{-/-}$ males phenocopied the dKO males' variations from WT in the open field. Interestingly, these two differences are connected: all the phenotypes that were aberrant in dKO males but not in dKO females were also aberrant in the *Dgki*$^{-/-}$ males. Therefore, the sex difference in open field can

be attributed to how *Dgki* deletion affects males differently from females, not necessarily how double *Dgkh/Dgki* deletion affects males differently.

Even in the assays where dKO females and males had the same results, there is potentially for the result to represent two different types of behavior. For example, both female and male dKO mice spent more time in the closed arms of the EPM (Figure 4.2); however, they may have behaved differently while they were in the closed arms (we were not able to see them in the closed arms). If the mice stayed in the corner, huddled against the tall, protective walls, this would represent an anxious phenotype. On the other hand, if the mice roamed up and down the long arms or engaged in frequent rearing behavior, this would represent a hyperactive or exploratory phenotype.

Both female and male dKO mice had decreased immobility time in the FST, as well (Figure 4.1). Females had normal behavior in other tests of activity, so we interpreted this as mania-like behavior. However, the dKO males had enhanced activity in both the FST and the open field. Therefore, in the dKO males, decreased immobility in the FST and the increases in horizontal distance covered, vertical movements, and center distance in the open field together paint a picture of a mouse that is hyperactive and hyperexploratory.

Detailed explorations of the molecular, cellular, and circuit-based mechanisms for these phenotypes are great future directions of this study. The many potential mechanisms that may be regulating these behaviors are discussed below.

Potential signaling pathways contributing to psychopathological behavior in dKO mice

Dgkh and *Dgki* are known to regulate multiple signaling pathways that have been linked to the phenotypes we uncovered. Activation of $G\alpha_q$-GPCRs induces calcium release and production of DAG, together leading to neuronal activity [25, 165]. We previously found that overexpression of *Dgkh* prolongs $G\alpha_q$-GPCR-stimulated calcium mobilization by attenuating the activation of PKC [45]. Using hippocampal slices from neonatal (2-week-old) *Dgki*-knockout

mice, others found that mGluR-LTD was dampened; although, they did not find this effect in adult tissue [32]. Impaired mGluR-LTD (a $G\alpha_q$-GPCR-dependent process) in the *Dgki*$^{-/-}$ mouse tissue required increased PKC activation, suggesting a mechanism analogous to that which we previously showed for *Dgkh*. In addition to negatively regulating PKC, both *Dgkh* and *Dgki* were found to positively regulate ERK signaling [20, 23, 48].

Disruptions in PKC and ERK activity have frequently been implicated in mood disorders. Increased PKC activity has been shown in mouse models of mania and anxiety [166, 167] and in bipolar manic patients [168], and PKC-null (*Prkcg*$^{-/-}$ and *Prkce*$^{-/-}$) mice demonstrate reduced anxiety [169, 170]. ERK dysfunction leads to poor maternal care and mania- and anxiety-like behavior in rodents [171-173]. Mood stabilizers that manage mania in human patients can decrease PKC activity [168] or increase ERK signaling [174] in neurons. Thus, loss of *Dgkh* and *Dgki* has the potential to affect behavior by enhancing PKC activity and/or attenuating ERK activity.

PKC and ERK have many signaling targets that could contribute to impaired behavior in dKO mice. PKC modulates the function of $GABA_A$ and 5-HT_{2A} receptors [175, 176], both of which regulate maternal behavior [177, 178] and anxiety [179, 180]. Altered PKC or ERK function resulting from *Dgkh* and *Dgki* loss may induce behavioral changes by modulating phosphorylation of GSK3β [181, 182], an enzyme implicated in the pathology of multiple mood disorders [183]. Indeed, other researchers found that phosphorylation (i.e. inactivation) of GSK3β was decreased in brains of their *Dgkh*$^{-/-}$ male mice (a different mutant than the *Dgkh*$^{-/-}$ mice used in this study), which showed manic behaviors [39].

However, it is difficult to link increased PKC activity or decreased ERK activity to the hyperactivity phenotype of the *Dgki*$^{-/-}$ and dKO male mice. ADHD treatments (amphetamines) enhance dopamine signaling by inhibiting the dopamine transporter (DAT), enabling dopamine to remain in the synapse [184]. Similarly, PKC activation leads to DAT internalization, thus inhibiting its function [185]. Whereas mice lacking ERK1 showed increased locomotion in the

open field test, their hyperactivity did not diminish with amphetamine treatment, suggesting they are not a model of ADHD [174]. Further investigations are needed to determine which signaling pathways are disrupted in the brains of dKO mice.

Brain regions that may mediate aberrant behaviors in dKO mice

Based on gene expression data from the Allen Brain Atlas [186], *Dgkh* and *Dgki* have highly overlapping regional expression patterns in the brain [25]. The high degree of overlap of *Dgkh* and *Dgki* expression presents the potential for compensation, which could account for why phenotypes were detected only when both genes were deleted. *Dgkh* and *Dgki* expression are enriched in the cerebral cortex, hippocampus, and striatum [25, 187]. Human and animal studies connect the pathology of both mania and anxiety to cortical and hippocampal function [141, 188-192], whereas striatal function has been implicated in the regulation of nurturing behaviors in rodents [154, 193, 194].

Disruptions in functions performed by the medial prefrontal cortex (mPFC), including decision-making and mood regulation, are primary symptoms of anxiety [188]. The connection between anxiety and mPFC dysfunction is bidirectional: mPFC lesions in rats induce anxiety-like behaviors [189], and anxiogenic treatments impair mPFC activity [190]. Ventral hippocampal function has a role in anxiety, as well [191]; however, *Dgkh* and *Dgki* are highly expressed in the dorsal hippocampus. In a study of bipolar disorder patients, decreases in frontal cortical volume and thickness were seen only in bipolar patients who experienced manic episodes over the six-year observation period [192]. Many mouse models of mania show shifts from excitatory to inhibitory synaptic function in the hippocampus or the cortex [141]. Mood stabilizers that effectively treat manic symptoms target hippocampal, cortical, and/or striatal excitability [141]. Male children with ADHD showed hypoactivation of the PFC segments during tests of motor response inhibition and cognitive flexibility, tasks which are challenging for ADHD patients [195].

Others found altered activation in both the PFC and the striatum during attentional tasks, and in most cases ADHD medications were able to reverse these alterations [196].

The preoptic area of the hypothalamus is a critical nucleus for expression of maternal behavior in rodents. In particular, preoptic area projections to the substantia nigra and the ventral tegmental area mediate various nurturing phenotypes [154]. It is likely that the substantia nigra and ventral tegmental area control maternal behavior through their inputs into the striatum, as dopaminergic activity in both the dorsal and ventral striatum impacts nurturing [193, 194].

Connections between psychopathological phenotypes and maternal care

Given the known links between different brain regions and the phenotypes we have shown here, it is possible that *Dgkh* and *Dgki* loss could affect mood by altering hippocampal and cortical activity, while their effects on maternal behavior may arise in the striatum. Alternatively, other mouse models of deficient maternal behavior have likewise shown comorbid psychological phenotypes, suggesting potential overlap in the pathology behind these behaviors. Mice lacking the δ subunit of $GABA_A$ receptors showed poor maternal care, anxiety, and depression [177]. Mice with loss of ephrin-A5 or central nervous system-specific ERK2 deletion had decreased nurturing behaviors and anxiety [171, 197], and mice bred for low anxiety were less maternal than their high-anxiety counterparts [198]. While these studies show variability in the phenotypes in each mouse model, they demonstrate that aberrant mood-related behaviors commonly coincide with disrupted maternal behavior in mice.

Extensive research has demonstrated that receiving poor maternal care as a young rodent increases the likelihood of developing anxiety-like behaviors as an adult [148-151, 199]. However, the influence of a rodent's anxiety on its ability to provide maternal care is underappreciated. One possible explanation of the poor survival of dKO-raised litters is that dKO females have exaggerated responses to stressful situations, including the presence of new pups in the cage, which cause them to neglect their offspring. From our observations of milk

spots, we found that pups raised by dKO mothers were receiving less milk (Figure 4.7E). It is unclear whether this is due to the moms failing to assist their pups in nursing or due to dKO females leaving the nest in response to stressful disturbances. During the pup retrieval assay, as well as while working with dKO females in the animal housing facility, we noticed that dKO females would dart around the cage, rear frequently, and not settle down like WT females, especially after opening or disturbing the cage. And, during the pup retrieval assay, the dKO females that failed to return all three pups to the nest (Figure 4.7D) displayed this manic-like exploratory behavior for the entire testing period. We speculate that this manic-like behavior might make it difficult for newborn pups to nurse, and hence could contribute to poor pup survival.

Parturition can induce depression and anxiety in mice and humans [177, 200, 201] and frequently exacerbates symptoms in patients with prepartum mood disorders [202]. Indeed, dKO mice appear to be predisposed to these deficits, as signs of mania and anxiety were observed in virgin dKO females. The disturbances in both mood phenotypes and in maternal behaviors, especially in the early postpartum period, suggest that *Dgki* and *Dgkh* may be interesting targets to investigate for their role in parturition-linked affective disorders.

METHODS

Mice

See: “Mice” under METHODS from Chapter 2.

Maternal behavior

For maternal behavior experiments, timed matings were set up in the evening within 2 hours of the start of the dark cycle, using one male mouse and one or two female mice per breeding cage. The male mouse was separated from the female mice after 48 or 72 hours. Female mice were single-housed at least one week prior to giving birth. Pup retrieval

experiments and observations of pup survival, weight, and milk spots were conducted in the evening within 3 hours of the start of the dark cycle. When handling pre-weanling mice, care was taken to rub gloves with used bedding from the home cage before touching the animals, particularly when removing pups for weighing or testing in the retrieval assay.

Fostering

Within an hour after the birth of the last pup from dKO female litters, the dKO dam was removed and replaced with a foster WT dam. Foster WT dams had given birth to a litter no more than seven days prior to being used for fostering. The 8 litters came from 7 different dKO mothers and were fostered with 8 different foster dams.

Pup retrieval

To examine pup retrieval [171, 203, 204], in a cage with a dam and her litter, the pups were removed from the home cage and kept warm on a SpaceGel heating pad (Braintree Scientific, Braintree, Massachusetts). With the nest in one corner of the home cage, one pup was placed in each of the three remaining corners. The mother was then placed in the cage at the site of the nest, and her latency to retrieve each pup and place them in the nest was timed. This assay was only performed when litters had at least three live pups. Mothers were tested on the day of or day after birth of the litter. After 15 min, all pups were returned to the nest by the experimenter. At P0, 22 WT mothers were assay with 25 litters, and 12 dKO mothers were assayed with 14 litters. At P1, 18 WT mothers were assay with 21 litters, and 8 dKO mothers were assayed with 9 litters. No mother was tested with more than 2 of her litters.

Psychopathological behavior

For the elevated plus maze, open field, forced swim test, and acoustic startle and prepulse inhibition experiments (tested in that order), we tested 2- to 4-month-old virgin female

or male mice during the light phase of their light:dark cycle. Mice were given at least 48 hours to recover after the elevated plus maze and open field assays, and at least one week to recover after the forced swim test. Because of the large number of animals required, the three genetic models (*Dgkh*$^{-/-}$, *Dgki*$^{-/-}$, and dKO) were tested in separate cohorts, each with an age-matched wild type (WT) cohort.

For the female assays, 15 WT mice were tested with 16 *Dgki*$^{-/-}$ mice; 14 WT mice were tested with 14 *Dgkh*$^{-/-}$ mice; and 19 WT mice were tested with 19 dKO mice (only 14 mice of each genotype from the dKO cohort were tested in the acoustic startle and prepulse inhibition experiments). For the male assays, 13 WT mice were tested with 13 *Dgki*$^{-/-}$ mice; 13 WT mice were tested with 12 *Dgkh*$^{-/-}$ mice; and 12 WT mice were tested with 13 dKO mice (only 5 WT and 3 dKO mice from the dKO cohort were tested in the acoustic startle and prepulse inhibition experiments). For each of these assays, outliers were identified using the interquartile range (IQR = $Q_3 - Q_1$). Any data points that were 1.5×IQR below Q_1 or 1.5×IQR above Q_3 were excluded.

Forced swim test

To model depression or mania [157, 158], activity was monitored in the forced swim test. Mice were placed into a 28 cm tall cylinder of 20 cm diameter filled to approximately 15 cm with 24-26°C water for 6 min. Activity was video recorded. The time spent immobile during the final 4 min in the chamber was tracked and scored using EthoVision XT 7.0 software (Noldus Information Technology, Leesburg, Virginia). Floating without actively swimming was counted as immobility. Animals were monitored during the experiment period to ensure their head stayed above the water.

Elevated plus maze

To model anxiety-like behavior [159], mice were placed into the 7.5 cm^2 center of a 52 cm high elevated plus maze, the two closed and two open arms of which are each 30 cm long and 7.5 cm wide. The height of the walls of the closed arms was 20 cm, and the lip surrounding the open arms was 1.5 cm high. Activity of the freely-exploring mouse was monitored by a human observer for 5 min. Time spent in the closed or open arms or the center of the maze was measured. Entry into the center or any arm was scored when three of the animal's paws crossed the threshold between each area.

Open field

To test for exploratory behavior and activity levels [160], mice were monitored in a 40 cm^2 open field of 28 cm depth, enclosed in a box with a light above the open field, for 60 min. Activity was analyzed using the VersaMax animal activity monitoring system (AccuScan Instruments, Columbus, Ohio) to determine total distance moved in the entire arena and total distance moved in the 25 cm x 25 cm center region, binned in 5-min segments.

Acoustic startle response and prepulse inhibition

To assess sensorimotor gating and startle reflex in these mice [164, 205], ENREF_41 mice were placed into an acrylic tube (7 cm long x 3.75 cm inner diameter) that was paired with a piezoelectric transducer that measured flinch responses. The tube and transducer were housed in a 29 cm^3 sound-attenuating chamber with a light, fan, and speaker. Responses to a 40-ms, 120-dB acoustic stimulus were measured, alone or with a 20-ms prepulse tone played 100 ms preceding the 120-dB stimulus. Following a 5-min acclimation to the startle chamber, testing sessions were 10 min and consisted of 42 randomized trials, 6 trials each of the following 7 conditions: 1) no acoustic stimulus, 2) 120-dB startle tone alone, or 3) prepulse tone of 74, 78, 82, 86, or 90 dB followed by the 120-dB startle tone. The startle response was

measured and analyzed with SR-LAB startle response system apparatus and software (San Diego Instruments, San Diego, California). The degree to which the prepulse tone inhibited the startle response to the 120-dB tone was calculated as: 100 – [(response to startle stimulus post-prepulse)/(response to startle stimulus alone) × 100]. Mouse weights were measured at the end of the session; however, neither *Dgkh*$^{-/-}$, *Dgki*$^{-/-}$, nor dKO mice differed in weight from their simultaneously-tested WT cohort, so we did not adjust the startle responses for weight in our analyses.

Statistics

After processing by the software programs mentioned above, data were analyzed with GraphPad Prism version 7.04. Survival curves of WT and dKO pups were compared with a log-rank (Mantel-Cox) test. The proportion of mothers retrieving all three pups was compared between genotypes with a binomial test. Total distance and center distance traveled in the open field were compared between WT and other genotypes using two-way repeated measures analysis of variance (ANOVA), with Sidak's multiple comparisons tests used for pairwise comparisons within 5-min time bins. All other assays were tested for significance using two-tailed t-tests with Welch's correction to compare WT and *Dgkh*$^{-/-}$, *Dgki*$^{-/-}$, or dKO, or to compare dKO and dKO Fostered, in the case of litter survival.

FIGURES

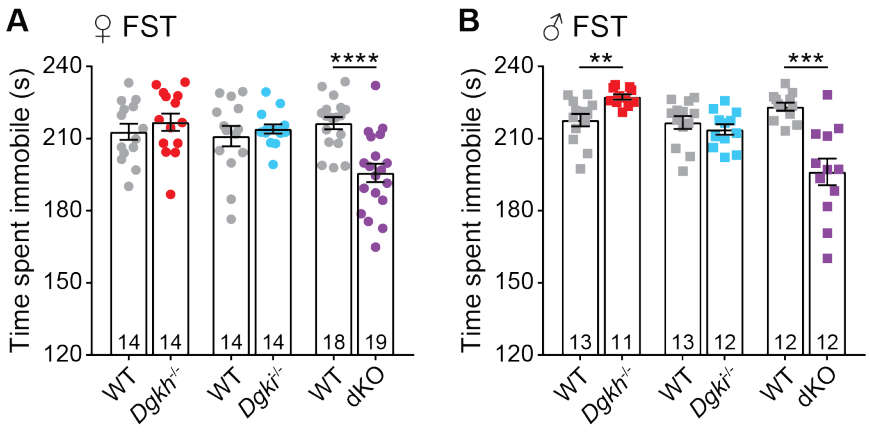

Figure 4.1. dKO mice show decreased immobility in the forced swim test (FST). In the FST, female (A) or male (B) mice were placed in a large cylinder of water for six minutes. Time spent immobile (i.e. not swimming) was measured for the final four minutes. Data represent mean ± SEM. Number of mice indicated on graphs. p< **0.01, ***0.001, ****0.0001 vs. WT.

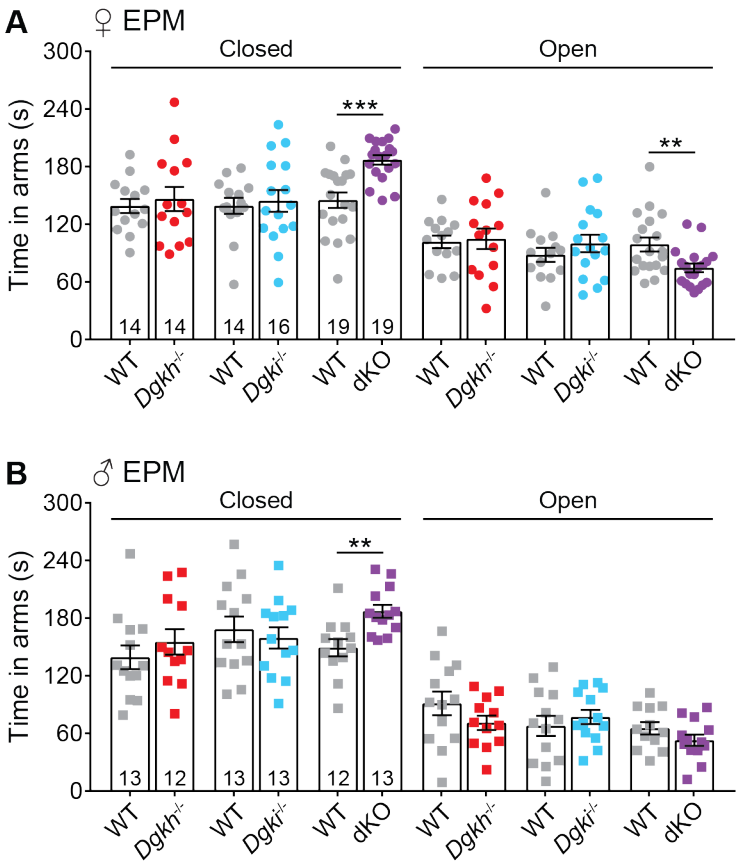

Figure 4.2. dKO mice spend more time in the closed arms of the elevated plus maze (EPM). Time that female (A) or male (B) mice spent in the closed or open arms of an EPM was measured in a five-minute period. Data represent mean ± SEM. Number of mice indicated on graphs. p< **0.01, ***0.001 vs. WT.

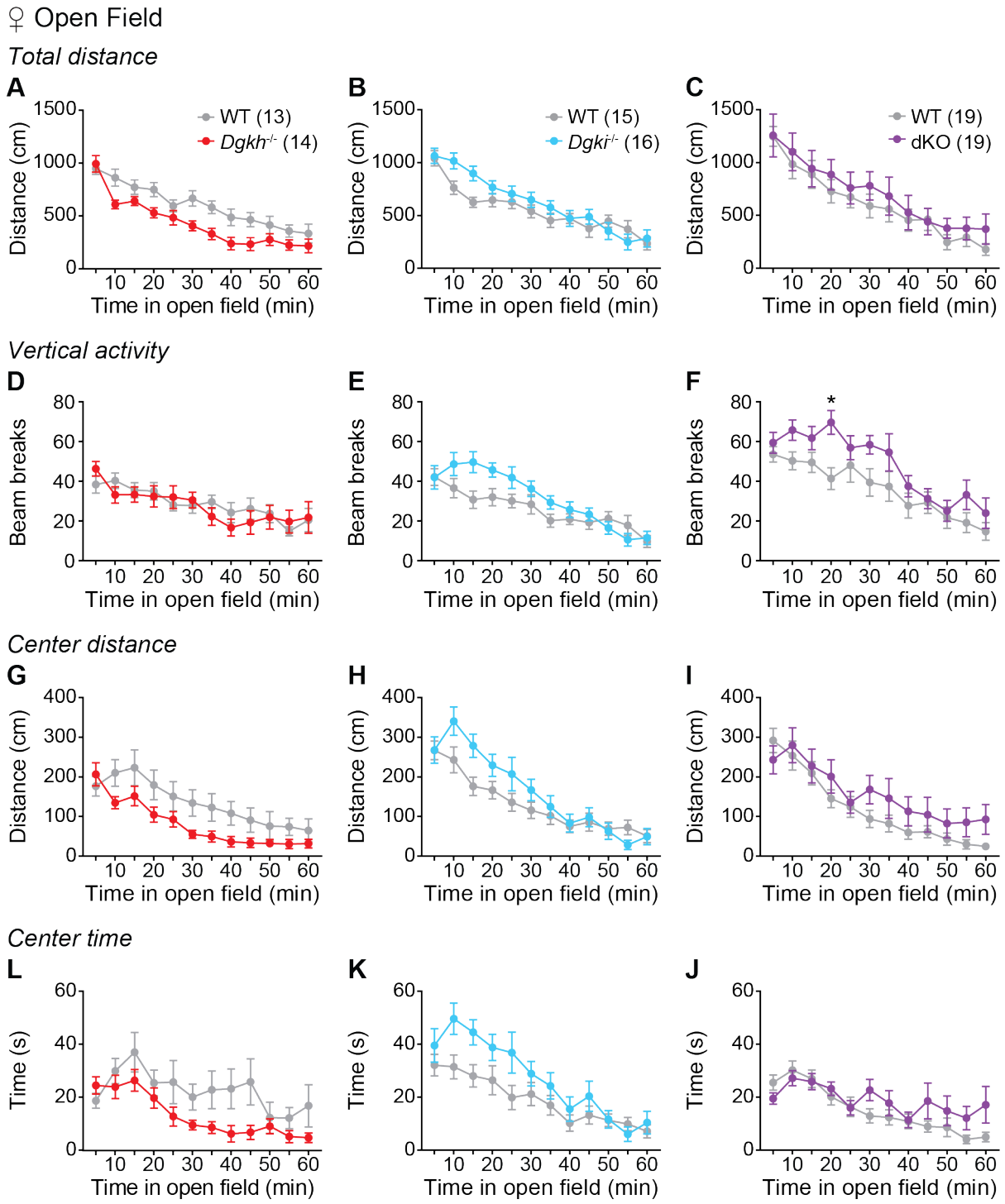

Figure 4.3. Locomotion and center behavior in an open field were unaffected by *Dgkh* and/or *Dgki* loss in female mice. In the 60-minute test, the total distance covered (A-C), vertical activity (D-F), distance covered in the center (G-I), and time spent in the center (L-J) of an open field were tracked for WT and *Dgkh*$^{-/-}$ (A,D,G,L), *Dgki*$^{-/-}$ (B,E,H,K), or dKO (C,F,I,J) female mice. Data represent mean ± SEM. Number of mice indicated in graphs.

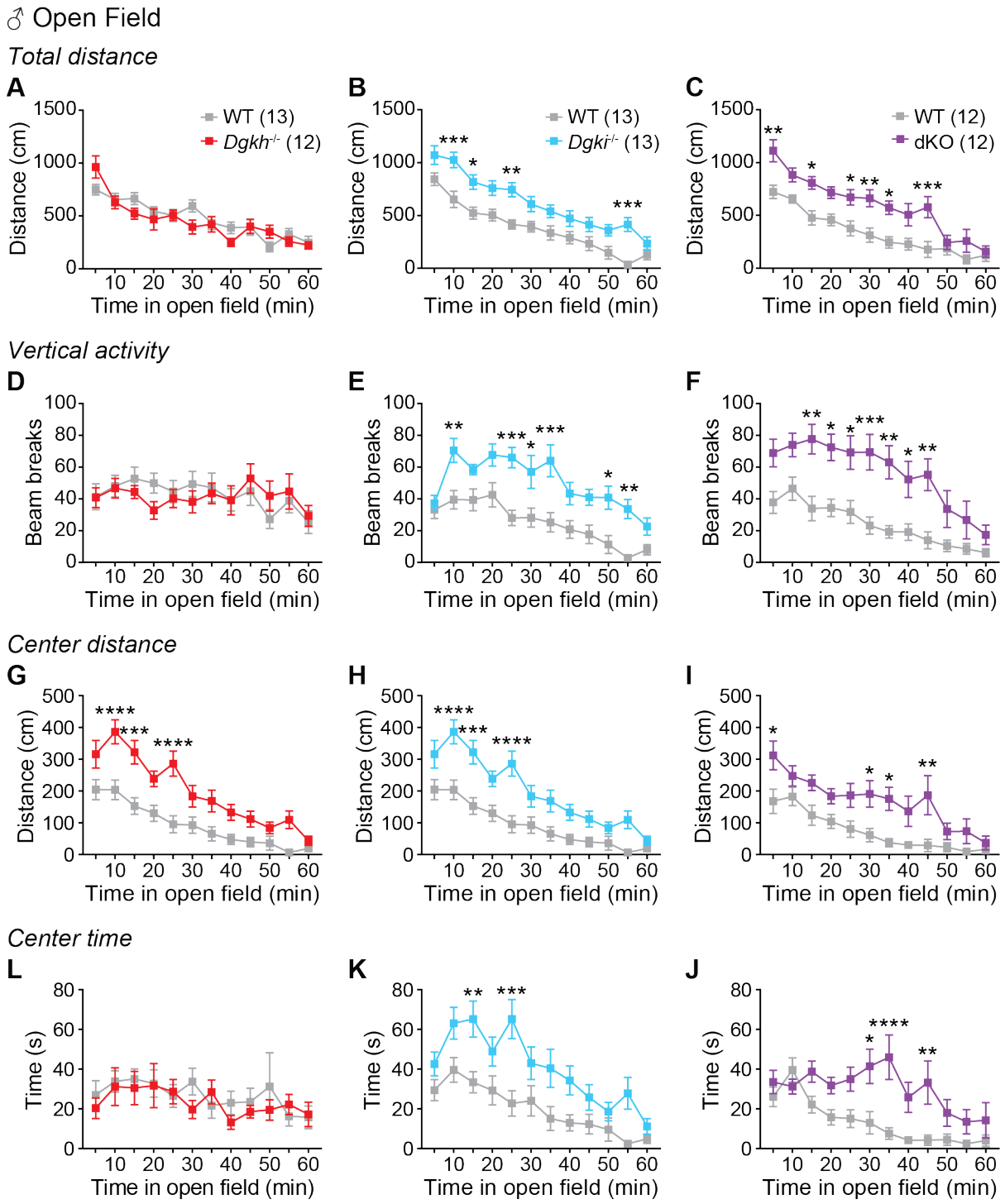

Figure 4.4. Locomotion and center behavior in an open field were enhanced by *Dgki* deletion, with or with *Dgkh* deletion, in male mice. In the 60-minute test, the total distance covered (A-C), vertical activity (D-F), distance covered in the center (G-I), and time spent in the center (L-J) of an open field were tracked for WT and *Dgkh*$^{-/-}$ (A,D,G,L), *Dgki*$^{-/-}$ (B,E,H,K), or dKO (C,F,I,J) male mice. Data represent mean ± SEM. Number of mice indicated in graphs. p< *0.05, **0.01, ***0.001, ****0.0001 vs. WT at individual time point.

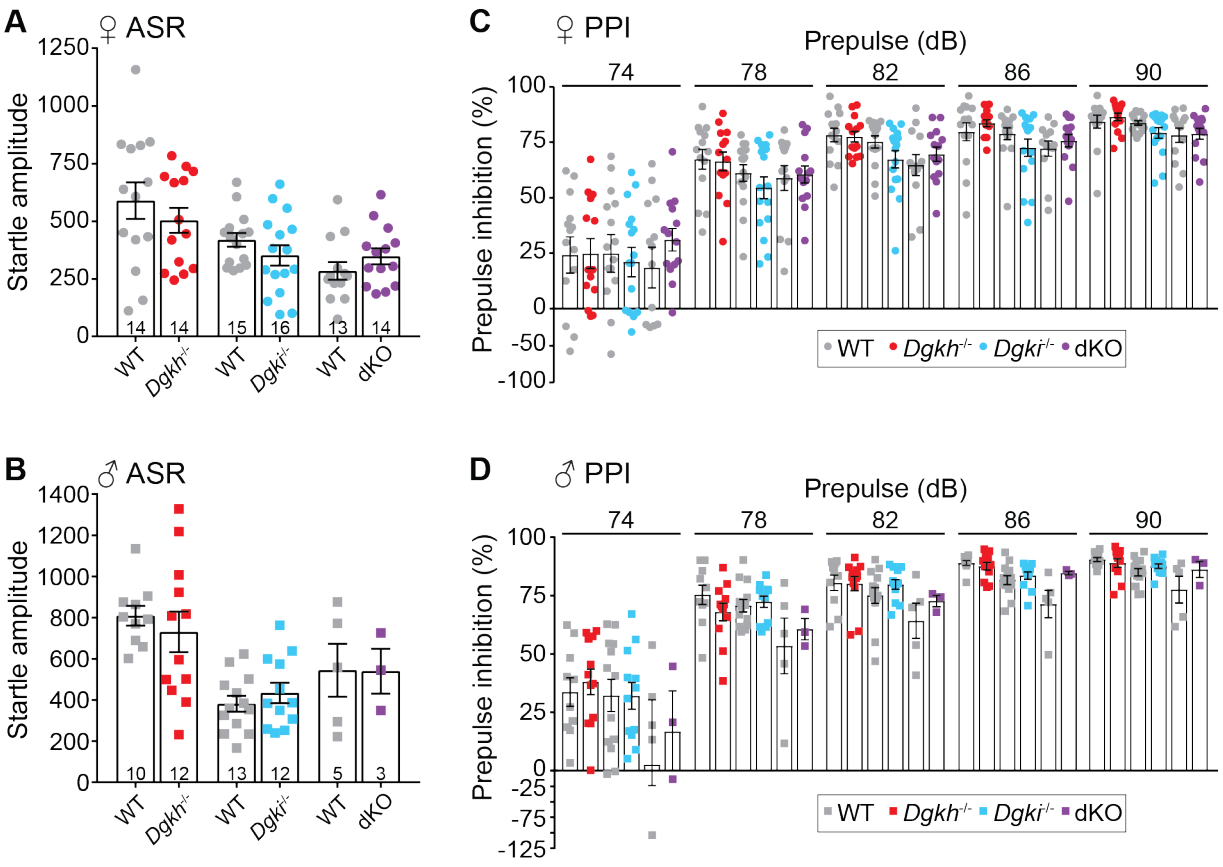

Figure 4.5. Deletion of *Dgkh* and/or *Dgki* does not alter responses or habituation to acoustic startle tone in mice. A-B) Acoustic startle response (ASR) to a 120-decibel (dB) tone in female (A) and male (B) mice. C-D) The prepulse inhibition (PPI) representing the % decrease in ASR shown in (A) and (B) when the 120-dB tone was preceded by a non-startling tone of 74, 78, 82, 86, or 90 dB in female (C) and male (D) mice. Data represent mean ± SEM. Same mice were used in (A) and (C) and in (B) and (D); number of mice indicated on graphs in (A) and (B).

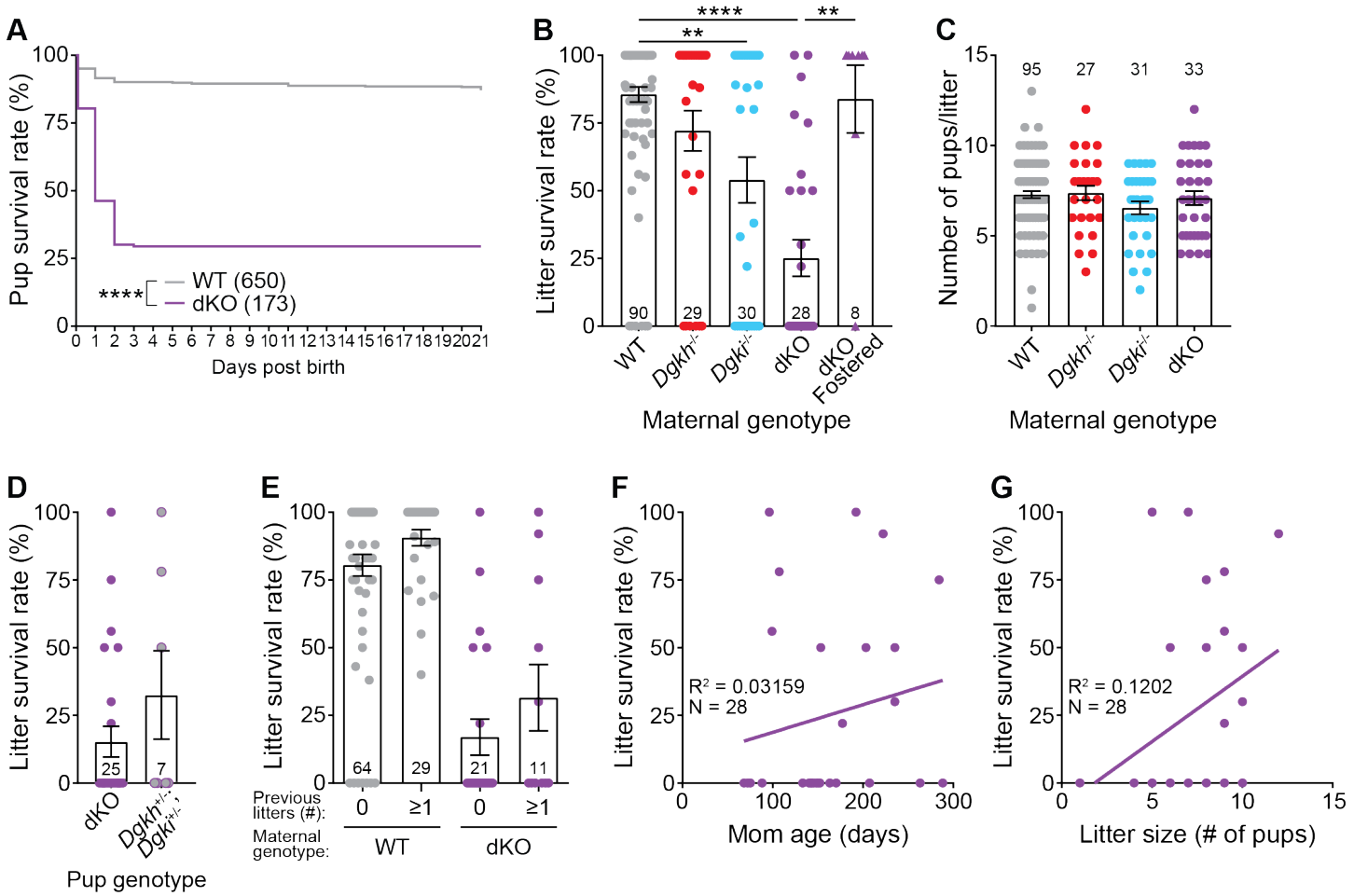

Figure 4.6. Poor survival of offspring raised by dKO females. A) Survival rate of pups born from dKO dams was significantly reduced after birth relative to those born from WT dams. B) The average proportion of each litter that survived to weaning was dependent on genotype of the mother. dKO fostered = litters born from dKO dams fostered with recently postpartum WT dams. C) Litter size on the day of birth based on the genotype of the mother. D-G) Litter survival rate of dKO-born litters based on the genotype of the pup (D), the number of previous litters the dam had given birth to (E), the age of the dam (F), or the size of the litter at birth (G). Number of pups indicated on graph in (A). Number of litters indicated on graphs in (B-G). Bars in (B-E) represent mean ± SEM. p < **0.01, ****0.0001, comparison indicated with bars.

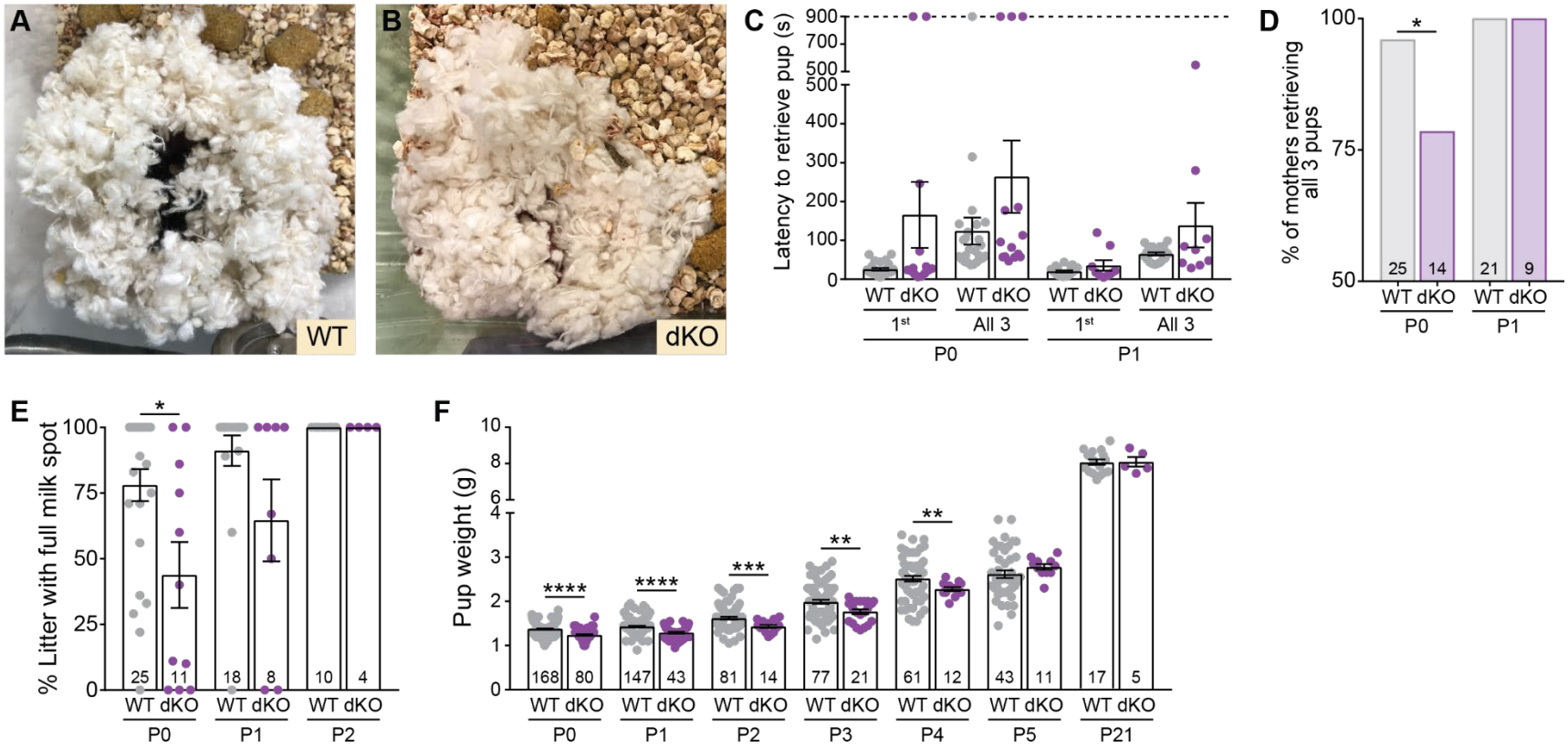

Figure 4.7. dKO females show deficits in nurturing. A-B) Representative nests by WT (A) and dKO (B) dams. Each nest contains a dam and her litter. C) Time taken to retrieve the first pup and all three pups in the pup retrieval assay, based on the genotype of the mother. D) Percentage of mothers, tested in (C), that retrieved all three pups to the nest. E) Percentage of a litter with a milk spot present, shown by genotype of the mother. F) Weight of pups raised by WT or dKO mothers. Number of litters indicated on graphs in (D-E). Number of pups indicated on graph in (F). Bars in (C), (E), and (F) represent mean ± SEM. p < *0.05, **0.01, ***0.001, ****0.0001, comparison indicated with bars.

	A Females			B Males		
Phenotype	*Dgkh*$^{-/-}$	*Dgki*$^{-/-}$	dKO	*Dgkh*$^{-/-}$	*Dgki*$^{-/-}$	dKO
FST: Immobility	=	=	↓****	↑**	=	↓****
EPM: Closed arm time	=	=	↑***	=	=	↑**
EPM: Open arm time	=	=	↓**	=	=	=
Open field: Total distance	=	=	=	=	↑***	↑***
Open field: Center distance	=	=	=	↑****	↑****	↑**
ASR	=	=	=	=	=	=
PPI	=	=	=	=	=	=
Offspring survival	=	↓**	↓****			

Table 4.1. Summary of psychopathological behavior tests in *Dgkh*$^{-/-}$, *Dgki*$^{-/-}$, and dKO female and male mice. Response of female (A) or male (B) *Dgkh*$^{-/-}$, *Dgki*$^{-/-}$, and dKO mice in each assay relative to WT mice of the respective sex. Arrows indicate the direction of the change from WT. Asterisks indicate the p-value of the difference from WT. "=" symbolizes no difference from WT. For the open field, the 5-min period in which the difference from WT was most significant over the 60-min period is represented. This may not represent the behavior over the entire 60-min period. p < **0.01, ***0.001, ****0.0001 vs WT.

CHAPTER 5: CONCLUSIONS

Important findings

Building on our previous findings showing that overexpression of *Dgkh* enhances $G\alpha_q$-GPCR signaling, we found that overexpression of *Dgki* has the same effect on $G\alpha_q$-GPCR-stimulated calcium activity. Additionally, we discovered that overexpression of *Dgkh* or *Dgki* enhances phosphorylation of both DAG and MAG substrates, revealing a previously-unknown function of DGKs in lipid metabolism. We developed knockout mice lacking *Dgki* and/or *Dgkh* to study these kinases *in vivo*. Whereas there was no increase in expression levels of either DGK isoform in the others absence, *Dgki* and *Dgkh* appeared to compensate for each other functionally in some cases.

While others have identified the expression of *Dgk* isoforms in rodent peripheral sensory neurons [90], this study was the first to examine the role of any *Dgk* isoform in itch or pain behavior. Here, we have demonstrated that *Dgki* negatively regulates behavioral responses to histamine in male and female mice, as loss of *Dgki* significantly enhances histamine-induced scratching. Conversely, *Dgkh* acts in the opposite direction, as loss of *Dgkh* reduces histamine-induced scratching in males. *Dgkh* deletion in reduced both DAG and MAG phosphorylation in DRG tissue. dKO mice lacking both *Dgki* and *Dgkh* phenocopied the *Dgki*$^{-/-}$ animals' *in vivo* histamine sensitivity and the *Dgkh*$^{-/-}$ animals' DRG kinase activity. Further experiments are needed to determine the mechanisms by which *Dgki* and *Dgkh* may function to regulate responses to histamine.

In exploring the role of *Dgki* and *Dgkh* in neurological behaviors, we found that dKO mothers showed poor nurturing behavior, evidenced by fewer milk spots, reduced weight, and impaired survival of dKO-raised litters. Additionally, we observed that dKO females—but not

Dgkh$^{-/-}$ or *Dgki*$^{-/-}$ females—showed mania- and anxiety-like behaviors, without disrupting baseline activity, exploration, startle reflexes, or sensorimotor gating. dKO males showed hyperactivity and hyperexploratory behavior, with some of these phenotypes presenting in the *Dgki*$^{-/-}$ and *Dgkh*$^{-/-}$ male mice, as well. Our research shows that *Dgkh* and *Dgki* have functional compensation in each other's absence, perhaps due to the high degree of overlapping expression. These results should be investigated further to understand the mechanism of by which loss of these genes induces deficits in maternal care and psychopathological behavior.

Connecting molecular, sensory, and psychopathological phenotypes

Our research on the molecular functions of *Dgki* and *Dgkh* (Chapter 2) informed the design some of our *in vivo* experiments. For example, having found that overexpressed *Dgki* and *Dgkh* modulated $G\alpha_q$-GPCR activity, when studying sensory signaling in the *Dgk* mutant mice (Chapter 3) we included stimuli that activate $G\alpha_q$-GPCR signaling (e.g. histamine) in our analyses. Our molecular findings also helped us understand some of the aberrant phenotypes we observed in our *Dgk* mutant mice. For example, when we observed psychopathological behavior in our dKO mice (Chapter 4), we hypothesized that PKC or ERK signaling may be disrupted in dKO mouse brains, as *Dgki* and *Dgkh* were shown to control these signaling pathways *in vitro*.

In addition to coupling the molecular studies in Chapter 2 with the subsequent behavioral studies, we can also compare the data on cellular functions analyzed by overexpressing *Dgki* or *Dgkh* in HEK293 cells (Chapter 2) versus deleting *Dgki* or *Dgkh* in DRGs (Chapter 3). In Chapter 2, we showed that when overexpressed in HEK293 cells, *Dgki* phosphorylated DAG and MAG substrates more than *Dgkh* (Figure 2.2B-C). However, when analyzing *Dgki* or *Dgkh* in mouse DRG in Chapter 3, we found that *Dgkh* loss had a much larger impact on acylglycerol phosphorylation (Figure 3.17). Further, our lab had previously shown that *Dgkh* kinase activity is required for overexpressed *Dgkh* to enhance $G\alpha_q$-GPCR signaling [45]. However, when *Dgkh*

was deleted in DRGs, we found that kinase activity in DRGs was reduced, but $G\alpha_q$-GPCR signaling was not affected. These experiments underscore the importance of analyzing the molecular behavior of proteins in the tissues in which they are endogenously expressed.

Whereas the molecular experiments done in HEK293 cells did not fully translate to mouse neurons, it is more likely that *Dgk* function is comparable between mouse neuron subtypes (i.e. between DRG and cortex). Understanding the molecular, cellular, and/or physiological underpinnings of the sensory phenotypes would be helpful in developing hypotheses about the mechanisms involved in psychopathological behavior of *Dgk* mutant mice, and vice versa.

Future directions

Molecular experiments

Previously, our lab generated a series of truncated *Dgkh* constructs, yielding DGKH mutants with different functional domains truncated from the N- and/or C-termini. Overexpressing these truncated constructs revealed how each protein domain controls kinase activity and $G\alpha_q$-GPCR signaling activity [45]. For example, DAG phosphorylation and $G\alpha_q$-GPCR-stimulated calcium activity were enhanced by the loss of the PH domain but were attenuated by the loss of both the PH and C1 domains. It would be useful to do a similar analysis of the protein domains of DGKI, as the functional domains greatly differ from DGKH [4]. Understanding the roles of the functional domains of both proteins may explain why disrupting *Dgki* or *Dgkh* genes has different effects on mammalian biology. A long-term goal of this research is to develop treatments for itch and the psychopathological behaviors controlled by *Dgki* and *Dgkh*. Identifying the protein segments to manipulate to increase or decrease DGKH or DGKI activity would be useful for creating future pharmacological treatments.

Sensory experiments

Our investigation into *Dgki* and *Dgkh* began because of their enriched expression in mouse DRG (Table 3.1), an important sensory organ. Through our studies, we discovered critical roles for *Dgki* and *Dgkh* in regulating histamine behavioral responses in mice. In our corresponding studies of DRG function *in vitro*, we were surprised to see that *Dgki* and *Dgkh* loss had minor influences on kinase activity and no effect on either GPCR- or TRP-stimulated calcium activity or RTK-stimulated ERK phosphorylation. Thus far, our data reject the hypothesis that the *in vivo* histamine phenotypes seen in *Dgki*$^{-/-}$ and *Dgkh*$^{-/-}$ mice are mediated by the DRG. However, there are other readouts of DRG function that could be investigated in future experiments. For example, electrophysiological excitability of rodent DRG neurons is enhanced by injury, leading to increased firing in response to a histamine-containing inflammatory cocktail [206]. *Dgki* deletion may likewise enhanced mouse DRG neuron excitability, contributing to the immediately-elevated scratching response to histamine injection *in vivo*.

As mentioned in the discussion of Chapter 3, there is the potential for mast cells to cause the altered histamine sensitivity in the *Dgki*$^{-/-}$ mice. The involvement of mast cells in *Dgki*-dependent histamine itch behaviors could be tested by monitoring histamine-induced scratching in *Dgki*$^{+/+}$ and *Dgki*$^{-/-}$ mast-cell-deficient mice. Also, the functions of primary mast cells from WT and *Dgki*$^{-/-}$ mice could be analyzed *in vitro* by examining mast cell infiltration, degranulation, and/or calcium mobilization in response to histamine exposure.

Among the neuronal tissues in which *Dgkh* and *Dgki* are expressed, the DRG has the highest expression levels. However, among the *Dgk* genes that are expressed in the DRG, *Dgkz* is more highly expressed than either *Dgkh* or *Dgki* in both mouse and human [87]. *Dgkd* and *Dgkq* are also found at higher levels than *Dgki* in the DRG. In our kinase activity assay, we found that loss of both *Dgkh* and *Dgki* only reduced DAG and MAG phosphorylation in the DRG

by about 50% (Figure 3.17). Therefore, it would be worth investigating the role that other *Dgk* isoforms may be playing in DRG neuron function and sensory behaviors.

Psychopathological experiments

Mania is a complex condition, characterized by disruptions in mood, energy, or sleep and engagement in impulsive behaviors [129]. We found that dKO females showed one sign of mania: decreased immobility in the FST, representing increased goal-directed activity. However, we cannot suggest that this mouse is a true model of mania without testing additional facets of this condition. To further explore mania-like behaviors in dKO mice, we could assess reward-seeking behavior, sleep patterns, aggression, and hypersexuality; these characteristics are disrupted in human mania patients, and these behaviors can be assessed in mice [207-209].

Because deficient maternal care of pups is known to impair mood-related behaviors in adulthood [148-151, 199], the dKO mice used in the psychopathological behavior studies were raised by WT foster moms. Having characterized the neurological behaviors caused by deletion of *Dgki* and *Dgkh*, it would now be interesting to determine how poor maternal care in the neonatal period would affect dKO pups compared to WT pups. Likewise, now that we have determined how deletion of *Dgki* and *Dgkh* manifests in behavioral abnormalities in virgin females, it would be interesting to examine the postpartum phenotypes of dKO females. Parturition can exacerbate mood-related disorders in humans [202], and may do so in dKO female mice, as well. This would also have implications for our understanding of the pathology behind their maternal behavior deficits. Differences in pre- and post-partum psychopathological behaviors in dKO mice would suggest that parturition alters behavior in dKO females, which may explain why their nurturing behaviors are impaired in the first few days after the birth of a new litter. In Chapter 4, I discussed the potential for mood-related phenotypes to cause the deficient nurturing phenotype in the dKO females, as well as the potential for these phenotypes to arise by independent mechanisms. This could be tested in the mice by treating pregnant dKO

dams with a pregnancy-safe dose of a mood stabilizer (e.g. lithium) and observing whether this improves their ability to care for their young.

Further studies are also needed to discover the signaling mechanisms by which *Dgki* and *Dgkh* loss lead to anxious and/or hyperactive behavior. Both *Dgkh*$^{-/-}$ and *Dgkb*$^{-/-}$ male mice developed by other researchers showed signs of mania and/or hyperactivity that were reversed with lithium treatment [29, 39]. Phosphorylation of GSK3β was reduced in cortices of both mouse models. Because our *Dgki*$^{-/-}$, *Dgkh*$^{-/-}$, and dKO mice also showed altered mood-related phenotypes following *Dgk* deletion, it is possible that GSK3β phosphorylation may also be reduced in the brains of our mouse models.

Lingering questions

In the discussion of each chapter, I have suggested potential mechanisms that could explain the phenotypes we observed from loss of *Dgki* and/or *Dgkh* in mice. In this chapter, I have added additional hypotheses that connect the findings of multiple chapters and have proposed experiments to test those hypotheses. Developing a more detailed understanding of how *Dgki* and *Dgkh* regulate mammalian biology may help to answer some of the following remaining questions.

Why do dKO mice resemble the Dgki*$^{-/-}$ *mice in some behavioral assays rather than the Dgkh*$^{-/-}$ *mice?

In many tests performed with our three mouse models, using either the animals or their tissues, only one of the single *Dgk*-knockout mice differed from WT. For these cases, loss of *Dgkh* or *Dgki* was sufficient to affect behavior, and thus the mice lacking both *Dgki* and *Dgkh* phenocopied the affected single knockout mouse. However, in tests of *in vivo* histamine sensitivity, *Dgki*$^{-/-}$ and *Dgkh*$^{-/-}$ both differed from WT in opposite directions, but the dKO mice resembled the *Dgki*$^{-/-}$ mice. Histamine-induced scratching was increased in *Dgki*$^{-/-}$ mice and

decreased in *Dgkh*$^{-/-}$ mice, and was increased in dKO mice. Comparing the many phenotypes that differ between the three mouse models helped us speculate how the individual *Dgk* genes may regulate somatosensation (discussed in Chapter 3 above). However, why the *Dgki*$^{-/-}$ phenotype masks the *Dgkh*$^{-/-}$ phenotype in the dKO mice remains to be determined.

Do the sensory and psychopathological phenotypes have a common pathology?

The expression of *Dgki* and *Dgkh* in a wide range of neuronal tissues leads to the knockout mice having many neurological phenotypes, including disruptions in histamine-induced itch, mood regulation, and maternal behaviors. The connections between mood phenotypes and maternal behaviors were discussed in Chapter 4 above, but it would also be interesting to explore the potential connections between these phenotypes and itch. For example, does histamine hypersensitivity in dKO females contribute to reduced nursing behaviors? Certainly, we need to keep in mind all the phenotypes observed in the *Dgk* mutant mice in determining how to modulate one particular phenotype. For example, treating histamine-induced itch by enhancing *Dgki* function may influence psychopathological behaviors in males. In addition to being an interesting thought experiment, the potential overlaps in the development of itch- and mood-related symptoms may have clinical relevance.

Why are there sex differences in the effects of* Dgk *deletion in mice?

In many tests of sensory and psychopathological behavior, males were more sensitive to *Dgki* or *Dgkh* loss than females. *Dgkh* loss only affected *in vivo* histamine response in the males (Figure 3.4). *Dgkh* or *Dgki* loss only affected exploratory behavior and/or activity levels in the open field test in males (Figure 4.4). DGKI and DGKH protein levels are not higher in neuronal tissues of WT males versus females (see westerns in Figure 2.3 and Figure 2.4E-G, quantification not shown) and, thus, would not explain why *Dgkh*/*Dgki* disruption have a greater

impact on males. Once we identify the mechanism by which *Dgki* or *Dgkh* loss disrupts mouse behavior, we will be able to probe differences in those systems between males and females.

Why does our Dgkh$^{-/-}$ mouse behave differently from the Dgkh$^{-/-}$ mouse created by other researchers?

To analyze the role of *Dgkh* in mammalian biology, we developed a *Dgkh*$^{-/-}$ mouse using CRISPR-Cas9 technology to disrupt the *Dgkh* gene at exon 9 (Figure 2.4). Researchers in the lab of Fumio Sakane recently developed a *Dgkh*$^{-/-}$ mouse using traditional homologous recombination methods targeting exon 6 [39]. In the FST, used as an assay of depression- and mania-like behavior, we found that our *Dgkh*$^{-/-}$ male mice showed increased immobility relative to WT male mice, suggesting a slight depression-like phenotype (Figure 4.1). The *Dgkh*$^{-/-}$ mutant mouse generated by the Sakane lab was tested on the tail suspension assay, which is analogous to the FST. In this assay, mice are suspended upside-down by their tails and immobility time is measured. The Sakane lab's *Dgkh*$^{-/-}$ males showed decreased immobility relative to WT in this assay [39]. Additionally, the Sakane lab found that their *Dgkh*-knockout males spent more time in the open arms of the EPM than WT males, whereas we found that our *Dgkh*$^{-/-}$ males did not differ from WT males in the EPM (Figure 4.2). However, we both demonstrated that our respective *Dgkh* mutant males showed increased activity in the center of the open field (Figure 4.4G). Mouse behavior varies greatly depending on factors including the testing environment, the experimenter, the time of day, and the housing conditions [125, 210-214]. These two *Dgkh* mutant models were tested in different environments, and these variations in testing conditions likely evoked variable phenotypes in the mice.

Broad implications

As discussed above, our findings have implications for the treatment of histamine-induced itch, anxiety, mania, hyperactivity, and parturition-associated mood disorders. *Dgki* and

Dgkh have also be implicated in biological pathways not covered by our study. *Dgki* has a potential link to alcoholism, as *Dgki* RNA expression is 25% higher in the brains of alcohol-accepting rats relative to alcohol-avoiding rats [187]. Inhibition of *DGKI* decreased epithelial sodium channel (ENaC) activity and rescued aberrant functions of lung cells from human cystic fibrosis patients [215]. *DGKI* methylation was increased in human hepatocellular carcinoma samples [216] and was associated with decreased survival and poor treatment response in glioblastoma patients [217, 218]. Additionally, DGKH was detected in human lung cancer cell lines and lung tissue in a mouse with EGFR-mutant lung cancer [20].

We showed that *Dgki* and *Dgkh* can modulate $G\alpha_q$-GPCR signaling and lipid phosphorylation in the context of overexpression in HEK293 cells, but they have different effects on molecular activity in mouse neurons. Therefore, researchers studying *Dgki* and *Dgkh* in other contexts should focus their analyses of the molecular functions of these kinases on their tissue/cell type of interest. However, while our HEK293 findings did not translate to mouse DRG, the effects we found of *Dgki* and *Dgkh* on signaling in HEK293 cells may still translate well to other cells types.

Overall, our research reveals the potential of *Dgki* and *Dgkh* to mediate histamine-dependent itch and mood-related behaviors. Further research will help us understand the molecular functions of *Dgki* and *Dgkh* by defining how they affect receptor signaling and modulate phosphorylation of DAG and/or MAG in order to alter behavior. Characterizing these functions may help identify future therapies for patients with chronic allergen-mediated itch and patients with mental health disorders, including those whose symptoms present during the postpartum period.

APPENDIX: ANALYSIS OF LIPIDS IN DKO NEURONAL TISSUE VIA MASS SPECTROMETRY

INTRODUCTION

As presented in the introduction to Chapter 3, DAG and MAG are important signaling lipids that can regulate DRG neuron activity. DAG and 2-AG are able to regulated pathways that inhibit or enhance itch and pain signaling (Figure 3.1). DAG activates PKC [5], which phosphorylates pain and itch receptors [45, 80], desensitizing $G\alpha_q$-GPCRs [81] and sensitizing TRPV1 [80]. DAG and 2-AG are partial agonists for TRPV1 [7, 83], and 2-AG is a full agonist for CB1 [82].

Decreasing the metabolism of DAG by inhibiting a DAG lipase attenuates pain signaling [84]. Increasing 2-AG levels by inhibiting its metabolism into either arachidonic acid (AA; by blocking monoacylglycerol lipase) [219] and prostaglandins (PG; by blocking cyclooxygenase-2) [220] can provide analgesia. Both AA and PG are pronociceptive agents [220, 221]. It is unclear whether elevating endogenous 2-AG alone is sufficient to relieve pain or if it is also necessary to block production of these proalgesic metabolites. Overall, previous research suggests that changing the levels of lipids in this network can control somatosensory responses. Disruption of DAG lipase and MAG lipase functions also impact lipid metabolism in the brain [86, 222], although the behavioral implications are not yet fully appreciated. DAG and MAG levels can also be altered through phosphorylation, which converts them into PA and LPA, both of which have been implicated in the regulation of sensory signaling [8, 106, 223, 224].

Not only can *Dgki* and *Dgkh* regulate the activity of various signaling molecules, but they may also alter the balance of signaling lipids in the DRG and the brain. In the DRG kinase activity assay, deletion of *Dgkh* reduced phosphorylation of all DAG and MAG substrates tested (Figure 3.17). Therefore, metabolism of acylglycerols is reduced in the absence of *Dgkh*, and levels of these lipids may be altered in neuronal tissues of dKO mice. We aimed to delineate how this lipid balance was regulated in neurons lacking *Dgki* and *Dgkh* expression, with the goal

of understanding the pathology underlying the somatosensory and psychopathological phenotypes observed in dKO mice.

RESULTS

We collaborated with the NIH West Coast Metabolomics Center to identify and quantify the lipid components in DRG and cortical tissue from dKO mice using mass spectrometry. Our goal was to use this technology to determine how the levels of various lipids change in neurons of the brain and the DRG in the absence of *Dgki* and *Dgkh*, including DAG and MAG species, PA and LPA, as well as 2-AG and its metabolites. Experts at the NIH West Coast Metabolomics Center analyzed DRG and cortex samples from WT and dKO male and female mice via liquid chromatography coupled with mass spectrometry [225]. Details of this analysis are described in the Methods below. For each tissue (cortex and DRG) and each ionization mode (positive and negative), the fold change (dKO/WT) for each lipid was calculated, as was the significance of that change. The results are shown in Figure 0.1. Lipids whose identity is unknown are formatted with numbers representing “retention time_m/z.”

DISCUSSION

The lipid profiles in both the DRG and the brain were disrupted by deletion of *Dgki* and *Dgkh*, with several lipids showing significant up- or down-regulation in dKO tissues relative to WT. The data presented here show genotype-specific changes for both sexes combined. Some significantly-altered lipids were specific to male or female tissue (data not shown), but most of the lipids shown to significantly differ from WT in Figure 0.1 were altered in both sexes. Of the identifiable lipids marked as hits, the only pattern that emerges is a disruption in triglyceride balance in the DRG (Figure 0.1A); however, triglycerides are both up- and down-regulated in dKO DRG tissue.

One obvious feature of the lipids marked as “hits” in Figure 0.1 is that the identity of many lipids are unknown (labeled as "#.##_###.##" representing "retention time_m/z"). The identity of a lipid cannot be confirmed as a “known” without evidence of the matching experimental mass spectrum. Even with the availability of mass spectrum databases, a small fraction of known chemicals have experimental mass spectra [226], and *in silico* modeling does not always accurately predict mass spectroscopy results [227]. With many of our top hits being unknowns, our data cannot yet tell us which lipids are disrupted in dKO neuronal tissue; however, as more unknowns become knowns in the future, we will be able to reanalyze these data sets.

METHODS

DRG and right front cortex tissue was dissected from twenty 2- to 3-month-old mice: five each of WT male, dKO male, WT female, and dKO female. Tissues were placed in microcentrifuge tubes with no buffer and frozen at -80°C. Within 48 hours, samples were shipped to the NIH West Coast Metabolomics Center (Davis, California), where lipids were extracted and processed for mass spectrometry. Metabolites were separated with ultra-high-pressure liquid chromatography. Electrospray ionization was performed in both positive and negative mode; both were used, as each method yields variation in the metabolites captured. Metabolites were detected with quadrupole time-of-flight mass spectrometry. Spectral profiles, retention times, and mass-to-charge ratios (m/z) were compared to databases of known lipids to identify lipids in our samples, and peak intensities were quantified. For analysis of the data, males and females were combined within each genotype. The dKO/WT fold change was calculated for each lipid, and the significance of that change was calculated via Student’s t-test, using the MetaBox online platform for analysis of metabolomics data [228].

FIGURES

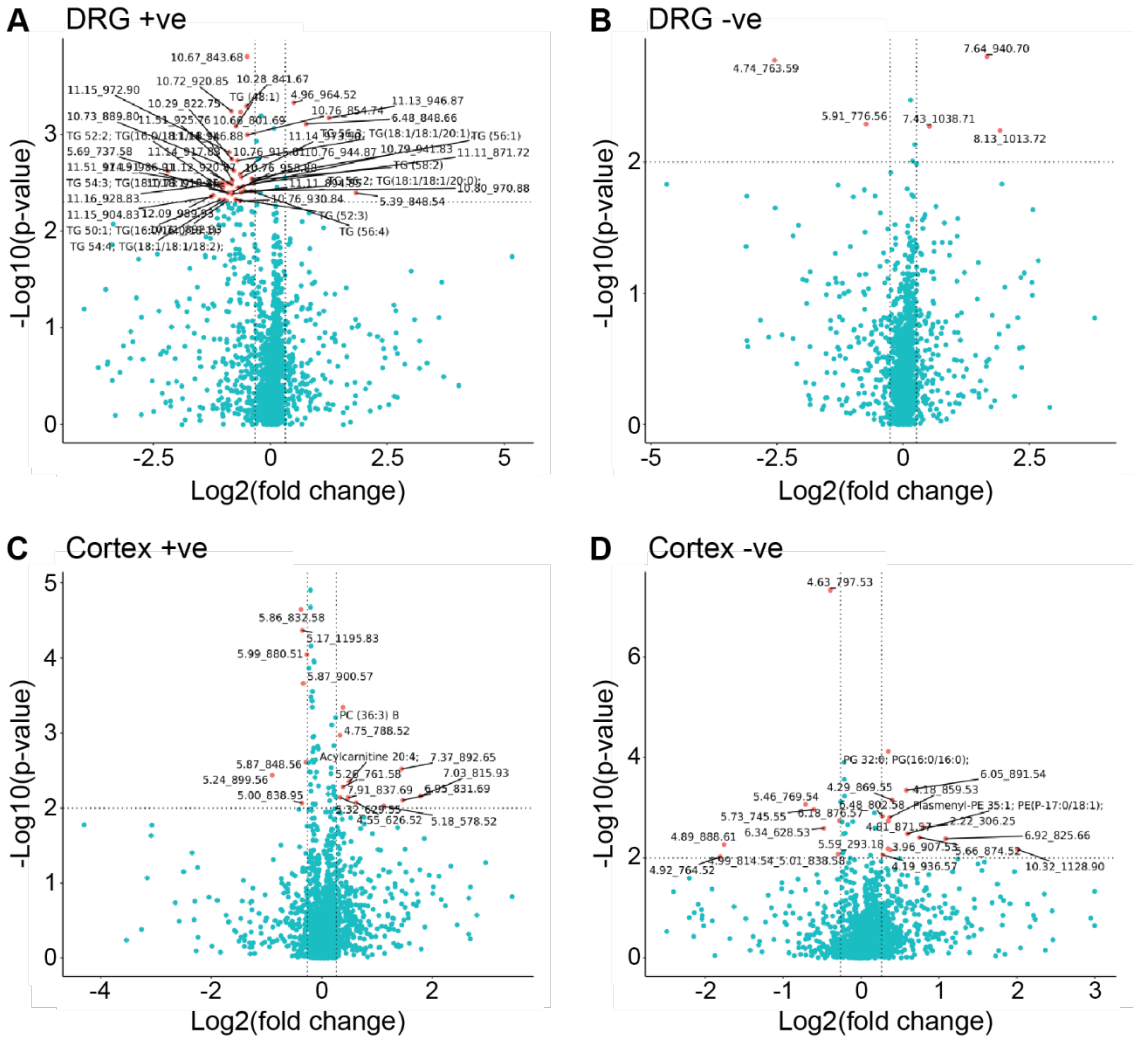

Figure 0.1. Top hits of mass spectrometry analysis comparing lipid levels in WT and dKO mouse neuronal tissue. Volcano plots indicate the magnitude (fold change) and significance (p-value) of lipids whose levels differed between WT and dKO DRG (A,B) and cortex (C,D) when positive (A,C) or negative (B,D) ionization was used. All lipids with a p-value lower than 0.01 and a fold change of ± 25% (dotted lines) are shown in red and are labeled.

REFERENCES

1. Topham MK, Epand RM. Mammalian diacylglycerol kinases: molecular interactions and biological functions of selected isoforms. Biochim Biophys Acta. 2009;1790(6):416-24. Epub 2009/04/15. doi: 10.1016/j.bbagen.2009.01.010. PMID: 19364481.

2. Merida I, Avila-Flores A, Merino E. Diacylglycerol kinases: at the hub of cell signalling. Biochem J. 2008;409(1):1-18. Epub 2007/12/08. doi: 10.1042/bj20071040. PMID: 18062770.

3. Shulga YV, Topham MK, Epand RM. Regulation and functions of diacylglycerol kinases. Chem Rev. 2011;111(10):6186-208. Epub 2011/08/02. doi: 10.1021/cr1004106. PMID: 21800853.

4. Sakane F, Imai S, Kai M, Yasuda S, Kanoh H. Diacylglycerol kinases: why so many of them? Biochim Biophys Acta. 2007;1771(7):793-806. Epub 2007/05/22. doi: 10.1016/j.bbalip.2007.04.006. PMID: 17512245.

5. Marignani PA, Epand RM, Sebaldt RJ. Acyl chain dependence of diacylglycerol activation of protein kinase C activity in vitro. Biochem Biophys Res Commun. 1996;225(2):469-73. doi: http://dx.doi.org/10.1006/bbrc.1996.1196.

6. Hall C, Lim L, Leung T. C1, see them all. Trends Biochem Sci. 2005;30(4):169-71. doi: https://doi.org/10.1016/j.tibs.2005.02.003.

7. Woo DH, Jung SJ, Zhu MH, Park CK, Kim YH, Oh SB, et al. Direct activation of transient receptor potential vanilloid 1(TRPV1) by diacylglycerol (DAG). Mol Pain. 2008;4:42. Epub 2008/10/02. doi: 10.1186/1744-8069-4-42. PMID: 18826653.

8. Cockcroft S. Phosphatidic acid regulation of phosphatidylinositol 4-phosphate 5-kinases. Biochim Biophys Acta. 2009;1791(9):905-12. doi: http://dx.doi.org/10.1016/j.bbalip.2009.03.007.

9. Fang Y, Vilella-Bach M, Bachmann R, Flanigan A, Chen J. Phosphatidic acid-mediated mitogenic activation of mTOR signaling. Science. 2001;294(5548):1942-5. Epub 2001/12/01. doi: 10.1126/science.1066015. PMID: 11729323.

10. Levitzki A. Protein kinase inhibitors as a therapeutic modality. Acc Chem Res. 2003;36(6):462-9. Epub 2003/06/18. doi: 10.1021/ar0201207. PMID: 12809533.

11. Hopkins AL, Groom CR. The druggable genome. Nature Reviews Drug Discovery. 2002;1(9):727-30. doi: http://www.nature.com/nrd/journal/v1/n9/suppinfo/nrd892_S1.html.

12. Sanjuan MA, Pradet-Balade B, Jones DR, Martinez AC, Stone JC, Garcia-Sanz JA, et al. T cell activation in vivo targets diacylglycerol kinase alpha to the membrane: a novel mechanism for Ras attenuation. J Immunol. 2003;170(6):2877-83. Epub 2003/03/11. PMID: 12626538.

13. Zha Y, Marks R, Ho AW, Peterson AC, Janardhan S, Brown I, et al. T cell anergy is reversed by active Ras and is regulated by diacylglycerol kinase-alpha. Nat Immunol. 2006;7(11):1166-73. Epub 2006/10/10. doi: 10.1038/ni1394. PMID: 17028589.

14. Topham MK, Prescott SM. Diacylglycerol kinase zeta regulates Ras activation by a novel mechanism. J Cell Biol. 2001;152(6):1135-43. Epub 2001/03/21. PMID: 11257115.

15. Zhong XP, Hainey EA, Olenchock BA, Zhao H, Topham MK, Koretzky GA. Regulation of T cell receptor-induced activation of the Ras-ERK pathway by diacylglycerol kinase zeta. J Biol Chem. 2002;277(34):31089-98. Epub 2002/06/19. doi: 10.1074/jbc.M203818200. PMID: 12070163.

16. Olenchock BA, Guo R, Carpenter JH, Jordan M, Topham MK, Koretzky GA, et al. Disruption of diacylglycerol metabolism impairs the induction of T cell anergy. Nat Immunol. 2006;7(11):1174-81. Epub 2006/10/10. doi: 10.1038/ni1400. PMID: 17028587.

17. Niizeki T, Takeishi Y, Kitahara T, Arimoto T, Koyama Y, Goto K, et al. Diacylglycerol kinase zeta rescues G alpha q-induced heart failure in transgenic mice. Circ J. 2008;72(2):309-17. Epub 2008/01/26. PMID: 18219172.

18. Niizeki T, Takeishi Y, Kitahara T, Arimoto T, Ishino M, Bilim O, et al. Diacylglycerol kinase-epsilon restores cardiac dysfunction under chronic pressure overload: a new specific regulator of Galpha(q) signaling cascade. Am J Physiol Heart Circ Physiol. 2008;295(1):H245-55. Epub 2008/05/20. doi: 10.1152/ajpheart.00066.2008. PMID: 18487437.

19. Takeishi K, Taketomi A, Shirabe K, Toshima T, Motomura T, Ikegami T, et al. Diacylglycerol kinase alpha enhances hepatocellular carcinoma progression by activation of Ras-Raf-MEK-ERK pathway. J Hepatol. 2012;57(1):77-83. Epub 2012/03/20. doi: 10.1016/j.jhep.2012.02.026. PMID: 22425622.

20. Nakano T, Iravani A, Kim M, Hozumi Y, Lohse M, Reichert E, et al. Diacylglycerol kinase eta modulates oncogenic properties of lung cancer cells. Clin Transl Oncol. 2014;16(1):29-35. Epub 2013/04/11. doi: 10.1007/s12094-013-1036-y. PMID: 23572183.

21. Cai J, Crotty TM, Reichert E, Carraway KL, Stafforini DM, Topham MK. Diacylglycerol Kinase δ and Protein Kinase Cα Modulate Epidermal Growth Factor Receptor Abundance and Degradation through Ubiquitin-specific Protease 8. J Biol Chem. 2010;285(10):6952-9. doi: 10.1074/jbc.M109.055731. PMID: 20064931.

22. Cai K, Mulatz K, Ard R, Nguyen T, Gee SH. Increased diacylglycerol kinase zeta expression in human metastatic colon cancer cells augments Rho GTPase activity and contributes to enhanced invasion. BMC Cancer. 2014;14:208. Epub 2014/03/22. doi: 10.1186/1471-2407-14-208. PMID: 24646293.

23. Regier DS, Higbee J, Lund KM, Sakane F, Prescott SM, Topham MK. Diacylglycerol kinase ı regulates Ras guanyl-releasing protein 3 and inhibits Rap1 signaling. Proc Natl Acad Sci U S A. 2005;102(21):7595-600. doi: 10.1073/pnas.0500663102.

24. Kai M, Yamamoto E, Sato A, Yamano HO, Niinuma T, Kitajima H, et al. Epigenetic silencing of diacylglycerol kinase gamma in colorectal cancer. Mol Carcinog. 2017;56(7):1743-52. Epub 2017/02/22. doi: 10.1002/mc.22631. PMID: 28218473.

25. Tu-Sekine B, Raben DM. Regulation and roles of neuronal diacylglycerol kinases: a lipid perspective. Crit Rev Biochem Mol Biol. 2011;46(5):353-64. Epub 2011/05/05. doi: 10.3109/10409238.2011.577761. PMID: 21539478.

26. Shirai Y, Saito N. Diacylglycerol kinase as a possible therapeutic target for neuronal diseases. J Biomed Sci. 2014;21:28. Epub 2014/04/09. doi: 10.1186/1423-0127-21-28. PMID: 24708409.

27. Kim K, Yang J, Kim E. Diacylglycerol kinases in the regulation of dendritic spines. J Neurochem. 2010;112(3):577-87. Epub 2009/11/20. doi: 10.1111/j.1471-4159.2009.06499.x. PMID: 19922438.

28. Lee D, Kim E, Tanaka-Yamamoto K. Diacylglycerol kinases in the coordination of synaptic plasticity. Front Cell Dev Biol. 2016;4(92). doi: 10.3389/fcell.2016.00092.

29. Kakefuda K, Oyagi A, Ishisaka M, Tsuruma K, Shimazawa M, Yokota K, et al. Diacylglycerol kinase beta knockout mice exhibit lithium-sensitive behavioral abnormalities. PLoS One. 2010;5(10):e13447. Epub 2010/10/27. doi: 10.1371/journal.pone.0013447. PMID: 20976192.

30. Frere SG, Di Paolo G. A lipid kinase controls the maintenance of dendritic spines. EMBO J. 2009;28(8):999-1000. doi: 10.1038/emboj.2009.77.

31. Tabet R, Moutin E, Becker JAJ, Heintz D, Fouillen L, Flatter E, et al. Fragile X Mental Retardation Protein (FMRP) controls diacylglycerol kinase activity in neurons. Proc Natl Acad Sci U S A. 2016;113(26):E3619-E28. doi: 10.1073/pnas.1522631113. PMID: PMC4932937.

32. Yang J, Seo J, Nair R, Han S, Jang S, Kim K, et al. DGKι regulates presynaptic release during mGluR-dependent LTD. EMBO J. 2011;30(1):165-80. Epub 2010/12/02. doi: 10.1038/emboj.2010.286. PMID: 21119615.

33. Seo J, Kim K, Jang S, Han S, Choi SY, Kim E. Regulation of hippocampal long-term potentiation and long-term depression by diacylglycerol kinase zeta. Hippocampus. 2012;22(5):1018-26. Epub 2010/11/12. doi: 10.1002/hipo.20889. PMID: 21069783.

34. Shirai Y, Kouzuki T, Kakefuda K, Moriguchi S, Oyagi A, Horie K, et al. Essential role of neuron-enriched diacylglycerol kinase (DGK), DGKβ in neurite spine formation, contributing to cognitive function. PLoS One. 2010;5(7):e11602. Epub 2010/07/27. doi: 10.1371/journal.pone.0011602. PMID: 20657643.

35. Rodriguez de Turco EB, Tang W, Topham MK, Sakane F, Marcheselli VL, Chen C, et al. Diacylglycerol kinase ε regulates seizure susceptibility and long-term potentiation through arachidonoyl– inositol lipid signaling. Proc Natl Acad Sci U S A. 2001;98(8):4740-5. doi: 10.1073/pnas.081536298.

36. Kim K, Yang J, Zhong X-P, Kim M-H, Kim YS, Lee HW, et al. Synaptic removal of diacylglycerol by DGKζ and PSD-95 regulates dendritic spine maintenance. EMBO J. 2009;28(8):1170-9. doi: 10.1038/emboj.2009.44. PMID: PMC2683696.

37. Leach NT, Sun Y, Michaud S, Zheng Y, Ligon KL, Ligon AH, et al. Disruption of diacylglycerol kinase delta (DGKD) associated with seizures in humans and mice. Am J Hum Genet. 2007;80(4):792-9. PMID: PMC1852716.

38. Ishisaka M, Tsuruma K, Shimazawa M, Shirai Y, Saito N, Hara H. Increased seizure susceptibility in a mouse with diacylglycerol kinase β deficiency. Neurosci Med. 2013;04(02):117–22. doi: 10.4236/nm.2013.42019.

39. Isozaki T, Komenoi S, Lu Q, Usuki T, Tomokata S, Matsutomo D, et al. Deficiency of diacylglycerol kinase eta induces lithium-sensitive mania-like behavior. J Neurochem. 2016;138(3):448-56. Epub 2016/05/12. doi: 10.1111/jnc.13661. PMID: 27167678.

40. Baum AE, Akula N, Cabanero M, Cardona I, Corona W, Klemens B, et al. A genome-wide association study implicates diacylglycerol kinase eta (DGKH) and several other genes in the etiology of bipolar disorder. Mol Psychiatry. 2008;13(2):197-207. Epub 2007/05/09. doi: 10.1038/sj.mp.4002012. PMID: 17486107.

41. Weber H, Kittel-Schneider S, Gessner A, Domschke K, Neuner M, Jacob CP, et al. Cross-disorder analysis of bipolar risk genes: further evidence of DGKH as a risk gene for bipolar disorder, but also unipolar depression and adult ADHD. Neuropsychopharmacology. 2011;36(10):2076-85. Epub 2011/06/10. doi: 10.1038/npp.2011.98. PMID: 21654738.

42. Moskvina V, Craddock N, Holmans P, Nikolov I, Pahwa JS, Green E, et al. Gene-wide analyses of genome-wide association data sets: evidence for multiple common risk alleles for schizophrenia and bipolar disorder and for overlap in genetic risk. Mol Psychiatry. 2009;14(3):252-60. Epub 2008/12/10. doi: 10.1038/mp.2008.133. PMID: 19065143.

43. Schizophrenia Working Group of the Psychiatric Genomics C. Biological insights from 108 schizophrenia-associated genetic loci. Nature. 2014;511(7510):421-7. doi: 10.1038/nature13595 http://www.nature.com/nature/journal/v511/n7510/abs/nature13595.html#supplementary-information.

44. Ruderfer DM, Ripke S, McQuillin A, Boocock J, Stahl EA, Pavlides JMW, et al. Genomic dissection of bipolar disorder and schizophrenia, including 28 subphenotypes. Cell. 2018;173(7):1705-15.e16. doi: 10.1016/j.cell.2018.05.046.

45. Rittiner JE, Brings VE, Zylka MJ. Overexpression of diacylglycerol kinase eta enhances Gαq-coupled G protein-coupled receptor signaling. Mol Pharmacol. 2014;85(5):800-10. Epub 2014/03/13. doi: 10.1124/mol.113.091280. PMID: 24608858.

46. van Baal J, de Widt J, Divecha N, van Blitterswijk WJ. Diacylglycerol kinase theta counteracts protein kinase C-mediated inactivation of the EGF receptor. Int J Biochem Cell Biol. 2012;44(11):1791-9. Epub 2012/06/27. doi: 10.1016/j.biocel.2012.06.021. PMID: 22732145.

47. Crotty T, Cai J, Sakane F, Taketomi A, Prescott SM, Topham MK. Diacylglycerol kinase delta regulates protein kinase C and epidermal growth factor receptor signaling. Proc Natl Acad Sci U S A. 2006;103(42):15485-90. Epub 2006/10/06. doi: 10.1073/pnas.0604104103. PMID: 17021016.

48. Yasuda S, Kai M, Imai S-i, Takeishi K, Taketomi A, Toyota M, et al. Diacylglycerol kinase η augments C-Raf activity and B-Raf/C-Raf heterodimerization. J Biol Chem. 2009;284(43):29559-70. doi: 10.1074/jbc.M109.043604.

49. Yasuda S, Kai M, Imai S, Kanoh H, Sakane F. Diacylglycerol kinase gamma interacts with and activates beta2-chimaerin, a Rac-specific GAP, in response to epidermal growth factor. FEBS Lett. 2007;581(3):551-7. Epub 2007/01/27. doi: 10.1016/j.febslet.2007.01.022. PMID: 17254573.

50. Yakubchyk Y, Abramovici H, Maillet JC, Daher E, Obagi C, Parks RJ, et al. Regulation of neurite outgrowth in N1E-115 cells through PDZ-mediated recruitment of diacylglycerol kinase zeta. Mol Cell Biol. 2005;25(16):7289-302. Epub 2005/08/02. doi: 10.1128/mcb.25.16.7289-7302.2005. PMID: 16055737.

51. Tang W, Bunting M, Zimmerman GA, McIntyre TM, Prescott SM. Molecular cloning of a novel human diacylglycerol kinase highly selective for arachidonate-containing substrates. J Biol Chem. 1996;271(17):10237-41. Epub 1996/04/26. PMID: 8626589.

52. Madani S, Hichami A, Legrand A, Belleville J, Khan NA. Implication of acyl chain of diacylglycerols in activation of different isoforms of protein kinase C. FASEB J. 2001;15(14):2595-601. Epub 2001/12/01. doi: 10.1096/fj.01-0753int. PMID: 11726535.

53. Marignani PA, Epand RM, Sebaldt RJ. Acyl chain dependence of diacylglycerol activation of protein kinase C activity in vitro. Biochem Biophys Res Commun. 1996;225(2):469-73. Epub 1996/08/14. doi: 10.1006/bbrc.1996.1196. PMID: 8753785.

54. Eichberg J, Zhu X. Diacylglycerol composition and metabolism in peripheral nerve. Adv Exp Med Biol. 1992;318:413-25. Epub 1992/01/01. PMID: 1636507.

55. Shim YH, Lin CH, Strickland KP. The purification and properties of monoacylglycerol kinase from bovine brain. Biochem Cell Biol. 1989;67(4-5):233-41. Epub 1989/04/01. PMID: 2550036.

56. Kanoh H, Iwata T, Ono T, Suzuki T. Immunological characterization of sn-1,2-diacylglycerol and sn-2-monoacylglycerol kinase from pig brain. J Biol Chem. 1986;261(12):5597-602. Epub 1986/04/25. PMID: 3007514.

57. Obata K, Noguchi K. MAPK activation in nociceptive neurons and pain hypersensitivity. Life Sci. 2004;74(21):2643-53. doi: http://dx.doi.org/10.1016/j.lfs.2004.01.007.

58. Wang H, Yang H, Shivalila Chikdu S, Dawlaty Meelad M, Cheng Albert W, Zhang F, et al. One-step generation of mice carrying mutations in multiple genes by CRISPR/Cas-mediated genome engineering. Cell. 2013;153(4):910-8. doi: http://dx.doi.org/10.1016/j.cell.2013.04.025.

59. Tanino F, Maeda Y, Sakai H, Sakane F. Induction of filopodia-like protrusions in N1E-115 neuroblastoma cells by diacylglycerol kinase gamma independent of its enzymatic activity: potential novel function of the C-terminal region containing the catalytic domain of diacylglycerol kinase gamma. Mol Cell Biochem. 2013;373(1-2):85-93. Epub 2012/10/12. doi: 10.1007/s11010-012-1477-6. PMID: 23054194.

60. Sato Y, Murakami C, Yamaki A, Mizuno S, Sakai H, Sakane F. Distinct 1-monoacylglycerol and 2-monoacylglycerol kinase activities of diacylglycerol kinase isozymes. Biochimica et Biophysica Acta (BBA) - Proteins and Proteomics. 2016;1864(9):1170-6. doi: https://doi.org/10.1016/j.bbapap.2016.06.012.

61. Institutes of Medicine Committee on Advancing Pain Research C, and Education. Relieving pain in America: a blueprint for transforming prevention, care, education, and research: The National Academies Press; 2011. 382 p.

62. Coates MD, Lahoti M, Binion DG, Szigethy EM, Regueiro MD, Bielefeldt K. Abdominal pain in ulcerative colitis. Inflamm Bowel Dis. 2013;19(10):2207-14. Epub 2013/08/10. doi: 10.1097/MIB.0b013e31829614c6. PMID: 23929261.

63. Chronic pain and depression: Does the evidence support a relationship? [Internet]. US: American Psychological Association; 1985

64. Benyamin R, Trescot AM, Datta S, Buenaventura R, Adlaka R, Sehgal N, et al. Opioid complications and side effects. Pain Physician. 2008;11(2 Suppl):S105-20. Epub 2008/06/17. PMID: 18443635.

65. Ong CKS, Lirk P, Tan CH, Seymour RA. An evidence-based update on nonsteroidal anti-inflammatory drugs. Clinical Medicine and Research. 2007;5(1):19-34. doi: 10.3121/cmr.2007.698. PMID: PMC1855338.

66. Hong J, Buddenkotte J, Berger TG, Steinhoff M. Management of itch in atopic dermatitis. Semin Cutan Med Surg. 2011;30(2):71-86. doi: 10.1016/j.sder.2011.05.002. PMID: 21767767.

67. Akiyama T, Carstens E. Neural processing of itch. Neuroscience. 2013;250:697-714. Epub 2013/07/31. doi: 10.1016/j.neuroscience.2013.07.035. PMID: 23891755.

68. Bautista DM, Wilson SR, Hoon MA. Why we scratch an itch: the molecules, cells and circuits of itch. Nat Neurosci. 2014;17(2):175-82. doi: 10.1038/nn.3619.

69. Basbaum AI, Bautista DM, Scherrer G, Julius D. Cellular and molecular mechanisms of pain. Cell. 2009;139(2):267-84. Epub 2009/10/20. doi: 10.1016/j.cell.2009.09.028. PMID: 19837031.

70. Voscopoulos C, Lema M. When does acute pain become chronic? Br J Anaesth. 2010;105 Suppl 1:i69-85. Epub 2010/12/22. doi: 10.1093/bja/aeq323. PMID: 21148657.

71. Zhang J, Cavanaugh DJ, Nemenov MI, Basbaum AI. The modality-specific contribution of peptidergic and non-peptidergic nociceptors is manifest at the level of dorsal horn nociresponsive neurons. The Journal of Physiology. 2013;591(Pt 4):1097-110. doi: 10.1113/jphysiol.2012.242115. PMID: PMC3591717.

72. Zylka MJ, Rice FL, Anderson DJ. Topographically distinct epidermal nociceptive circuits revealed by axonal tracers targeted to Mrgprd. Neuron. 2005;45(1):17-25. doi: http://dx.doi.org/10.1016/j.neuron.2004.12.015.

73. Ikoma A, Fartasch M, Heyer G, Miyachi Y, Handwerker H, Schmelz M. Painful stimuli evoke itch in patients with chronic pruritus: central sensitization for itch. Neurology. 2004;62(2):212-7. Epub 2004/01/28. PMID: 14745056.

74. Shim WS, Oh U. Histamine-induced itch and its relationship with pain. Mol Pain. 2008;4:29. Epub 2008/08/01. doi: 10.1186/1744-8069-4-29. PMID: 18667087.

75. Liu T, Ji R-R. New insights into the mechanisms of itch: are pain and itch controlled by distinct mechanisms? Pflugers Archiv. 2013;465(12):1671-85. doi: 10.1007/s00424-013-1284-2. PMID: PMC3796138.

76. Stone LS, Molliver DC. In search of analgesia: emerging roles of GPCRs in pain. Mol Interv. 2009;9(5):234-51. doi: 10.1124/mi.9.5.7. PMID: PMC2861805.

77. Geppetti P, Veldhuis Nicholas A, Lieu T, Bunnett Nigel W. G Protein-Coupled Receptors: Dynamic Machines for Signaling Pain and Itch. Neuron. 2015;88(4):635-49. doi: https://doi.org/10.1016/j.neuron.2015.11.001.

78. Wilson SR, Gerhold KA, Bifolck-Fisher A, Liu Q, Patel KN, Dong X, et al. TRPA1 is required for histamine-independent, Mas-related G protein-coupled receptor-mediated itch. Nat Neurosci. 2011;14(5):595-602. Epub 2011/04/05. doi: 10.1038/nn.2789. PMID: 21460831.

79. Tanimura A, Yamazaki M, Hashimotodani Y, Uchigashima M, Kawata S, Abe M, et al. The endocannabinoid 2-arachidonoylglycerol produced by diacylglycerol lipase alpha mediates retrograde suppression of synaptic transmission. Neuron. 2010;65(3):320-7. Epub 2010/02/18. doi: 10.1016/j.neuron.2010.01.021. PMID: 20159446.

80. Bhave G, Hu H-J, Glauner KS, Zhu W, Wang H, Brasier DJ, et al. Protein kinase C phosphorylation sensitizes but does not activate the capsaicin receptor transient receptor potential vanilloid 1 (TRPV1). Proceedings of the National Academy of Sciences. 2003;100(21):12480-5. doi: 10.1073/pnas.2032100100.

81. Kelly E, Bailey CP, Henderson G. Agonist-selective mechanisms of GPCR desensitization. Br J Pharmacol. 2008;153(Suppl 1):S379-S88. doi: 10.1038/sj.bjp.0707604. PMID: PMC2268061.

82. Sugiura T, Kodaka T, Nakane S, Miyashita T, Kondo S, Suhara Y, et al. Evidence that the cannabinoid CB1 receptor is a 2-arachidonoylglycerol receptor: structure-activity relationship of 2-arachidonoylglycerol, ether-linked analogues, and related compounds. J Biol Chem. 1999;274(5):2794-801. doi: 10.1074/jbc.274.5.2794.

83. Zygmunt PM, Ermund A, Movahed P, Andersson DA, Simonsen C, Jonsson BA, et al. Monoacylglycerols activate TRPV1--a link between phospholipase C and TRPV1. PLoS One. 2013;8(12):e81618. Epub 2013/12/07. doi: 10.1371/journal.pone.0081618. PMID: 24312564.

84. Wilkerson JL, Ghosh S, Bagdas D, Mason BL, Crowe MS, Hsu KL, et al. Diacylglycerol lipase β inhibition reverses nociceptive behaviour in mouse models of inflammatory and neuropathic pain. Br J Pharmacol. 2016;173(10):1678-92. doi: 10.1111/bph.13469.

85. Long JZ, Li W, Booker L, Burston JJ, Kinsey SG, Schlosburg JE, et al. Selective blockade of 2-arachidonoylglycerol hydrolysis produces cannabinoid behavioral effects. Nat Chem Biol. 2009;5(1):37-44. Epub 2008/11/26. doi: 10.1038/nchembio.129. PMID: 19029917.

86. Zhong P, Pan B, Gao XP, Blankman JL, Cravatt BF, Liu QS. Genetic deletion of monoacylglycerol lipase alters endocannabinoid-mediated retrograde synaptic depression in the cerebellum. The Journal of Physiology. 2011;589(Pt 20):4847-55. Epub 2011/09/14. doi: 10.1113/jphysiol.2011.215509. PMID: 21911610.

87. Ray P, Torck A, Quigley L, Wangzhou A, Neiman M, Rao C, et al. Comparative transcriptome profiling of the human and mouse dorsal root ganglia: an RNA-seq-based resource for pain and sensory neuroscience research. Pain. 2018;159(7):1325-45. Epub 2018/03/22. doi: 10.1097/j.pain.0000000000001217. PMID: 29561359.

88. Wu C, Orozco C, Boyer J, Leglise M, Goodale J, Batalov S, et al. BioGPS: an extensible and customizable portal for querying and organizing gene annotation resources. Genome Biol. 2009;10(11):R130. doi: 10.1186/gb-2009-10-11-r130.

89. Usoskin D, Furlan A, Islam S, Abdo H, Lonnerberg P, Lou D, et al. Unbiased classification of sensory neuron types by large-scale single-cell RNA sequencing. Nat Neurosci. 2015;18(1):145-53. doi: 10.1038/nn.3881.

90. Sasaki H, Hozumi Y, Hasegawa H, Ito T, Takagi M, Ogino T, et al. Gene expression and localization of diacylglycerol kinase isozymes in the rat spinal cord and dorsal root ganglia. Cell Tissue Res. 2006;326(1):35-42. Epub 2006/06/08. doi: 10.1007/s00441-006-0219-z. PMID: 16758180.

91. Liu Q, Sikand P, Ma C, Tang Z, Han L, Li Z, et al. Mechanisms of itch evoked by beta-alanine. The Journal of Neuroscience. 2012;32(42):14532-7. Epub 2012/10/19. doi: 10.1523/jneurosci.3509-12.2012. PMID: 23077038.

92. Wang JJ, Ho ST, Hu OY, Chu KM. An innovative cold tail-flick test: the cold ethanol tail-flick test. Anesth Analg. 1995;80(1):102-7. Epub 1995/01/01. PMID: 7802265.

93. Janssen PA, Niemegeers CJ, Dony JG. The inhibitory effect of fentanyl and other morphine-like analgesics on the warm water induced tail withdrawl reflex in rats. Arzneimittelforschung. 1963;13:502-7. Epub 1963/06/01. PMID: 13957426.

94. Nishihara I, Minami T, Uda R, Ito S, Hyodo M, Hayaishi O. Effect of NMDA receptor antagonists on prostaglandin E2-induced hyperalgesia in conscious mice. Brain Res. 1995;677(1):138-44. Epub 1995/04/17. PMID: 7606458.

95. Brenner DS, Golden JP, Gereau RW. A novel behavioral assay for measuring cold sensation in mice. PLoS One. 2012;7(6):e39765. doi: 10.1371/journal.pone.0039765. PMID: PMC3382130.

96. Mogil JS, Ritchie J, Smith SB, Strasburg K, Kaplan L, Wallace MR, et al. Melanocortin-1 receptor gene variants affect pain and μ-opioid analgesia in mice and humans. J Med Genet. 2005;42(7):583-7. doi: 10.1136/jmg.2004.027698.

97. Garrison SR, Dietrich A, Stucky CL. TRPC1 contributes to light-touch sensation and mechanical responses in low-threshold cutaneous sensory neurons. J Neurophysiol. 2012;107(3):913-22. doi: 10.1152/jn.00658.2011. PMID: PMC3289471.

98. McCoy ES, Taylor-Blake B, Street SE, Pribisko AL, Zheng J, Zylka MJ. Peptidergic CGRPα primary sensory neurons encode heat and itch and tonically suppress sensitivity to cold. Neuron. 2013;78(1):138-51. Epub 2013/03/26. doi: 10.1016/j.neuron.2013.01.030. PMID: 23523592.

99. Cunha TM, Verri Jr. WA, Vivancos GG, Moreira IF, Reis S, Parada CA, et al. An electronic pressure-meter nociception paw test for mice. Braz J Med Biol Res. 2004;37:401-7.

100. Hargreaves K, Dubner R, Brown F, Flores C, Joris J. A new and sensitive method for measuring thermal nociception in cutaneous hyperalgesia. Pain. 1988;32(1):77-88. Epub 1988/01/01. PMID: 3340425.

101. Decosterd I, Woolf CJ. Spared nerve injury: an animal model of persistent peripheral neuropathic pain. Pain. 2000;87(2):149-58. Epub 2000/08/05. PMID: 10924808.

102. Shields SD, Eckert WA, 3rd, Basbaum AI. Spared nerve injury model of neuropathic pain in the mouse: a behavioral and anatomic analysis. J Pain. 2003;4(8):465-70. Epub 2003/11/19. PMID: 14622667.

103. Chaplan SR, Bach FW, Pogrel JW, Chung JM, Yaksh TL. Quantitative assessment of tactile allodynia in the rat paw. J Neurosci Methods. 1994;53(1):55-63. Epub 1994/07/01. PMID: 7990513.

104. Pingle SC, Matta JA, Ahern GP. Capsaicin receptor: TRPV1 a promiscuous TRP channel. Handb Exp Pharmacol. 2007;(179):155-71. Epub 2007/01/16. doi: 10.1007/978-3-540-34891-7_9. PMID: 17217056.

105. Renback K, Inoue M, Yoshida A, Nyberg F, Ueda H. Vzg-1/lysophosphatidic acid-receptor involved in peripheral pain transmission. Molecular Brain Research. 2000;75(2):350-4. Epub 2000/02/25. PMID: 10686359.

106. Inoue M, Rashid MH, Fujita R, Contos JJ, Chun J, Ueda H. Initiation of neuropathic pain requires lysophosphatidic acid receptor signaling. Nat Med. 2004;10(7):712-8. Epub 2004/06/15. doi: 10.1038/nm1060. PMID: 15195086.

107. Gerevich Z, Illes P. P2Y receptors and pain transmission. Purinergic Signal. 2004;1(1):3-10. doi: 10.1007/s11302-004-4740-9. PMID: 18404394.

108. Hockley JRF, Tranter MM, McGuire C, Boundouki G, Cibert-Goton V, Thaha MA, et al. P2Y Receptors Sensitize Mouse and Human Colonic Nociceptors. J Neurosci. 2016;36(8):2364-76. doi: 10.1523/jneurosci.3369-15.2016. PMID: 26911685.

109. Michael GJ, Priestley JV. Differential expression of the mRNA for the vanilloid receptor subtype 1 in cells of the adult rat dorsal root and nodose ganglia and its downregulation by axotomy. The Journal of Neuroscience. 1999;19(5):1844-54. Epub 1999/02/19. PMID: 10024368.

110. Elmes SJR, Millns PJ, Smart D, Kendall DA, Chapman V. Evidence for biological effects of exogenous LPA on rat primary afferent and spinal cord neurons. Brain Res. 2004;1022(1–2):205-13. doi: 10.1016/j.brainres.2004.07.005.

111. Jankowski MP, Koerber HR. Neurotrophic Factors and Nociceptor Sensitization. In: Kruger L, Light AR, editors. Translational Pain Research: From Mouse to Man. Boca Raton, FL: CRC Press/Taylor & Francis Llc.; 2010.

112. Carlos D, Sá-Nunes A, de Paula L, Matias-Peres C, Jamur MC, Oliver C, et al. Histamine modulates mast cell degranulation through an indirect mechanism in a model IgE-mediated reaction. Eur J Immunol. 2006;36(6):1494-503. doi: 10.1002/eji.200535464.

113. Hofstra CL, Desai PJ, Thurmond RL, Fung-Leung W-P. Histamine H_4 receptor mediates chemotaxis and calcium mobilization of mast cells. J Pharmacol Exp Ther. 2003;305(3):1212-21. doi: 10.1124/jpet.102.046581.

114. Olenchock BA. Impaired degranulation but enhanced cytokine production after FcεRI stimulation of diacylglycerol kinase ζ–deficient mast cells. 2006;203(6):1471-80. doi: 10.1084/jem.20052424. PMID: 16717114.

115. Sakuma M, Shirai Y, Ueyama T, Saito N. Diacylglycerol kinase γ regulates antigen-induced mast cell degranulation by mediating Ca2+ influxes. Biochem Biophys Res Commun. 2014;445(2):340-5. doi: 10.1016/j.bbrc.2014.01.197.

116. Valtcheva MV, Davidson S, Zhao C, Leitges M, Gereau RW. Protein kinase Cδ mediates histamine-evoked itch and responses in pruriceptors. Mol Pain. 2015;11. doi: 10.1186/1744-8069-11-1. PMID: 25558916.

117. Ross SE, Mardinly AR, McCord AE, Zurawski J, Cohen S, Jung C, et al. Loss of inhibitory interneurons in the dorsal spinal cord and elevated itch in Bhlhb5 mutant mice. Neuron. 2010;65(6):886-98. Epub 2010/03/30. doi: 10.1016/j.neuron.2010.02.025. PMID: 20346763.

118. Wang X, Zhang J, Eberhart D, Urban R, Meda K, Solorzano C, et al. Excitatory superficial dorsal horn interneurons are functionally heterogeneous and required for the full behavioral expression of pain and itch. Neuron. 2013;78(2):312-24. Epub 2013/04/30. doi: 10.1016/j.neuron.2013.03.001. PMID: 23622066.

119. Ishiuji Y, Coghill RC, Patel TS, Dawn A, Fountain J, Oshiro Y, et al. Repetitive scratching and noxious heat do not inhibit histamine-induced itch in atopic dermatitis. Br J Dermatol. 2008;158(1):78-83. Epub 2007/11/08. doi: 10.1111/j.1365-2133.2007.08281.x. PMID: 17986304.

120. Shimada SG, LaMotte RH. Behavioral differentiation between itch and pain in mouse. Pain. 2008;139(3):681-7. Epub 2008/09/16. doi: 10.1016/j.pain.2008.08.002. PMID: 18789837.

121. Ikoma A, Steinhoff M, Stander S, Yosipovitch G, Schmelz M. The neurobiology of itch. Nat Rev Neurosci. 2006;7(7):535-47. Epub 2006/06/23. doi: 10.1038/nrn1950. PMID: 16791143.

122. Su AI, Wiltshire T, Batalov S, Lapp H, Ching KA, Block D, et al. A gene atlas of the mouse and human protein-encoding transcriptomes. Proc Natl Acad Sci U S A. 2004;101(16):6062-7. doi: 10.1073/pnas.0400782101. PMID: 15075390.

123. Lattin JE, Schroder K, Su AI, Walker JR, Zhang J, Wiltshire T, et al. Expression analysis of G Protein-Coupled Receptors in mouse macrophages. Immunome Res. 2008;4:5. Epub 2008/04/30. doi: 10.1186/1745-7580-4-5. PMID: 18442421.

124. McCoy ES, Taylor-Blake B, Zylka MJ. CGRPα-Expressing Sensory Neurons Respond to Stimuli that Evoke Sensations of Pain and Itch. PLoS One. 2012;7(5). doi: 10.1371/journal.pone.0036355. PMID: 22563493.

125. Langford DJ, Crager SE, Shehzad Z, Smith SB, Sotocinal SG, Levenstadt JS, et al. Social Modulation of Pain as Evidence for Empathy in Mice. Science. 2006;312(5782):1967-70. doi: 10.1126/science.1128322.

126. Zhuang ZY, Xu H, Clapham DE, Ji RR. Phosphatidylinositol 3-kinase activates ERK in primary sensory neurons and mediates inflammatory heat hyperalgesia through TRPV1 sensitization. J Neurosci. 2004;24(38):8300-9. Epub 2004/09/24. doi: 10.1523/jneurosci.2893-04.2004. PMID: 15385613.

127. Otte C, Gold SM, Penninx BW, Pariante CM, Etkin A, Fava M, et al. Major depressive disorder. Nature Reviews Disease Primers. 2016;2:16065. doi: 10.1038/nrdp.2016.65.

128. Goldstein BI, Birmaher B. Prevalence, Clinical Presentation, and Differential Diagnosis of Pediatric Bipolar Disorder. Isr J Psychiatry Relat Sci. 2012;49(1):3-14. PMID: 22652925.

129. Dubovsky SL. Mania. CONTINUUM: Lifelong Learning in Neurology. 2015;21(3):737-55. doi: 10.1212/01.CON.0000466663.28026.6f. PMID: 00132979-201506000-00016.

130. Grande I, Berk M, Birmaher B, Vieta E. Bipolar disorder. The Lancet. 2016;387(10027):1561-72. doi: 10.1016/S0140-6736(15)00241-X.

131. Waraich P, Goldner EM, Somers JM, Hsu L. Prevalence and Incidence Studies of Mood Disorders: A Systematic Review of the Literature. The Canadian Journal of Psychiatry. 2004;49(2):124-38. doi: 10.1177/070674370404900208. PMID: 15065747.

132. Faraone SV, Asherson P, Banaschewski T, Biederman J, Buitelaar JK, Ramos-Quiroga JA, et al. Attention-deficit/hyperactivity disorder. Nature Reviews Disease Primers. 2015;1:15020. doi: 10.1038/nrdp.2015.20.

133. Craske MG, Stein MB, Eley TC, Milad MR, Holmes A, Rapee RM, et al. Anxiety disorders. Nature Reviews Disease Primers. 2017;3:17024. doi: 10.1038/nrdp.2017.24.

134. Gejman P, Sanders A, Duan J. The Role of Genetics in the Etiology of Schizophrenia. Psychiatr Clin North Am. 2010;33(1):35-66. doi: 10.1016/j.psc.2009.12.003. PMID: 20159339.

135. Perälä J, Suvisaari J, Saarni SI, et al. Lifetime prevalence of psychotic and bipolar I disorders in a general population. Arch Gen Psychiatry. 2007;64(1):19-28. doi: 10.1001/archpsyc.64.1.19.

136. Somers JM, Goldner EM, Waraich P, Hsu L. Prevalence and Incidence Studies of Anxiety Disorders: A Systematic Review of the Literature. The Canadian Journal of Psychiatry. 2006;51(2):100-13. doi: 10.1177/070674370605100206. PMID: 16989109.

137. McGuffin P, Rijsdijk F, Andrew M, Sham P, Katz R, Cardno A. The heritability of bipolar affective disorder and the genetic relationship to unipolar depression. Arch Gen Psychiatry. 2003;60(5):497-502. doi: 10.1001/archpsyc.60.5.497.

138. Butler M, Urosevic S, Desai P, Sponheim SR, Popp J, Nelson VA, et al. AHRQ Comparative Effectiveness Reviews. Treatment for Bipolar Disorder in Adults: A Systematic Review. Rockville (MD): Agency for Healthcare Research and Quality (US); 2018.

139. Patel KR, Cherian J, Gohil K, Atkinson D. Schizophrenia: Overview and Treatment Options. Pharmacy and Therapeutics. 2014;39(9):638-45. PMID: PMC4159061.

140. Castle L, Aubert RE, Verbrugge RR, Khalid M, Epstein RS. Trends in Medication Treatment for ADHD. Journal of Attention Disorders. 2007;10(4):335-42. doi: 10.1177/1087054707299597. PMID: 17449832.

141. Lee Y, Zhang Y, Kim S, Han K. Excitatory and inhibitory synaptic dysfunction in mania: an emerging hypothesis from animal model studies. Exp Mol Med. 2018;50(4):12. doi: 10.1038/s12276-018-0028-y. PMID: PMC5938027.

142. Zeng Z, Wang T, Li T, Li Y, Chen P, Zhao Q, et al. Common SNPs and haplotypes in DGKH are associated with bipolar disorder and schizophrenia in the Chinese Han population. Mol Psychiatry. 2010;16:473. doi: 10.1038/mp.2010.86 https://www.nature.com/articles/mp201086#supplementary-information.

143. Takata A, Kawasaki H, Iwayama Y, Yamada K, Gotoh L, Mitsuyasu H, et al. Nominal association between a polymorphism in DGKH and bipolar disorder detected in a meta-analysis of East Asian case–control samples. Psychiatry Clin Neurosci. 2011;65(3):280-5. doi: doi:10.1111/j.1440-1819.2011.02193.x.

144. Yosifova A, Mushiroda T, Kubo M, Takahashi A, Kamatani Y, Kamatani N, et al. Genome-wide association study on bipolar disorder in the Bulgarian population. Genes Brain Behav. 2011;10(7):789-97. Epub 2011/07/21. doi: 10.1111/j.1601-183X.2011.00721.x. PMID: 21771265.

145. Moya PR, Murphy DL, McMahon FJ, Wendland JR. Increased gene expression of diacylglycerol kinase eta in bipolar disorder. The International Journal of Neuropsychopharmacology. 2010;13(8):1127-8. doi: 10.1017/S1461145710000593. PMID: PMC2928712.

146. Machado-Vieira R, Manji HK, Zarate CA. The role of lithium in the treatment of bipolar disorder: convergent evidence for neurotrophic effects as a unifying hypothesis. Bipolar Disord. 2009;11(Suppl 2):92-109. doi: 10.1111/j.1399-5618.2009.00714.x. PMID: PMC2800957.

147. Caricasole A, Bettini E, Sala C, Roncarati R, Kobayashi N, Caldara F, et al. Molecular Cloning and Characterization of the Human Diacylglycerol Kinase β (DGKβ) Gene: ALTERNATIVE SPLICING GENERATES DGKβ ISOTYPES WITH DIFFERENT PROPERTIES. J Biol Chem. 2002;277(7):4790-6. doi: 10.1074/jbc.M110249200.

148. Romeo RD, Mueller A, Sisti HM, Ogawa S, McEwen BS, Brake WG. Anxiety and fear behaviors in adult male and female C57BL/6 mice are modulated by maternal separation. Horm Behav. 2003;43(5):561-7. doi: https://doi.org/10.1016/S0018-506X(03)00063-1.

149. Weaver ICG, Meaney MJ, Szyf M. Maternal care effects on the hippocampal transcriptome and anxiety-mediated behaviors in the offspring that are reversible in adulthood. Proc Natl Acad Sci U S A. 2006;103(9):3480-5. doi: 10.1073/pnas.0507526103.

150. van der Kooij MA, Grosse J, Zanoletti O, Papilloud A, Sandi C. The effects of stress during early postnatal periods on behavior and hippocampal neuroplasticity markers in adult male mice. Neuroscience. 2015;311:508-18. Epub 2015/11/10. doi: 10.1016/j.neuroscience.2015.10.058. PMID: 26548415.

151. Ishikawa J, Nishimura R, Ishikawa A. Early-life stress induces anxiety-like behaviors and activity imbalances in the medial prefrontal cortex and amygdala in adult rats. Eur J Neurosci. 2015;41(4):442-53. Epub 2015/01/13. doi: 10.1111/ejn.12825. PMID: 25581710.

152. Pearson RM, Campbell A, Howard LM, Bornstein MH, O'Mahen H, Mars B, et al. Impact of dysfunctional maternal personality traits on risk of offspring depression, anxiety and self-harm at age 18 years: a population-based longitudinal study. Psychol Med. 2018;48(1):50-60. Epub 2017/06/07. doi: 10.1017/s0033291717001246. PMID: 28583221.

153. Bosch OJ, Neumann ID. Both oxytocin and vasopressin are mediators of maternal care and aggression in rodents: From central release to sites of action. Horm Behav. 2012;61(3):293-303. doi: https://doi.org/10.1016/j.yhbeh.2011.11.002.

154. Numan M, Stolzenberg DS. Medial preoptic area interactions with dopamine neural systems in the control of the onset and maintenance of maternal behavior in rats. Front Neuroendocrinol. 2009;30(1):46-64. doi: https://doi.org/10.1016/j.yfrne.2008.10.002.

155. Smith JW, Seckl JR, Evans AT, Costall B, Smythe JW. Gestational stress induces post-partum depression-like behaviour and alters maternal care in rats. Psychoneuroendocrinology. 2004;29(2):227-44. doi: https://doi.org/10.1016/S0306-4530(03)00025-8.

156. Fleming AS, Corter C. Factors influencing maternal responsiveness in humans: Usefulness of an animal model. Psychoneuroendocrinology. 1988;13(1):189-212. doi: https://doi.org/10.1016/0306-4530(88)90014-5.

157. Flaisher-Grinberg S, Einat H. A possible utilization of the mice forced swim test for modeling manic-like increase in vigor and goal-directed behavior. J Pharmacol Toxicol Methods. 2009;59(3):141-5. Epub 2009/04/04. doi: 10.1016/j.vascn.2009.03.003. PMID: 19341808.

158. Porsolt RD, Bertin A, Jalfre M. Behavioral despair in mice: a primary screening test for antidepressants. Arch Int Pharmacodyn Ther. 1977;229(2):327-36. Epub 1977/10/01. PMID: 596982.

159. Walf AA, Frye CA. The use of the elevated plus maze as an assay of anxiety-related behavior in rodents. Nat Protoc. 2007;2(2):322-8. doi: 10.1038/nprot.2007.44. PMID: PMC3623971.

160. Walsh RN, Cummins RA. The open-field test: a critical review. Psychol Bull. 1976;83(3):482-504. Epub 1976/05/01. PMID: 17582919.

161. Geyer MA, Braff DL. Startle habituation and sensorimotor gating in schizophrenia and related animal models. Schizophr Bull. 1987;13(4):643-68. Epub 1987/01/01. PMID: 3438708.

162. Goto SH, Conceicao IM, Ribeiro RA, Frussa-Filho R. Comparison of anxiety measured in the elevated plus-maze, open-field and social interaction tests between spontaneously

hypertensive rats and Wistar EPM-1 rats. Rev Bras Pesqui Med Biol. 1993;26(9):965-9. Epub 1993/09/01. PMID: 8298531.

163. Carola V, D'Olimpio F, Brunamonti E, Mangia F, Renzi P. Evaluation of the elevated plus-maze and open-field tests for the assessment of anxiety-related behaviour in inbred mice. Behav Brain Res. 2002;134(1-2):49-57. Epub 2002/08/23. PMID: 12191791.

164. Swerdlow NR, Braff DL, Geyer MA. Cross-species studies of sensorimotor gating of the startle reflex. Ann N Y Acad Sci. 1999;877:202-16. Epub 1999/07/23. PMID: 10415651.

165. Berridge MJ. Neuronal calcium signaling. Neuron. 1998;21(1):13-26. doi: 10.1016/S0896-6273(00)80510-3.

166. Garzón-Niño J, Rodríguez-Muñoz M, Cortés-Montero E, Sánchez-Blázquez P. Increased PKC activity and altered GSK3β/NMDAR function drive behavior cycling in HINT1-deficient mice: bipolarity or opposing forces. Sci Rep. 2017;7:43468. doi: 10.1038/srep43468. PMID: PMC5327482.

167. Varadarajulu J, Lebar M, Krishnamoorthy G, Habelt S, Lu J, Bernard Weinstein I, et al. Increased anxiety-related behaviour in Hint1 knockout mice. Behav Brain Res. 2011;220(2):305-11. Epub 2011/02/15. doi: 10.1016/j.bbr.2011.02.012. PMID: 21316396.

168. Hahn CG, Friedman E. Abnormalities in protein kinase C signaling and the pathophysiology of bipolar disorder. Bipolar Disord. 1999;1(2):81-6. Epub 2001/03/17. PMID: 11252663.

169. Bowers BJ, Collins AC, Tritto T, Wehner JM. Mice lacking PKCγ exhibit decreased anxiety. Behav Genet. 2000;30(2):111-21. doi: 10.1023/a:1001951104208.

170. Hodge CW, Raber J, McMahon T, Walter H, Sanchez-Perez AM, Olive MF, et al. Decreased anxiety-like behavior, reduced stress hormones, and neurosteroid supersensitivity in mice lacking protein kinase Cε. J Clin Invest. 2002;110(7):1003-10. doi: 10.1172/JCI15903.

171. Satoh Y, Endo S, Nakata T, Kobayashi Y, Yamada K, Ikeda T, et al. ERK2 contributes to the control of social behaviors in mice. J Neurosci. 2011;31(33):11953-67. Epub 2011/08/19. doi: 10.1523/jneurosci.2349-11.2011. PMID: 21849556.

172. Ailing F, Fan L, Li S, Manji S. Role of extracellular signal-regulated kinase signal transduction pathway in anxiety. J Psychiatr Res. 2008;43(1):55-63. Epub 2008/03/20. doi: 10.1016/j.jpsychires.2008.01.018. PMID: 18348889.

173. Engel SR, Creson TK, Hao Y, Shen Y, Maeng S, Nekrasova T, et al. The extracellular signal-regulated kinase pathway contributes to the control of behavioral excitement. Mol Psychiatry. 2009;14(4):448-61. doi: 10.1038/sj.mp.4002135. PMID: PMC2804878.

174. Chen G, Manji HK. The extracellular signal-regulated kinase pathway: an emerging promising target for mood stabilizers. Curr Opin Psychiatry. 2006;19(3):313-23. Epub 2006/04/14. doi: 10.1097/01.yco.0000218604.63463.cd. PMID: 16612219.

175. Bhattacharyya S, Puri S, Miledi R, Panicker MM. Internalization and recycling of 5-HT_{2A} receptors activated by serotonin and protein kinase C-mediated mechanisms. Proc Natl Acad Sci U S A. 2002;99(22):14470-5. doi: 10.1073/pnas.212517999.

176. Brandon NJ, Delmas P, Kittler JT, McDonald BJ, Sieghart W, Brown DA, et al. GABAA receptor phosphorylation and functional modulation in cortical neurons by a protein kinase C-dependent pathway. J Biol Chem. 2000;275(49):38856-62. doi: 10.1074/jbc.M004910200.

177. Maguire J, Mody I. GABA(A)R plasticity during pregnancy: relevance to postpartum depression. Neuron. 2008;59(2):207-13. doi: 10.1016/j.neuron.2008.06.019. PMID: PMC2875248.

178. Gao J, Wu R, Davis C, Li M. Activation of 5-HT2A receptor disrupts rat maternal behavior. Neuropharmacology. 2018;128:96-105. Epub 2017/10/03. doi: 10.1016/j.neuropharm.2017.09.037. PMID: 28965828.

179. Aznar S, Hervig ME-S. The 5-HT2A serotonin receptor in executive function: Implications for neuropsychiatric and neurodegenerative diseases. Neurosci Biobehav Rev. 2016;64:63-82. doi: https://doi.org/10.1016/j.neubiorev.2016.02.008.

180. Nuss P. Anxiety disorders and GABA neurotransmission: a disturbance of modulation. Neuropsychiatr Dis Treat. 2015;11:165-75. doi: 10.2147/NDT.S58841. PMID: PMC4303399.

181. Ding Q, Xia W, Liu JC, Yang JY, Lee DF, Xia J, et al. Erk associates with and primes GSK-3beta for its inactivation resulting in upregulation of beta-catenin. Mol Cell. 2005;19(2):159-70. Epub 2005/07/26. doi: 10.1016/j.molcel.2005.06.009. PMID: 16039586.

182. Goode N, Hughes K, Woodgett JR, Parker PJ. Differential regulation of glycogen synthase kinase-3 beta by protein kinase C isotypes. J Biol Chem. 1992;267(24):16878-82. Epub 1992/08/25. PMID: 1324914.

183. Jope RS, Roh M-S. Glycogen synthase kinase-3 (GSK3) in psychiatric diseases and therapeutic interventions. Curr Drug Targets. 2006;7(11):1421-34. PMID: PMC1850891.

184. Boudanova E, Navaroli DM, Melikian HE. Amphetamine-induced decreases in dopamine transporter surface expression are protein kinase C-independent. Neuropharmacology. 2008;54(3):605-12. Epub 2008/01/01. doi: 10.1016/j.neuropharm.2007.11.007. PMID: 18164041.

185. Loder MK, Melikian HE. The dopamine transporter constitutively internalizes and recycles in a protein kinase C-regulated manner in stably transfected PC12 cell lines. J Biol Chem. 2003;278(24):22168-74. Epub 2003/04/19. doi: 10.1074/jbc.M301845200. PMID: 12682063.

186. Lein ES, Hawrylycz MJ, Ao N, Ayres M, Bensinger A, Bernard A, et al. Genome-wide atlas of gene expression in the adult mouse brain. Nature. 2006;445:168. doi: 10.1038/nature05453 https://www.nature.com/articles/nature05453#supplementary-information.

187. Sommer W, Arlinde C, Caberlotto L, Thorsell A, Hyytia P, Heilig M. Differential expression of diacylglycerol kinase iota and L18A mRNAs in the brains of alcohol-preferring AA

and alcohol-avoiding ANA rats. Mol Psychiatry. 2001;6(1):103-8. Epub 2001/03/13. PMID: 11244494.

188. Martin EI, Ressler KJ, Binder E, Nemeroff CB. The neurobiology of anxiety disorders: brain imaging, genetics, and psychoneuroendocrinology. Psychiatr Clin North. 2009;32(3):549-75. doi: 10.1016/j.psc.2009.05.004. PMID: PMC3684250.

189. Blanco E, Castilla-Ortega E, Miranda R, Begega A, Aguirre JA, Arias JL, et al. Effects of medial prefrontal cortex lesions on anxiety-like behaviour in restrained and non-restrained rats. Behav Brain Res. 2009;201(2):338-42. doi: https://doi.org/10.1016/j.bbr.2009.03.001.

190. Park J, Wood J, Bondi C, Del Arco A, Moghaddam B. Anxiety evokes hypofrontality and disrupts rule-relevant encoding by dorsomedial prefrontal cortex neurons. J Neurosci. 2016;36(11):3322-35. doi: 10.1523/jneurosci.4250-15.2016.

191. Kheirbek MA, Drew LJ, Burghardt NS, Costantini DO, Tannenholz L, Ahmari SE, et al. Differential control of learning and anxiety along the dorso-ventral axis of the dentate gyrus. Neuron. 2013;77(5):955-68. doi: 10.1016/j.neuron.2012.12.038. PMID: PMC3595120.

192. Abé C, Ekman C-J, Sellgren C, Petrovic P, Ingvar M, Landén M. Manic episodes are related to changes in frontal cortex: a longitudinal neuroimaging study of bipolar disorder 1. Brain. 2015;138(11):3440-8. doi: 10.1093/brain/awv266.

193. Henschen CW, Palmiter RD, Darvas M. Restoration of dopamine signaling to the dorsal striatum is sufficient for aspects of active maternal behavior in female mice. Endocrinology. 2013;154(11):4316-27. doi: 10.1210/en.2013-1257.

194. Hansen S, Harthon C, Wallin E, Löfberg L, Svensson K. The effects of 6-OHDA-induced dopamine depletions in the ventral or dorsal striatum on maternal and sexual behavior in the female rat. Pharmacol Biochem Behav. 1991;39(1):71-7. doi: https://doi.org/10.1016/0091-3057(91)90399-M.

195. Smith AB, Taylor E, Brammer M, Toone B, Rubia K. Task-specific hypoactivation in prefrontal and temporoparietal brain regions during motor inhibition and task switching in medication-naive children and adolescents with attention deficit hyperactivity disorder. Am J Psychiatry. 2006;163(6):1044-51. Epub 2006/06/03. doi: 10.1176/ajp.2006.163.6.1044. PMID: 16741205.

196. Spencer TJ, Brown A, Seidman LJ, Valera EM, Makris N, Lomedico A, et al. Effect of Psychostimulants on Brain Structure and Function in ADHD: A Qualitative Literature Review of MRI-Based Neuroimaging Studies. The Journal of clinical psychiatry. 2013;74(9):902-17. doi: 10.4088/JCP.12r08287. PMID: PMC3801446.

197. Sheleg M, Yu Q, Go C, Wagner GC, Kusnecov AW, Zhou R. Decreased maternal behavior and anxiety in ephrin-A5$^{-/-}$ mice. Genes Brain Behav. 2017;16(2):271-84. Epub 2016/08/19. doi: 10.1111/gbb.12319. PMID: 27535576.

198. Kessler MS, Bosch OJ, Bunck M, Landgraf R, Neumann ID. Maternal care differs in mice bred for high vs. low trait anxiety: impact of brain vasopressin and cross-fostering. Soc Neurosci. 2011;6(2):156-68. Epub 2010/07/28. doi: 10.1080/17470919.2010.495567. PMID: 20661836.

199. Pedersen C, Vadlamudi S, Boccia M, Moy S. Variations in maternal behavior in C57BL/6J mice: behavioral comparisons between adult offspring of high and low pup-licking mothers. Front Psychiatry. 2011;2(42). doi: 10.3389/fpsyt.2011.00042.

200. O'Hara MW, Swain AM. Rates and risk of postpartum depression—a meta-analysis. Int Rev Psychiatry. 1996;8(1):37-54. doi: 10.3109/09540269609037816.

201. C. R, K. S, M. B, U. S, K. R, T. F, et al. Prevalence, onset and comorbidity of postpartum anxiety and depressive disorders. Acta Psychiatr Scand. 2008;118(6):459-68. doi: doi:10.1111/j.1600-0447.2008.01264.x.

202. Katon W, Russo J, Gavin A. Predictors of postpartum depression. J Womens Health. 2014;23(9):753-9. Epub 2014/08/15. doi: 10.1089/jwh.2014.4824. PMID: 25121562.

203. Brown JR, Ye H, Bronson RT, Dikkes P, Greenberg ME. A defect in nurturing in mice lacking the immediate early gene fosB. Cell. 1996;86(2):297-309. doi: https://doi.org/10.1016/S0092-8674(00)80101-4.

204. Wang Z, Storm DR. Maternal behavior is impaired in female mice lacking type 3 adenylyl cyclase. Neuropsychopharmacology. 2011;36(4):772-81. doi: 10.1038/npp.2010.211. PMID: 21150908.

205. Valsamis B, Schmid S. Habituation and prepulse inhibition of acoustic startle in rodents. J Visualized Exp. 2011;(55):3446. doi: 10.3791/3446. PMID: PMC3217252.

206. Ma C, Greenquist KW, Lamotte RH. Inflammatory mediators enhance the excitability of chronically compressed dorsal root ganglion neurons. J Neurophysiol. 2006;95(4):2098-107. Epub 2005/12/31. doi: 10.1152/jn.00748.2005. PMID: 16381809.

207. Roybal K, Theobold D, Graham A, DiNieri JA, Russo SJ, Krishnan V, et al. Mania-like behavior induced by disruption of CLOCK. Proceedings of the National Academy of Sciences. 2007;104(15):6406-11. doi: 10.1073/pnas.0609625104.

208. Scotti M-AL, Lee G, Stevenson SA, Ostromecki AM, Wied TJ, Kula DJ, et al. Behavioral and pharmacological assessment of a potential new mouse model for mania. Physiol Behav. 2011;103(3):376-83. doi: https://doi.org/10.1016/j.physbeh.2011.03.005.

209. Sharma AN, Fries GR, Galvez JF, Valvassori SS, Soares JC, Carvalho AF, et al. Modeling mania in preclinical settings: A comprehensive review. Prog Neuropsychopharmacol Biol Psychiatry. 2016;66:22-34. doi: https://doi.org/10.1016/j.pnpbp.2015.11.001.

210. Crabbe JC, Wahlsten D, Dudek BC. Genetics of Mouse Behavior: Interactions with Laboratory Environment. Science. 1999;284(5420):1670-2. doi: 10.1126/science.284.5420.1670.

211. Wahlsten D, Metten P, Phillips TJ, Boehm SL, Burkhart-Kasch S, Dorow J, et al. Different data from different labs: Lessons from studies of gene–environment interaction. J Neurobiol. 2003;54(1):283-311. doi: doi:10.1002/neu.10173.

212. Bohlen M, Hayes ER, Bohlen B, Bailoo JD, Crabbe JC, Wahlsten D. Experimenter effects on behavioral test scores of eight inbred mouse strains under the influence of ethanol. Behav Brain Res. 2014;272:46-54. doi: https://doi.org/10.1016/j.bbr.2014.06.017.

213. Lewejohann L, Reinhard C, Schrewe A, Brandewiede J, Haemisch A, Görtz N, et al. Environmental bias? Effects of housing conditions, laboratory environment and experimenter on behavioral tests. Genes Brain Behav. 2006;5(1):64-72. doi: doi:10.1111/j.1601-183X.2005.00140.x.

214. Loss CM, Binder LB, Muccini E, Martins WC, de Oliveira PA, Vandresen-Filho S, et al. Influence of environmental enrichment vs. time-of-day on behavioral repertoire of male albino Swiss mice. Neurobiol Learn Mem. 2015;125:63-72. doi: https://doi.org/10.1016/j.nlm.2015.07.016.

215. Almaça J, Faria D, Sousa M, Uliyakina I, Conrad C, Sirianant L, et al. High-Content siRNA Screen Reveals Global ENaC Regulators and Potential Cystic Fibrosis Therapy Targets. Cell. 2013;154(6):1390-400. doi: https://doi.org/10.1016/j.cell.2013.08.045.

216. Revill K, Wang T, Lachenmayer A, Kojima K, Harrington A, Li J, et al. Genome-Wide Methylation Analysis and Epigenetic Unmasking Identify Tumor Suppressor Genes in Hepatocellular Carcinoma. Gastroenterology. 2013;145(6):1424-35.e25. doi: https://doi.org/10.1053/j.gastro.2013.08.055.

217. Etcheverry A, Aubry M, Idbaih A, Vauleon E, Marie Y, Menei P, et al. DGKI Methylation Status Modulates the Prognostic Value of MGMT in Glioblastoma Patients Treated with Combined Radio-Chemotherapy with Temozolomide. PLoS One. 2014;9(9):e104455. doi: 10.1371/journal.pone.0104455.

218. Etcheverry A, Aubry M, de Tayrac M, Vauleon E, Boniface R, Guenot F, et al. DNA methylation in glioblastoma: impact on gene expression and clinical outcome. BMC Genomics. 2010;11:701. Epub 2010/12/16. doi: 10.1186/1471-2164-11-701. PMID: 21156036.

219. Sakin YS, Dogrul A, Ilkaya F, Seyrek M, Ulas UH, Gulsen M, et al. The effect of FAAH, MAGL, and Dual FAAH/MAGL inhibition on inflammatory and colorectal distension-induced visceral pain models in Rodents. J Neurogastroenterol Motil. 2015;27(7):936-44. Epub 2015/04/15. doi: 10.1111/nmo.12563. PMID: 25869205.

220. Lee Y, Rodriguez C, Dionne RA. The role of COX-2 in acute pain and the use of selective COX-2 inhibitors for acute pain relief. Curr Pharm Des. 2005;11(14):1737-55. Epub 2005/05/17. PMID: 15892672.

221. Higgs GA. Arachidonic acid metabolism, pain and hyperalgesia: the mode of action of non-steroidal mild analgesics. Br J Clin Pharmacol. 1980;10(Suppl 2):233S-5S. PMID: PMC1430162.

222. Ogasawara D, Deng H, Viader A, Baggelaar MP, Breman A, den Dulk H, et al. Rapid and profound rewiring of brain lipid signaling networks by acute diacylglycerol lipase inhibition. Proc Natl Acad Sci U S A. 2016;113(1):26-33. Epub 2015/12/17. doi: 10.1073/pnas.1522364112. PMID: 26668358.

223. Nieto-Posadas A, Picazo-Juárez G, Llorente I, Jara-Oseguera A, Morales-Lázaro S, Escalante-Alcalde D, et al. Lysophosphatidic acid directly activates TRPV1 through a C-terminal binding site. Nat Chem Biol. 2012;8(1):78-85. doi: http://www.nature.com/nchembio/journal/v8/n1/abs/nchembio.712.html#supplementary-information.

224. Park KA, Vasko MR. Lipid mediators of sensitivity in sensory neurons. Trends Pharmacol Sci. 2005;26(11):571-7. doi: http://dx.doi.org/10.1016/j.tips.2005.09.010.

225. Sommer U, Herscovitz H, Welty FK, Costello CE. LC-MS-based method for the qualitative and quantitative analysis of complex lipid mixtures. J Lipid Res. 2006;47(4):804-14. Epub 2006/01/31. doi: 10.1194/jlr.M500506-JLR200. PMID: 16443931.

226. Tumanov S, Kamphorst JJ. Recent advances in expanding the coverage of the lipidome. Curr Opin Biotechnol. 2017;43:127-33. doi: https://doi.org/10.1016/j.copbio.2016.11.008.

227. Kind T, Fiehn O. Seven Golden Rules for heuristic filtering of molecular formulas obtained by accurate mass spectrometry. BMC Bioinformatics. 2007;8:105. Epub 2007/03/29. doi: 10.1186/1471-2105-8-105. PMID: 17389044.

228. Wanichthanarak K, Fan S, Grapov D, Barupal DK, Fiehn O. Metabox: A Toolbox for Metabolomic Data Analysis, Interpretation and Integrative Exploration. PLoS One. 2017;12(1):e0171046. doi: 10.1371/journal.pone.0171046.